Investigating the Geochemistry of Selenium in the Residual from Biologically Treated Mine-Impacted Water

by

Laura Marie Desaunoy

B.Sc., University of Calgary, 2012

Thesis Submitted in Partial Fulfillment of the
Requirements for the Degree of
Master of Science

in the
Department of Earth Sciences
Faculty of Science

SIMON FRASER UNIVERSITY
Spring 2018

Approval

Name:	**Laura Marie Desaunoy**
Degree:	**Master of Science**
Title:	**Investigating the Geochemistry of Selenium in the Residual from Biologically Treated Mine-Impacted Water**
Examining Committee:	**Chair:** **Andy Calvert** Professor
	Dr. Dirk Kirste Senior Supervisor Assistant Professor
	Dr. Robert Gordon Supervisor Adjunct Professor
	Dr. Mario Bianchin Supervisor Hydrogeochemist, Wood plc
	Dr. Peter Winterburn External Examiner Research Chair in Exploration Geochemistry Department of Earth, Ocean, and Atmospheric Sciences University of British Columbia
Date Defended/Approved:	April, 16, 2018

Abstract

Bacterially-mediated wastewater treatment is commonly used to prevent selenium (Se) release to the environment. This research focuses on the characterization of a selenium-rich residual, the by-product of industrial wastewater treatment. Solid-phase selenium speciation was investigated through sequential extraction procedures (SEP) and X-ray Absorption near Edge Spectroscopy (XANES). Selenium mobility and changes in Se speciation were tested through batch experiments under varying redox and pH conditions. The residual exhibits some inhomogeneity, and is dominated by metal selenide species, with some evidence for less-reduced Se species. The greatest Se mobility was in mildly oxidizing conditions at neutral pH which also showed the least speciation change in the residual. Under highly-oxidizing and/or low-pH conditions Se mobilization was lower and reaction was dominated by oxidation of the metal-selenides to Se^0 and/or SeS_2. Additionally, speciation changes in the solid phase during the SEP were observed.

Keywords: selenium; geochemistry; waste; environment; mining; XANES

For Guy and Florence

Acknowledgements

I would first like to acknowledge my senior supervisor, Dirk, for his endless support, approachability and enthusiasm. Without his dedication, hours spent in the lab, and shared wealth of both funds and knowledge this would not have been possible.

Robert Gordon, without whom I would not have ever understood synchrotron physics or achieved beamtime to conduct my research.

I would like to recognize Mario Bianchin, not only for his support and guidance but for his integral role in this project coming to fruition. Without him I would not have had the opportunity to work on such an interesting project.

I would like to thank Peter Winterburn for volunteering his time and efforts to be the external examiner for the defense of this thesis.

I would like to thank Clemente Miranda for his central role in this project including support from an industrial perspective as well as additional resources.

Deserving of the highest level of acknowledgement is Andrew Allen, who spent countless hours in the lab conducting experiments with me, running analytical and assisting with my research. His support was central in a timely completion of this project and sustained sanity throughout.

I would like to highlight the role of my parents, Guy and Florence, who provided me with every opportunity to succeed in life and encouraged me to do so every step along the way. I would also like to acknowledge my partner, Dustin, for emotional, financial and unconditional support through this process.

As a work of this magnitude is never a solo effort, I would like to acknowledge my fellow researchers and lab mates not only for their support but for selfless time spent editing, reading and discussing my work as well as everyone in the Earth Science Department who helped make this project, and all projects, possible.

The authors thank the Society of Contaminated Sites Approved Professionals of BC, SRK Consulting, Teck Resources Limited, Geoscience BC, the Canadian Light Source

and funding provided to D. Kirste as part of the Hydrogeochemistry Research Group Project for the funds and resources required to carry out this research.

Use of the Advanced Photon Source, an Office of Science User Facility operated for the United States Department of Energy (DOE) Office of Science by Argonne National Laboratory, was supported by the DOE under Contract No. DE-AC02-06CH11357. The authors extend a special thanks to T. Wu and G. Sterbinsky for their support during the experiments.

Research described in this thesis was performed at the Canadian Light Source, which is supported by the Canada Foundation for Innovation, the Natural Sciences and Engineering Research Council of Canada, the University of Saskatchewan, the Government of Saskatchewan, Western Economic Diversification Canada, National Research Council Canada and the Canadian Institutes of Health Research. The authors extend a special thanks to R. Feng and P. Blanchard for their support during the experiments.

Table of Contents

List of Tables

List of Figures

List of Acronyms

APS	Advanced Photon Source
BM	Bending Magnet
CLS	Canadian Light Source
COD	Chemical Oxygen Demand
DI	De-Ionized
FBR	Fluid Bed Reactor
GCWB	Geochemists' Workbench
GSS	Geochemists' Spreadsheet
IC	Ion Chromatography
ICP-AES	Inductively Coupled Plasma Atomic Emission Spectroscopy
ICP-MS	Inductively Coupled Plasma Mass Spectroscopy
LCF	Linear Combinations Fitting
MBBR	Moving Bed Biological Reactor
ORP	Oxidation-Reduction Potential
SEP	Sequential Extraction Procedure
SFU	Simon Fraser University
VESPERS	Very Sensitive Elemental and Structural Probe Employing Radiation from a Synchrotron
XANES	X-ray Absorption Near Edge Spectroscopy

Chapter 1. Introduction

Although selenium (Se) is an essential element for human, animal and vegetation health, an over- or under-abundance may cause adverse health effects and ecological problems. Due to the onset of industrialization, Se has become a contaminant of concern in many parts of the world, including North America. It is naturally occurring in many environments and can become mobile under the right chemical conditions, potentially affecting aquatic habitats and drinking-water sources. While Se occurs naturally at elevated concentrations in sediments, soils and rocks, many anthropogenic activities have been shown to facilitate its mobility. Mining, agriculture and nuclear-power generation have all been demonstrated to increase the potential for mobilizing Se into both groundwater and surface water (Chapman et al., 2010). Elevated Se concentrations in the environment as a result of mining practices have been documented in both Canada and the United States.

Once Se reaches the aquatic environment, it can quickly attain high concentrations due to rapid bioaccumulation within food chains (Lemly, 2004). Selenium in high concentrations can be fatal and, even in lower doses, has the potential to negatively affect human health and reproduction in fish, birds, amphibians and reptiles (Chapman et al., 2010). For example, larval deformities in northern pike were attributed by Muscatello et al. (2006) to exposure to Se in mining effluent from a uranium operation in Saskatchewan. Holm et al. (2003) described harmful impacts of elevated Se from active coal mining on wild rainbow trout and brook trout. Moreover, Se deficiencies can result in humans experiencing growth retardation and impaired bone metabolism (Kang et al., 2013).

Selenium mobility is directly related to 1) the redox state, which controls the speciation in aqueous solution; 2) the sorption properties of the coinciding solid state; and 3) the stability of Se minerals (White and Dubrovsky, 1994). In general, the more oxidizing the environment is, the more mobile Se can be, with the solid-state species of Se occurring under reducing conditions (White et al., 1991). A significant control on Se mobility is the tendency for the element to adsorb onto mineral surfaces. The extent of adsorption is largely dependent on pH, redox conditions and adsorption-site density, with either a decrease in pH or the presence of mildly oxidizing conditions causing a higher

rate of Se adsorption (Balistrieri and Chao, 1990). In the aqueous phase, Se species consist of selenate (SeO_4^{2-}) and selenite (SeO_3^{2-}) which incorporate Se in the (VI) and (IV) valence states, respectively. Selenite adsorbs much more strongly than selenate, with the presence of each species dependent upon the redox and pH conditions of the system (Neal and Sposito, 1989). The reduction and oxidation of Se can occur in the absence of microbes, but the reaction rates are often faster when microbially mediated (Dowdle and Oremland, 1998).

Although the release of Se from industrial wastes to natural waterways and associated impacts are documented (Muscatello et al., 2006; Chapman et al., 2010), technology exists to actively remove Se from industrial effluents. Suspended-growth biological wastewater-treatment systems are currently being used as a way to remove Se from contaminated waters (Lenz et al., 2008; Jain et al., 2015). While wastewater treatment has been proven effective in removing Se from water, it produces a sludge residual with high concentrations of Se that requires disposal or tertiary treatment. Due to the recent emergence of this technology, there has been little research into the potential for Se to remobilize from a biologically fixed state (i.e., in sludge), and the risks associated with landfilling of this material are not understood.

The purpose of this research is to determine the Se speciation within the solid-phase fraction of the residual produced from biological wastewater treatment, and to advance the understanding of mobilization mechanisms within this residual. By addressing both aspects, it will be possible to determine the conditions under which the risk of remobilization is high and which Se species are the most vulnerable to remobilization. Understanding the geochemistry of Se mobility and transport is essential to the development of strategies for mitigating the negative effects of Se in the environment.

1.1. Geochemistry of Selenium

Selenium can occur in a variety of different oxidation states that are subject to oxidation-reduction processes and complex biogeochemical cycling (White and Dubrovsky, 1994). The mobility of selenium is directly related to the redox state, which controls the speciation in aqueous solution, sorption properties of the solid state and solubility (White and Dubrovsky, 1994). Under natural conditions, selenium can occur in

four different oxidation states. Selenium can exist in the Se (VI) oxidation state as selenate (SeO_4^{2-}), in the Se(IV) oxidation state as selenite (SeO_3^{2-}), in the zero oxidation state as elemental Se(0), and in the Se(-II) oxidation state as selenide (Se^{2-}) (White et al., 1991). Selenate and selenite, the two higher oxidation states, occur as aqueous species or in solid compounds (Maiers et al., 1988). Selenium can also exist as crystalline and amorphous polymorphs in the elemental state (Pejova and Grozdanov, 2001). The reduced form of selenium, selenide, can be present as aqueous species, as a solid bound with transition metals, or as gaseous forms of hydrogen selenide (White and Dubrovsky, 1994). Selenium can also exist as (0) or (-II) valence state organic compounds (Weres et al., 1989). Selenium readily substitutes for sulfur in compounds where zero-valent sulfur atoms are bonded to other sulfur atoms (Weres et al., 1989). In addition to inorganic forms of selenium, non-volatile organic selenides, such as selenoamino acids and volatile methylated forms, mainly as dimethyl selenide and dimethyldiselenide, can occur in surface and groundwater (Cutter, 1982).

Selenium can cycle through these different species depending on the biogeochemical conditions of each specific system (Presser and Swain, 1990). The stability of each selenium species is related to the electrochemical potential of the solution it is in (Figure 1) (Shaheen et al., 2016). The redox conditions have been demonstrated to be the main control on selenium solubility, mobilization and sequestration (Shwartz et al., 2016). The processes can be microbially or inorganically facilitated (Jayaweera and Biggar, 1996). Thermodynamic data indicate that selenide (Se^{1-} and Se^{2-}) and elemental Se (Se_0) should be dominant in reducing environments whereas selenite (SeO_3^{2-}) is dominant in mildly reducing environments to slightly oxidizing, and selenate (SeO_4^{2-}) in oxidizing environments (White et al., 1991). In addition, different allotropes of elemental selenium have been found to be more readily mobilized than others under changing redox conditions. Geering et al. (1968) found that the red and black amorphous allotropes are the most readily oxidized where the grey-hexagonal allotrope is found to be the most inert. The redox state of selenium may not, however, always be subject to thermodynamic equilibrium controls, and the role of microbes in affecting selenium speciation can be important (Février et al., 2007). It has been demonstrated that as conditions become more oxic, the predominance of the water-soluble forms of selenium increases, and as conditions become more reduced the selenium is removed from the solution phase possibly by adsorption or precipitation

(Jayaweera and Biggar, 1996). Once selenium has been removed by reducing conditions, however, the process by which it is released under re-oxidation is slower, and therefore, remobilization to the aqueous phase is protracted (Jayaweera and Biggar, 1996).

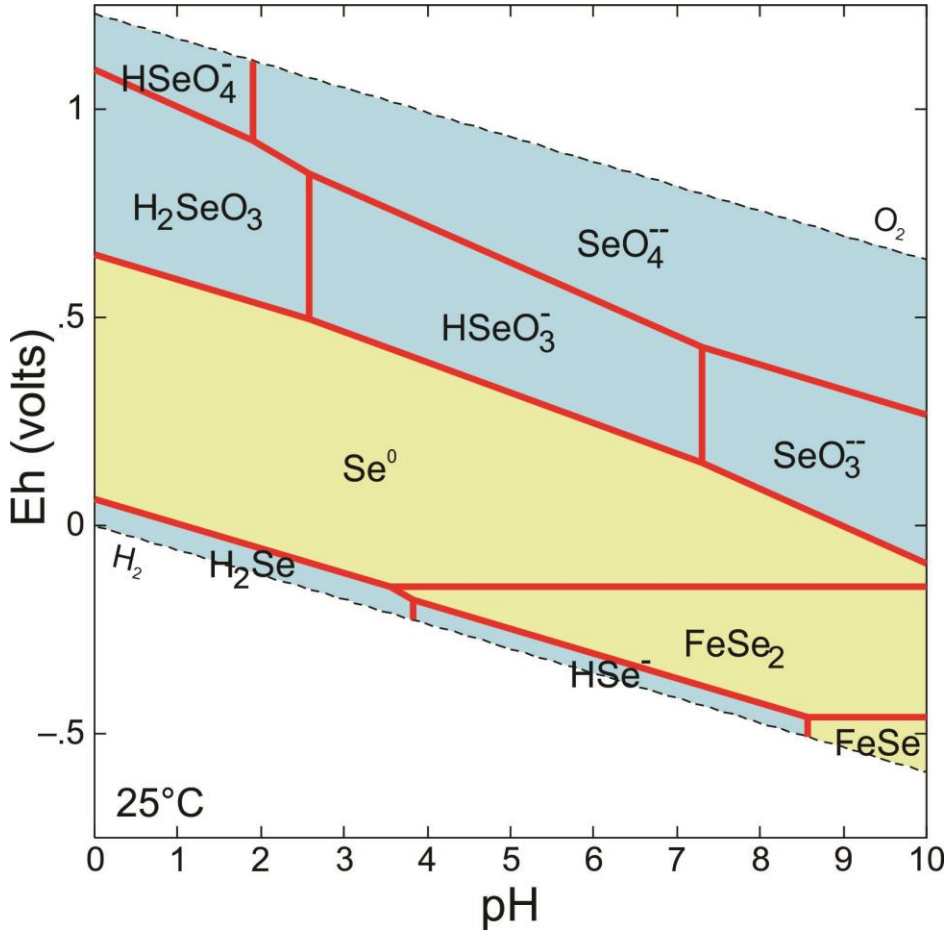

Figure 1-1 Thermodynamic stability diagram of selenium in a system with iron (activity = $1x10^{-4}$) present.

Important agents of the reductive portion of the selenium cycle are the selenate-respiring bacteria which oxidize organic matter by coupling electron flow to the reduction of selenate to form elemental selenium (Se_0) (Dowdle et al., 1998). Elemental selenium is a major repository for selenium in contaminated and natural sediments, the bulk of which remains immobilized as long as anoxic conditions persist (Dowdle et al., 1998). Not only is the reduction of selenium to elemental form mediated by microbes, but it has been shown that the oxidation of Se_0 to selenate and selenite is also carried out by a number of different aerobic microbes (Dowdle et al., 1998). Thiols, a type of organosulfur compounds, are also thought to have an effect on the solubility of selenium. Because

selenium is an analog of sulfur, it can substitute for sulfur in thiols (Stolz et al., 2002). Glutathione, a specific thiol, has the ability to form selenium complexes and is thought to be essential to the intracellular biochemistry of selenium (Weres et al., 1989). The reaction of glutathione, along with other thiols, with elemental selenium could potentially be one of the first processes to take place during the microbial oxidation of selenium in soil (Weres et al., 1989). It has been suggested that reducing the pH of a system can block the dissolution of elemental selenium by reaction with thiols, meaning it could be possible to reduce the cycling of selenium in water bodies by simply reducing the pH of the system. Conversely, increased pH and addition of thiols will enhance the conversion of selenium to soluble species and its volatile form, H_2Se (Weres et al., 1989).

Adsorption of selenium onto iron oxyhydroxides, which are commonly found in sediments and soils, has been shown to be controlled largely by pH (Balistrieri and Chao, 1987; Bleiman and Mishael, 2010). Selenite and selenate, the two aqueous forms of selenium, tend to behave differently when it comes to adsorption. Under similar pH conditions, selenite will adsorb much more strongly than selenate (Balistrieri and Chao, 1987; Neal and Sposito, 1989). This occurrence can be explained if selenite forms inner-sphere complexes and selenate forms outer-sphere complexes (Balistrieri and Chao, 1990). Since selenate has a weaker affinity for adsorption, it is mobile in groundwater and surface water and more readily available for uptake by plants (Balistrieri and Chao, 1990). Particle concentration and pH both influence the adsorption of selenium and either an increase in pH or a decrease in particle concentration cause a decrease in the amount of selenium adsorbed (Balistrieri and Chao, 1990). In addition, the presence of specific ions has shown to impact selenite adsorption. Szlachta and Chubar (2013) found that with high phosphate and at pH > 9, dissolved silica concentrations tended to decrease the amount of selenite adsorbed, while the presence of sulphate and carbonate did not have a notable effect.

1.2. Biological Wastewater Treatment

While the release of Se from industrial wastes to natural waterways has been documented (Chapman et al., 2010; Muscatello et al., 2006), technology exists to treat selenium impacted water. Suspended growth biological wastewater treatment systems are currently being used as a way to remove selenium from contaminated waters (Lenz et al., 2008; Jain et al., 2015). These systems work by adding a carbon source to

promote activity and growth in the native bacterial populations, thereby creating conditions where the selenium is reduced from its aqueous form to an immobile species, which is incorporated into a solid state residual. The systems are comprised of a series of reactors in a specific succession. Initially, heat exchangers are used to bring the temperature of the water to 10°C, after which the water is fed into the first fluid bed reactor (FBR1). Oxygen and nitrate are reduced in FBR1 (reactions 1 and 2).

$$1.5\ O_2 + CH_3OH = 2\ H_2O + CO_2 \quad (1)$$

$$6NO_3^- + CO_2 + 5\ CH_3OH = 7\ H_2O + 6HCO_3^- + 3\ N_2 \quad (2)$$

The water is then fed into the second fluid bed reactor (FBR2) by gravity drainage through a sand media. In FBR2, any unreacted nitrates are removed by adding a sugar-based electron donor (reactions 3 and 4). After the water is fed through FBR2, selenium is reduced to its elemental form (reaction 5).

$$4NO_{3-} + {}^5/_6\ C_6H_{12}O_6 = 7\ H_2O + 4HCO_3^- + 2\ N_2 + CO_2 \quad (3)$$

$$NO_3^- + {}^7/_6\ C_6H_{12}O_6 = 3\ H_2O + CO_2 + C_5H_7O_2N \quad (4)$$

$$SeO_4^{2-} + 0.5\ CO_2 + {}^1/_4\ C_6H_{12}O_6 = 0.5\ H_2O + 2HCO_3^- + Se^0 \quad (5)$$

When the water leaves FBR2 it enters a ballasted sand clarifier which removes biological solids, including selenium, from the effluent. The excess chemical oxygen demand (COD) is then removed by oxidation in the moving bed bioreactor (MBBR).

While the wastewater treatment has been proven effective in removing selenium from the water, it produced a solid state residual high in selenium and organic matter (Figure 2). This residual is currently being stored at industrial sites with a limited understanding of its properties and the risks associated with the remobilization of selenium from it.

Figure 1-2 Photos of two residual samples collected in the spring and summer of 2016.

1.3. Research Purpose and Objectives

The purpose of this research is to determine the selenium speciation within the solid state residual produced from biological wastewater treatment, and to advance the understanding of mobilization mechanisms for selenium within this residual

There are two main objectives that will be addressed in order to fulfill this purpose. The first objective is to characterize the occurrence of selenium in the solid state residual produced by the biological wastewater treatment, specifically the oxidation state(s) that is/are present. The second objective is to determine the mobility controls on selenium within the residual by conducting a suite of aqueous geochemical batch experiments. The batch experiments will address the question of whether the efficacy of the different remobilization pathways is dependent on the selenium speciation within the residual and whether that speciation is affected by the oxidation process. In particular, determining if preferential species mobilization occurs under different oxidation pathways when multiple species are present in the residual is undertaken. These two objectives in combination with one another will provide useful insight into the behavior of different selenium species with regards to their mobility in different redox and pH conditions.

1.4. Scope of Work

The following is a summary of the scope of work that was conducted throughout the duration of this research in order to accomplish the objectives set forth in section 1.3.

1. Objective 1: Solid State Characterization

    a. Bulk chemical analysis was performed by a third party laboratory to provide total elemental concentrations;

    b. Sequential extraction procedures were carried out to determine selenium speciation within the residual;

    c. X-ray Absorption Near Edge Structure (XANES) analysis was performed at the Canadian Light Source and the Advanced Photon Source to verify selenium speciation in the starting residual, samples following each fraction of the SEP and post-batch experiment samples to assess speciation change; and

    d. Linear combination fitting was used to analyze the XANES results in order to determine the relative amount of each selenium species present in the residual.

2. Objective 2: Mobility Mechanisms of Selenium

    a. Batch experiments were conducted on the residual samples and 4 selenium standards to determine under what pH and redox conditions the selenium in the residual was vulnerable to mobilization. Controls on the experiments were as follows:

        i. Varying redox state ranging from mildly to highly oxidizing using three different oxidants (O_2, NO_3^- and Fe^{3+}); and

        ii. Varying pH conditions including the natural state of the system once the oxidant was added and a controlled pH of 2.5.

    b. Aqueous characterization was performed on samples collected throughout the duration of the batch experiments including Ion Chromatography (IC), Inductively Coupled Plasma Mass Spectroscopy (ICP-MS) and Inductively Coupled Plasma Atomic Emission Spectroscopy (ICP-AES) to determine concentrations of selenium and other major elements; and

    c. Geochemical modelling was performed using Geochemist Workbench to identify trends within the chemistry data.

1.5. Thesis Outline

The following is a summary of the structure of this thesis. It should be noted that Chapters 3 and 4 were written in the format of journal articles and there may be redundancies in the methodology originally presented in Chapter 2.

1. Chapter 1 provides an introduction to the research topic including a summary of the reviewed literature, a background and description of the biological treatment process used to treat selenium containing wastewaters, the main research purpose and specific objectives along with the scope of work that was performed to achieve the objectives and lastly, this outline;

2. Chapter 2 includes the detailed methodology used to address each objective since the main research chapters are written in the form of publications and do not provide complete details;

3. Chapter 3 addresses Objective 1 by providing the results of the solid state characterization of the residual, including the comparison of sequential extraction procedures to XANES analysis;

4. Chapter 4 addresses Objective 2 by focusing on the results of the batch experiments and discusses the mobility mechanisms that were identified and the subsequent rate of the reactions; and

5. Chapter 5 provides a summary of the main conclusions from this research as well as recommendations for research going forward.

Chapter 2. Methodology

Three residual samples were collected from the filter press of a suspended growth biological treatment system for mine impacted waters over the summer of 2016 at 2 month intervals. The first of the three samples (RES 1) was collected from a pilot scale facility and the remaining two samples (RES 2 and RES 3) were collected from a full scale plant. In order to understand the mechanisms governing selenium (Se) mobility in the residual it is important to understand its chemical composition in terms of Se oxidation state and elemental associations. Bulk chemical characterization provides background information that can be used to identify elemental associations, potential mineral phases and subsequent Se speciation. This information can then be used to design the experiments and analyses to verify the chemical properties of the residual. Two methods were employed to characterize the solid phase of the residual with respect to Se speciation. Sequential extraction procedures (SEP) were developed to target the suspected Se species, and repeated to try and optimize the experiment in terms of solid to solution ratio and reaction rates. X-ray absorption Near Edge Spectroscopy (XANES) was then used to verify the efficiency of the SEP by analyzing solid phase samples following each extraction step and the original residual samples. To gain insight into the mobility mechanisms governing Se in the residual, a series of aqueous geochemical batch experiments were conducted under varying redox and pH conditions. Post-experiment solid phase samples were analyzed using XANES to determine if specific Se species were more vulnerable to mobilization under different redox and pH conditions. The understanding of solid phase speciation and mobility mechanisms of Se in the residual will help to quantify the risk is poses and to develop safe disposal methods.

2.1. Bulk Characterization

Residual samples were submitted to ALS Laboratories in Vancouver, British Columbia for analysis of 35 elements (Ag, Al, As, B, Ba, Be, Bi, Ca, Cd, Co, Cr, Cu, Fe, Ga, Hg, K, La, Mg, Mn, Mo, Na, Ni, P, Pb, S, Sb, Sc, Sr, Th, Ti, Tl, U, V, W, Zn) by aqua regia digestion and for selenium content by four acid digestion. Sulphur as SO_4 was determined using a carbonate leach analysis, and Sulphur as S_2 and organic content as Carbon by way of LECO combustion analysis. By having a bulk chemical

characterization of the residual, more detailed characterization methods were able to be further refined in order to optimize the characterization process. Figure 2.1 provides a photo of the residual sample.

Figure 2-1 Photograph of the residual from biological treatment of mine-impacted wastewater. Sample tray pictured is 10cm in length and evidence of iron oxidation can been seen on the edges.

2.2. Analytical Methods

Oxidation Reduction Potential (ORP), temperature and pH were monitored throughout batch experiments using a Thermo Orion 9678BNWO redox/ORP probe, a Thermo Orion 013005MD temperature probe and a Thermo Orion 9107BNMD pH probe, connected to a Thermo Orion 5 Star meter.

The composition of the aqueous samples was analyzed at the SFU Hydrogeochemistry Laboratory and SFU 4D Laboratories. Trace elements were measured using two methods of spectroscopy with Na, Ca, Mg, Fe, S and Si measured using a Horiba Jobin Yvon Ultima 2 Inductively Coupled Plasma Atomic Emission Spectrometer (ICP-AES) and 44 additional elements using a Thermofisher iCAP QC Inductively Coupled Plasma Mass Spectrometer (ICP-MS) (Li, Be, Al, Sc, Ti, V, Cr, Mn, Co, Ni, Cu, Zn Ga, As, Se, Rb, Sr, Zr, Ag, Cd, Sn, Sb, Cs, Ba, La, Ce, Pr, Nd, Sm, Eu, Gd, Tb, Dy, Ho, Er, Tm, Yb, Lu, Hg, Tl, Pb, Bi, Th and U). The ICP-AES has a measurement error of ±3% where the ICP-MS has an error of ±10%. Elements that had potential mass interferences with argon were measured using a kinetic energy

discrimination collision cell where ions collide and react with He gas to eliminate these interferences.

Major anions (Cl^-, NO_3^-, NO_2^-, SO_4^{2-}, Br^-, F^- and PO_4^{3-}) were measured using a Dionex ICS-3000 SP Ion Chromatography System (IC), which as an error of ±3%.

2.3. Sequential Extraction Procedures

Sequential extraction procedures (SEP) were carried out in order to determine the selenium species present in the residual and their relative abundances. The method used was based on a study by Wright et al. (2003), who compared two different methods of SEPs for selenium in soils and sediments. The method identified as most relevant based on their study was originally developed by Zhang & Moore (1996). It was then modified for this study by adding a step to target acid-volatile sulphide compounds, which was identified by Chao & Sanzolone (1989) to also remove metal selenides. The additional selenide step was included after the study by Lenz et al. (2008) that used X-ray Absorption Near Edge Structure (XANES) analysis to critically evaluate the accuracy of the SEP found that elemental selenium was overestimated due to the concurrent mobilization of metal selenide. In addition to the residual samples, the SEP was performed on select Se standards ($BaSeO_4$, SeS_2, Se^0, ZnSe and FeSe) to help understand how each species behaves throughout the experiment. Total Se was also measured at the end of select SEP experiments by way of aqua regia digestion to determine if any Se remained in the residual following the procedure. Table 2.1 provides a summary of the six steps used and the selenium species targeted by each step.

To limit microbial activity residual samples were stored in re-sealable plastic bags at 4°C until analysis. All reagents used were analytical grade and, due to the oxidation sensitivity of the residual, all solutions were prepared in 1L polyethylene bottles under an N_2 atmosphere and bubbled with N_2 gas for at least 10 minutes. All sample preparation and handling was conducted under a N_2 atmosphere to prevent oxidation of the residual. Six replicates of each sample were prepared in order to provide sufficient material to analyze the residual after each SEP step using XANES. The SEP was performed twice, using two different methods of sample preparation. In the first method, the residual was frozen with liquid nitrogen, crushed and weighed. With the intention of maximizing surface area available for reaction in the second method, the residual samples were

prepared by weighing at room temperature and then stirred into the solution to create slurry.

To begin, 6 grams of residual was placed in 6 separate 50 mL centrifuge tubes. After each step, the samples were centrifuged at 10 000 rpm for 10 minutes and the supernatant was decanted to a 50 mL test tube. Following this, the samples were diluted with 10 mL of DI water, stirred for 5 minutes and centrifuged a second time. The second supernatant was combined with the first in the 50 mL test tube. The supernatant was then filtered using a 0.45 µm syringe filter, diluted with a 2% nitric acid solution to reach a 1 in 10 dilution factor and stored at 4°C until analysis. Following each extraction step, the solid fraction of one replicate was set aside and preserved for solid state characterization.

Table 2-1 Summary of the reagents used and the targeted selenium species for each of the fractions in the sequential extraction procedure.

Fraction	Concentration	Reagent	Targeted Se species	Temp (°C)	Duration (mins)
F1	0.25 M	KCl	Selenate	21	120
F2	0.1 M	K_2HPO_4	Selenite	21	120
F3	4 M	HCl	Selenide	95	45
F4	0.25 M	Na_2SO_3	Elemental Se	21	240
F5	5%	NaOCl	Organoselenium	90	60
-	-	Aqua Regia	Remaining Se	21	24 hrs

Fraction 1. 0.25M KCl solution was added to each centrifuge tube at a 1 in 8 solid to solution ratio, stirred with a glass rod for 2 minutes, capped and transferred to the shaker bench at 300 rpm for 5 minutes before leaving at room temperature for 2 hours.

Fraction 2. 0.1M K_2HPO_4 solution was added to each centrifuge tube at a 1 in 8 solid to solution ratio, adjusted to a pH of 8 using 6M HCl and stirred with a glass rod for 2 minutes. Samples were then transferred to the shaker bench at 300 rpm for 5 minutes before leaving at room temperature for 2 hours.

Fraction 3. 4M HCl solution was added to each centrifuge tube at a 1 in 8 solid to solution ratio and transferred to the shaker bench at 300 rpm for 5 minutes. Samples were then placed in a hot water bath at 95°C for 45 minutes. Due to the presence of iron

sulphides in the residual, a large amount of volatilization of sulphur gas was observed after the addition of HCl. Because of this, stirring was not required and the 50 mL centrifuge tubes were capped immediately following the addition of the reagent.

Fraction 4. 0.25M Na_2SO_3 solution was added to each centrifuge tube at a 1 in 8 solid to solution ratio and adjusted to a pH of 7 using 6M HCl and stirred with a glass rod for 2 minutes. Samples were then transferred to the shaker bench at 300 rpm for 4 hours.

Fraction 5. 4% NaOCl solution was added to each centrifuge tube at a 1 in 20 solid to solution ratio, stirred with a glass rod for 2 minutes and placed in a hot water bath at 90°C for 1 hour. Zhang & Moore (1996) originally used a 1 in 4 solid to solution ratio for this step, but in a trial run of this method, insufficient mobilization of the organoselenium was observed. Subsequently, the solution to solid ratio was adjusted to increase the proportion of reactant.

Following the SEP, the supernatant was analyzed for selenium concentrations along with 41 additional elements (Li, Be, Al, Sc, Ti, V, Cr, Mn, Fe, Co, Ni, Cu, Zn, As, Rb, Sr, Zr, Ag, Cd, Sn, Sb, Cs, Ba, La, Ce, Pr, Sm, Eu, Gd, Tb, Dy, Ho, Er, Tm, Yb, Lu, Hg, Tl, Pb, Th and U) using Inductively Coupled Plasma Mass Spectroscopy (ICP-MS) in the 4D Laboratories at Simon Fraser University.

Following Fraction 5, for select experiments, the remaining solid was analyzed for total Se by digestion in aqua regia, which was prepared by mixing nitric and hydrochloric acids at a 1:3 ratio and left to digest for 24 hours. The supernatant from the digestion was then analyzed for Se concentrations along with 44 other elements using ICP-MS.

Following the analysis, mass balance calculations were conducted and it was determined that the original SEP was not successful in mobilizing the majority of Se present in the original 6g samples. To correct for this, the procedure was repeated using the same reagents but decreasing the solid to solution ratios. The purpose of this change in ratio was to ensure there was enough SEP reagent solution present to react with the total mass of Se and other reactive phases. Due to the low initial masses required to enable the appropriate solid to solution ratio and still be able to centrifuge

after each step (50 mL centrifuge tubes), there was insufficient residual left for solid phase analysis. Table 2.2 outlines the ratios used and the subsequent sample weights.

Table 2-2 Solid to solution ratios tested during SEPs and the corresponding solid and solution weights used.

Ratio	Solid Wt. (g)	Solution Wt. (g)
1:40	0.75	30
1:80	0.38	30
1:120	0.25	30
1:160	0.19	30
1:200	0.15	30
1:300	0.1	30

Following the increased ratio testing, mass balance calculations showed that the percentage of Se being mobilized did not change from the original SEP. Consequently, the SEP was performed again to determine if the mobilization of Se was kinetically controlled by increasing the amount of reaction time for select fractions. Since the original SEP indicated the majority of Se to be elemental, Fraction 4 was targeted. Research conducted by Jain et al. (2015) found that selenium in similar treatment residuals was in the form of nanoparticles entrapped within the biomass. In order to address this at the same time as the potential kinetic control, Fraction 4 was repeated following Fraction 5 within the same experiment. The purpose of this was to determine if elemental Se was liberated when the organic matter dissolves during Fraction 5. The kinetic SEP was performed using a 1:40 solid to solution ratio and details of the different time steps can be found in Table 2.3. Samples were set aside at the end of the experiment for solid phase analysis on the synchrotron. The remaining material after the modified SEP was applied was then digested in aqua regia to determine how much Se was left in the solid phase.

Table 2-3 Duration of each fraction performed during a modified SEP to determine the potential for a kinetic control on the mobility of Se from the residual.

Sample ID	Time (hours since start of experiment)							
	0-2	2-4	4-5	5-29	29-53	53-77	77-78	78-82
RES 24	F1	F2	F3	F4			F5	F4
RES 24 DUP	F1	F2	F3	F4			F5	F4
RES 48	F1	F2	F3		F4		F5	F4
RES 48 DUP	F1	F2	F3		F4		F5	F4
RES 72	F1	F2	F3		F4		F5	F4
RES 72 DUP	F1	F2	F3		F4		F5	F4

2.4. Batch Experiments

Geochemical batch experiments were conducted on the residual (RES) and 4 selenium standards (Na_2SeO_3, SeS_2, Se^0 and ZnSe) to evaluate selenium oxidation reaction mechanisms and rates. The RES and SeS_2 were conducted simultaneously for 64 and 46 days, respectively. The experiments for the remaining standards were conducted approximately 10 weeks later for a total of 25 days. Batches were sampled on a 2 or 3 day interval for the first 2 weeks and then approximately every 4 days for the remainder of the experiment.

Three oxidants (O_2, Fe^{3+} and NO_3^-) at different concentrations were used to simulate mildly oxidizing or highly oxidizing conditions at either the natural pH of the solution or at a controlled pH of 2.5. Table 2.4 provides a summary of the redox and pH conditions for each sample. Ferric iron and nitrate solutions were prepared in an N_2 atmosphere and then bubbled with N_2 gas for 10 minutes to ensure the intended oxidant was isolated in solution. For the oxygen experiments, DI water was used and the reaction vessel was either left open to the atmosphere to simulate highly oxidizing conditions or sealed to limit the oxygen available and simulate mildly oxidizing conditions. $FeCl_3$ was used to prepare 0.1 mmol (mildly oxidizing) and 10 mmol (highly oxidizing) iron solutions and $NaNO_3$ was used to prepare 1.0 mmol (mildly oxidizing) and 100 mmol (highly oxidizing) nitrate solutions. All reagents used were analytical grade. Following the first round of experiments, the highest selenium mobilization was observed under mildly oxidizing conditions, therefore only the lower concentration of the two oxidants was used for the elemental Se and ZnSe experiments.

Table 2-4 Summary of the samples subjected to batch experiments, the oxidant and concentration associated with each one and the corresponding pH of each batch reactor.

Sample	Oxidant	Concentration	pH
RES	O_2	Open to atm.	Natural
RES	O_2	Open to atm.	2.5
RES	O_2	Closed to atm.	Natural
RES	O_2	Closed to atm.	2.5
RES	$NaNO_3$	1.0 mmol	Natural
RES	$NaNO_3$	1.0 mmol	2.5
RES	$NaNO_3$	100 mmol	Natural
RES	$NaNO_3$	100 mmol	2.5
RES	$FeCl_3$	0.1 mmol	Natural
RES	$FeCl_3$	0.1 mmol	2.5
RES	$FeCl_3$	10 mmol	Natural
RES	$FeCl_3$	10 mmol	2.5
SeS_2	O_2	Open to atm.	Natural
SeS_2	O_2	Open to atm.	2.5
SeS_2	O_2	Closed to atm.	Natural
SeS_2	O_2	Closed to atm.	2.5
SeS_2	$NaNO_3$	1.0 mmol	Natural
SeS_2	$NaNO_3$	1.0 mmol	2.5
SeS_2	$NaNO_3$	100 mmol	Natural
SeS_2	$NaNO_3$	100 mmol	2.5
SeS_2	$FeCl_3$	0.1 mmol	Natural
SeS_2	$FeCl_3$	0.1 mmol	2.5
SeS_2	$FeCl_3$	10 mmol	Natural
SeS_2	$FeCl_3$	10 mmol	2.5
Na_2SeO_3	O_2	Closed to atm.	Natural
Na_2SeO_3	O_2	Closed to atm.	2.5
Na_2SeO_3	$NaNO_3$	1.0 mmol	Natural
Na_2SeO_3	$NaNO_3$	1.0 mmol	2.5
Na_2SeO_3	$FeCl_3$	0.1 mmol	Natural
Na_2SeO_3	$FeCl_3$	0.1 mmol	2.5
Se^0	O_2	Closed to atm.	Natural
Se^0	O_2	Closed to atm.	2.5
Se^0	$NaNO_3$	1.0 mmol	Natural
Se^0	$NaNO_3$	1.0 mmol	2.5
Se^0	$FeCl_3$	0.1 mmol	Natural
Se^0	$FeCl_3$	0.1 mmol	2.5
ZnSe	O_2	Closed to atm.	Natural
ZnSe	O_2	Closed to atm.	2.5
ZnSe	$NaNO_3$	1.0 mmol	Natural
ZnSe	$NaNO_3$	1.0 mmol	2.5
ZnSe	$FeCl_3$	0.1 mmol	Natural
ZnSe	$FeCl_3$	0.1 mmol	2.5

Abbreviations: 'Closed to atm.', closed to atmosphere; 'Open to atm.', open to atmosphere; 'RES', residual.

Residual samples were prepared by freezing with liquid nitrogen and grinding to a coarse powder. Each batch reactor was prepared using a 500mL polyethylene, re-sealable bottle. A photograph of the batch reactors can be seen in Figure 2.2. A 1:10 solid to solution ratio was prepared by adding 30g of sample to 300g of oxidizing solution. For the selenium standards, the weight used was calculated to equal the amount of selenium present in 30g of the residual and 300g of oxidizing solution was used to ensure the same selenium to solution ratio. The batch reactors were left at room temperature for the duration of the experiment and hand shaken after each sampling event.

Figure 2-2 Photograph of select batch reactors.

Apart from the oxygen batches, sampling was done in an N_2 atmosphere to prevent unintentional oxidation. Prior to each sampling event, the pH and the Oxidation-Reduction Potential (ORP) of the solution were measured and recorded. In the controlled pH experiments, HCl was added prior to sampling to adjust the pH to 2.5. The solution was then sampled using a syringe and a 0.45µm filter. Following this, three separate 1 mL aliquots of the supernatant were transferred to 15mL test tubes and diluted to a ratio of 1 in 10 with either 2% nitric acid for analysis of cations by ICP-MS and Inductively Coupled Plasma Atomic Emission Spectroscopy (ICP-AES) or DI water for analysis of anions by Ion Chromatography (IC). At the end of the experiments the solid-phase fraction was retained for selenium-species characterization using XANES.

2.5. X-ray Absorption Near Edge Structure

X-ray Absorption Near Edge Structure (XANES) analysis was performed at the Canadian Light Source (CLS) in Saskatoon, Saskatchewan and the Advanced Photon Source (APS) at the Argonne National Laboratory in Lemont, Illinois, to characterize the selenium speciation in the residual before and after the batch and SEP experiments. The first run was performed at the CLS and included the starting residual and the samples associated with the batch experiments. The second run was performed at the APS and included samples associated with the SEPs and replicate samples of the starting residual. A third run was performed at the APS for the purpose of measuring the red allotrope of elemental Se as a standard and samples from the additional SEP's that were performed to test ratio and kinetic influences on the Se mobility. Table 2.5 provides a summary of the samples analyzed at each light source and the associated experiments.

Table 2-5 Summary of the residual samples analyzed using XANES at the Canadian Light Source and the Advanced Photon Source and the corresponding experiments.

Light source	Sample name	Experiment description
CLS	RES 2_1	Starting residual sample
CLS	RES 2_2	Starting residual sample - duplicate
CLS	RES 2_3	Starting residual sample - duplicate
CLS	O2-O	O_2 oxidant - open to atmosphere
CLS	O2-O 2.5	O_2 oxidant - open to atmosphere with pH at 2.5
CLS	O2-C	O_2 oxidant - closed to atmosphere
CLS	O2-C 2.5	O_2 oxidant - closed to atmosphere with pH at 2.5
CLS	NO3 1.0	NO_3 oxidant using 1.0 mmol $NaNO_3$
CLS	NO3 1.0 2.5	NO_3 oxidant using 1.0 mmol $NaNO_3$ with pH at 2.5
CLS	NO3 100	NO_3 oxidant using 100 mmol $NaNO_3$
CLS	NO3 100 2.5	NO_3 oxidant using 100 mmol $NaNO_3$ with pH at 2.5
CLS	Fe 0.1	Fe oxidant using 0.1 mmol FeCl
CLS	Fe 0.1 2.5	Fe oxidant using 0.1 mmol FeCl with pH at 2.5
CLS	Fe 10	Fe oxidant using 10 mmol FeCl
CLS	Fe 10 2.5	Fe oxidant using 10 mmol FeCl with pH at 2.5
APS	RES 2	Starting residual sample
APS	RES 2_B	Starting residual sample - duplicate
APS	RES 3	Starting residual sample - duplicate
APS	F1	Residual following Fraction 1 of the SEP (targets selenate)
APS	F2	Residual following Fraction 2 of the SEP (targets selenite)
APS	F3	Residual following Fraction 3 of the SEP (targets selenides)
APS	F4	Residual following Fraction 4 of the SEP (targets elemental)
APS	F5	Residual following Fraction 5 of the SEP (targets organic)
APS	RES 24	Residual following the SEP with Fraction 4 running for 24 hrs
APS	RES 48	Residual following the SEP with Fraction 4 running for 48 hrs
APS	RES 72	Residual following the SEP with Fraction 4 running for 72 hrs

Abbreviations: 'APS', Advanced Photon Source (Chicago, Illinois); 'CLS', Canadian Light Source (Saskatoon, Saskatchewan); 'SEP', sequential extraction procedure.

In addition to the samples, a series of selenium standards were run for the purpose of linear combination fitting. This method fits the known spectra of the standards to the unknown composition of the residual in order to determine the relative amounts of each selenium species in the residual. While this method can identify the composition of an unknown sample accurately, it requires knowledge of the general composition of the

material to account for the major selenium species so that the appropriate standards are selected. Based on the bulk characterization performed, ten selenium standards were identified to be of interest and were run at both the CLS and the APS. Table 2.6 provides a summary of these standards.

Table 2-6 Summary of the selenium standards analyzed using XANES at the Canadian Light Source and the Advanced Photon Source and their association valence state.

Standard	Se species
Barium selenate	Se^{6+}
Sodium selenite	Se^{4+}
Elemental Se (grey)	Se^{0}
Elemental Se (red)*	Se^{0}
Selenium sulphide	Se**
Iron selenide	Se^{2-}
Zinc selenide	Se^{2-}
Copper selenide	Se^{2-}
Seleno-DL-cystine	Se^{2-} (organoSe)
Seleno-L-methionine	Se^{2-} (organoSe)
Seleno-cystamine	Se^{2-} (organoSe)

* Indicates the standard was analyzed at the APS only. ** The formal valence state of Se in SeS_2 varies.

In all cases, samples were shipped to the light source under chilled conditions and kept at that temperature until analysis to limit biological activity and subsequent sample oxidation. Samples were prepared using Teflon washers sealed in Kapton tape and the standards were prepared by grinding the sample to a fine powder and then spreading the sample on and sealing between layers of Kapton tape.

2.5.1. Se K-Edge Data Collection

Canadian Light Source

Bulk Se K-edge XANES spectra were collected on the Very Sensitive Elemental and Structural Probe Employing Radiation from a Synchrotron (VESPERS) 07B2-1 beamline at the Canadian Light Source. On this beamline, samples were positioned in front of the X-ray beam at an angle of 45°. XANES spectra of the samples were collected in fluorescence mode using a 4-element silicon drift Vortex detector. Spectra of the selenium standards were collected in both transmission and fluorescence mode. Spectra were collected from ~200 eV to ~250 eV above the Se K-edge absorption edge

(12658 eV) with a step size of 0.5 eV near the edge. The energy range was selected using a silicon (111) double crystal monochromator, which provided a monochromatic flux of ~10^{10} photons/sec. The focused beam size was set to 0.8mm wide and 0.8 mm tall. A selenium reference standard (grey elemental selenium) was run periodically between samples for beamline energy calibration. Ion chambers were filled with 100% N_2 gas. Samples were initially measured by performing 3 scans on 3 separate spots for a total of nine scans. Due to evidence of beam damage in some samples, a second run was performed with 1 scan at 9 separate spots, for a total of nine scans. Figure 2.3 provides a schematic representation of the experimental set up that was used for XANES analysis on the VESPERS beamline.

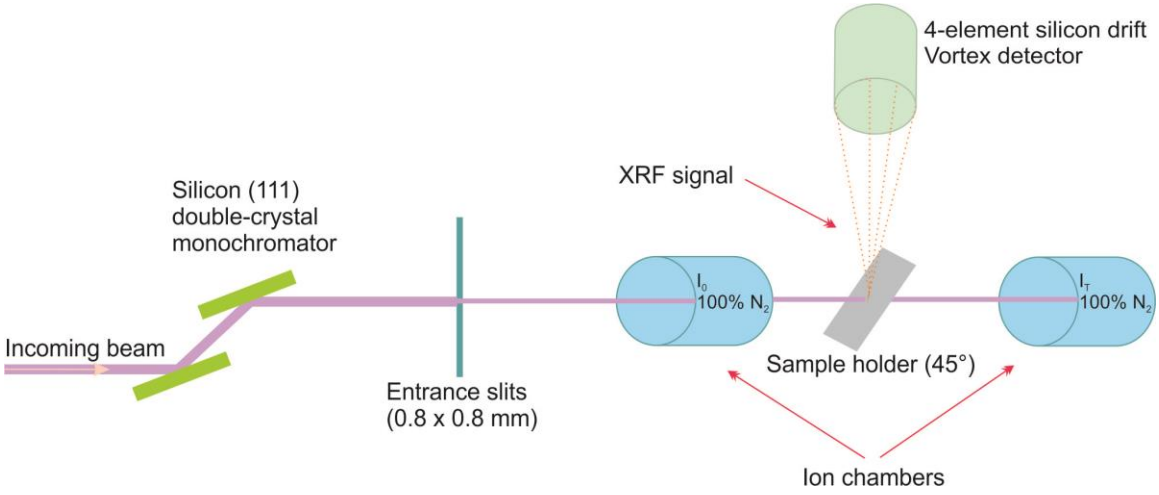

Figure 2-3 Schematic of the experimental set up used on the VESPERS beamline at the Canadian Light Source.

Advanced Photon Source

Bulk Se K-edge XANES spectra were collected for Se^0 (red) on 20-BM and for SeS_2 on 9BM bending magnet beamlines at the APS. Samples were positioned in front of the X-ray beam at an angle of 45°. XANES spectra of the samples were collected in both transmission and in fluorescence mode using a 12-element Ge solid state Canberra detector and a 4-element Vortex SDD detector on 20BM and 9BM, respectively. Spectra were collected from ~200 eV below the edge to ~250 eV above the Se K-edge absorption edge (12658 eV) with a step size of 0.5 eV through the edge region (-20/+30eV) itself. The energy range was selected using a silicon (111) double crystal monochromator which provided a monochromatic flux of ~10^{10} photons/sec. 20BM provided an unfocused beam which was set to 4.0x0.8mm where 9BM provided a

focused beam that was 0.25x0.25µm. A selenium reference standard was run concurrently in transmission with samples to monitor beamline energy calibration. Ion chambers were filled with N_2 gas at 1 atm on 20BM and 1/3 Ar gas with 2/3 N_2 gas at 1 atm on 9BM. On 9BM, the focused beam resulted in damage to the residual after multiple scans on the same location so nine scans were conducted on different locations. With the unfocused beam on 20BM, damage wasn't a concern and so three scans were run in fluorescence and transmission. Separate runs were merged in Athena (Ravel and Newville, 2005). Displayed spectra for residual samples were measured in fluorescence and in transmission for Se reference standards.Figure 3-1 provides a schematic representation of the experimental set up that was used for XANES analysis on the 9-BM for reference. Figure 2.4 provides a schematic representation of the experimental set up that was used for XANES analysis on 9BM.

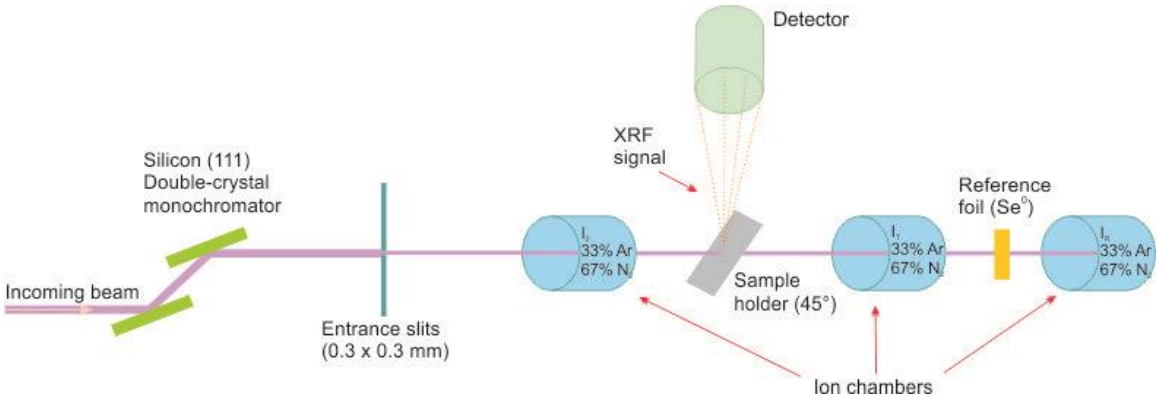

Figure 2-4 Schematic of the experimental set up used on 9-BM at the Advanced Photon Source. Set up was the same for 20BM but with 100% N2 gas in the ion chambers.

2.6. Data Analysis

ICP-MS data from the SEPs were brought into Microsoft Excel and analyzed for Se concentrations. Mass balance calculations were conducted to account for total Se in the starting residual sample and determine relative proportions of Se released during each fraction and the total Se recovery at the end of each experiment.

ICP-MS, ICP-AES and IC data from the batch experiments were combined and analyzed in The Geochemist's Workbench (Bethke, 2016). Specifically, GSS (Geochemist's Spreadsheet) and *Gtplot* were used to identify trends in Se and other elemental concentrations for the duration of the experiments.

XANES data were averaged and normalized and the background subtracted using standard procedures in the software program Athena (Ravel and Newville, 2005). Following visual inspection, linear combination fitting (LCF) was performed in an attempt to quantify the relative proportions of Se species in the samples. While this method provides a quantitative tool for data analysis, there are several limitations. If the unknown sample contains a species that was not included in the reference standards, the program is unable to accurately quantify relative proportions if that species is substantially different than the standards being used. Additionally, differences in the degree of crystalline order or particle size between reference standards and unknown sample will cause differences in spectra shape, particularly towards the end of the fit range in the extended region. In this case, the Se containing phases in the residual sample could be amorphous or nanoscale, while the reference standards are crystalline and highly ordered. The resulting differences in the extended region can be difficult for the LCF program to accurately fit, and is therefore used in combination with visual inspection.

Chapter 3. Solid Phase Characterization

3.1. Introduction

Selenium (Se) is an essential element for human, animal and vegetation health, however, an over- or under-abundance can cause adverse health effects and ecological problems. It is naturally occurring in a variety of different environments, however under appropriate conditions Se can become mobile, potentially affecting aquatic habitats and drinking water sources. Once Se enters the aquatic environment it can quickly reach high concentrations due to rapid bioaccumulation within food chains (Lemly, 2004). Selenium mobilization and introduction into aquatic systems at elevated levels can occur through anthropogenic activities such as mining and mineral processing, the extraction, processing and combustion of hydrocarbon fuels or intensive agriculture in regions with seleniferous soils (Plant et al., 2014). While the release of Se from industrial activities to natural waterways has been documented (Chapman et al., 2010; Muscatello et al., 2006), technology exists to treat Se impacted water. Suspended growth biological wastewater treatment systems are currently being used as a way to remove Se from contaminated waters (Lenz et al., 2008; Jain et al., 2015). This process produces a residual which is concentrated in Se and requires either disposal or tertiary treatment to reduce the potential risk it poses.

Selenium can occur in a variety of different oxidation states that are subject to oxidation-reduction processes and complex biogeochemical cycling (White and Dubrovsky, 1994). The mobility of Se is directly related to 1) the redox state, which controls the speciation in aqueous solution; 2) sorption properties of the coinciding solid state; and 3) the stability of Se minerals (White and Dubrovsky, 1994). Under natural conditions, selenium occurs in four main oxidation states: Se^{6+}, Se^{4+}, Se^{0}, Se^{2-} (White et al., 1991). The two highest oxidation states (Se^{6+} and Se^{4+}) form aqueous oxyanions known as selenate (SeO_4^{2-}) and selenite (SeO_3^{2-}), respectively (Maiers et al., 1988). In the elemental state, it can occur as crystalline and amorphous allotropes (Pejova and Grozdanov, 2001). Selenide, in the lowest oxidation state, can be present as aqueous species, as a solid bound with transition metals, or as gaseous hydrogen selenide (White and Dubrovsky, 1994). Selenium can also exist as (-II) valence state organic

compounds or as Se (0) within the cell walls of microbes (Weres et al., 1989; Jain et al., 2015).

Since the mobility and subsequent exposure pathway is directly related to the Se speciation, it is important to accurately determine the Se speciation in the solid phase to be able to identify the risks posed. This research aims to characterize the solid phase residual produced from biologically treated mine-impacted waters in bulk and in terms of the Se species present.

In this study, the solid phase of the residual was characterized using both Sequential extract procedures (SEPs) and X-ray Absorption Near Edge Structure (XANES) to determine which Se species were present. SEPs are a common tool for determining element speciation in soils and sediments. However, it is important to tailor the SEP to a specific material to ensure it is selective for the targeted species or fractions can be misinterpreted (Lenz et al., 2008). Modifications to the SEP used in this study were tested with the intention of finding a suitable SEP that is specifically adapted to Se in residuals from industrial water treatment. The XANES was additionally used to evaluate the accuracy of the SEP by analyzing Se speciation following each step of the SEP. Prior to these methods, bulk chemical characterization was done to provide adequate information to properly design the experiments and maximize the quality of the results. Once Se speciation is known, disposal methods can be sustainably developed to minimize the risk posed by the residual.

3.2. Methodology

3.2.1. Residual Samples

Residual samples were obtained from the filter press of a suspended growth biological treatment system for mine-impacted waters. Three separate samples were taken, the first of which was obtained from a pilot scale facility and was not used for the purpose of this study. Two samples (RES 2 and RES 3) were obtained from a full scale facility, 2 months apart in the summer of 2016. Samples were stored in re-sealable plastic bags and kept at 4°C to limit biological activity and subsequent oxidation. Prior to experimental work, subsamples were obtained from the center of the filter cake to ensure the samples had no prior contact with air. Bulk chemical characterization was

conducted on all three RES samples by ALS Laboratories in Vancouver, British Columbia for analysis of 35 elements (Ag, Al, As, B, Ba, Be, Bi, Ca, Cd, Co, Cr, Cu, Fe, Ga, Hg, K, La, Mg, Mn, Mo, Na, Ni, P, Pb, S, Sb, Sc, Sr, Th, Ti, Tl, U, V, W, Zn) by aqua regia digestion and for selenium content by four acid digestion followed by ICP-MS analysis. Sulphur as SO_4^{2} was measured using a sodium carbonate leach and gravimetric analysis, sulphur as S_2 and organic carbon concentrations were determined by combustion furnace infrared analysis.

3.2.2. Sequential Extraction Procedures

The SEP employed in this study was modified from published procedures and performed several times with modifications in order to optimize the procedure for residual samples. The initial method was based on a study by Wright et al. (2003), who compared two different methods of sequential extraction procedures for selenium in soils and sediments. The method identified as most relevant was originally developed by Zhang & Moore (1996). It was then modified by adding a step to remove metal selenide compounds (Chao & Sanzolone 1989). The additional selenide step was included based on the study done by Lenz et al. (2008) that used XANES to critically evaluate the accuracy of the SEP to show that elemental selenium was overestimated due to the concurrent mobilization of metal selenide. The modified SEP involved a five step procedure where each targets a different fraction, a summary of which can be found in Table 3-1. A final step was added where the remaining material after the modified SEP was digested using aqua regia and analyzed to determine the Se content.

Table 3-1 Summary of the reagents used and the targeted selenium species for each of the fractions in the SEP.

Fraction	Concentration	Reagent	Targeted Se species	Temp (°C)	Duration (mins)
F1	0.25 M	KCl	Selenate	21	120
F2	0.1 M	K_2HPO_4	Selenite	21	120
F3	4 M	HCl	Selenide	95	45
F4	0.25 M	Na_2SO_3	Elemental Se	21	240
F5	5%	NaOCl	Organoselenium	90	60
-	-	Aqua Regia	Remaining Se	21	24 hrs

Fraction 1. 0.25M KCl solution was added to each centrifuge tube at a 1 in 8 solid to solution ratio, stirred with a glass rod for 2 minutes, capped and transferred to the shaker bench at 300 rpm for 5 minutes before leaving at room temperature for 2 hours.

Fraction 2. 0.1M K_2HPO_4 solution was added to each centrifuge tube at a 1 in 8 solid to solution ratio, adjusted to a pH of 8 using 6M HCl and stirred with a glass rod for 2 minutes. Samples were then transferred to the shaker bench at 300 rpm for 5 minutes before leaving at room temperature for 2 hours.

Fraction 3. 4M HCl solution was added to each centrifuge tube at a 1 in 8 solid to solution ratio and transferred to the shaker bench at 300 rpm for 5 minutes. Samples were then placed in a hot water bath at 95°C for 45 minutes. Due to the presence of iron sulphides in the residual, a large amount of volatilization of sulphur gas was observed after the addition of HCl. Because of this, stirring was not required and the 50 mL centrifuge tubes were capped immediately following the addition of the reagent.

Fraction 4. 0.25M Na_2SO_3 solution was added to each centrifuge tube at a 1 in 8 solid to solution ratio and adjusted to a pH of 7 using 6M HCl and stirred with a glass rod for 2 minutes. Samples were then transferred to the shaker bench at 300 rpm for 4 hours.

Fraction 5. 4% NaOCl solution was added to each centrifuge tube at a 1 in 20 solid to solution ratio, stirred with a glass rod for 2 minutes and placed in a hot water bath at 90°C for 1 hour. Zhang & Moore (1996) originally used a 1 in 4 solid to solution ratio for this step, but in a trial run of this method, insufficient mobilization of the organoselenium was observed. Subsequently, the solution to solid ratio was adjusted to increase the proportion of reactant.

Following Fraction 5, the remaining solid was analyzed for total Se by digestion in aqua regia, which was prepared by mixing nitric and hydrochloric acids at a 1:3 ratio and left to digest for 24 hours. The supernatant from the digestion was then analyzed for Se concentrations along with 44 other elements using ICP-MS.

The SEP was performed a total of eleven times with the method outlined above using two different types of sample preparation. In the first type, the residual was frozen with liquid nitrogen, crushed, weighed and dispensed into the centrifuge tubes. In order

to maximize the surface area available for reaction, the experiment was replicated but the residual samples were prepared by weighing at room temperature and stirred into the initial SEP solution to create slurry. In both cases, six replicates of each sample were prepared by placing 6 grams of residual in separate 50 mL centrifuge tubes. Following each extraction step, the remaining solid fraction of one replicate was set aside and preserved for solid state characterization.

Following the initial SEPs, mass balance calculations were conducted and it was determined that the original SEP was not successful in mobilizing the majority of Se present in the original 6g samples. To address this, six additional modified SEPs were then performed using the same reagents but decreasing the solid to solution ratios and three additional procedures were run to investigate a rate control by increasing the amount of reaction time for select fractions. For each of the modified SEPs, samples were prepared using the slurry method, weighing at room temperature and stirring. The ratios tested and the subsequent sample weights can be found in Table 3-2. Samples from these ratio SEPs were not preserved for solid state analysis due to insufficient residual masses.

Table 3-2 Solid to solution ratios tested during SEPs and the corresponding solid and solution masses used.

Ratio	Solid Mass (g)	Solution Mass (g)
1:40	0.75	30
1:80	0.38	30
1:120	0.25	30
1:160	0.19	30
1:200	0.15	30
1:300	0.1	30

During the original SEPs, the majority of selenium liberated was during the elemental extraction step and so that fraction (F4) was targeted for dissolution rate control SEPs. In addition to dissolution rate controls, Jain et al. (2015) found that selenium in similar wastewater treatment residuals occurred as nanoparticles entrapped within the biomass and in order to address this, the Fraction 4 step was repeated after the Fraction 5 step within the same SEP. The purpose of this was to determine if elemental Se was liberated after the organic matter dissolved during Fraction 5. The rate control SEP was performed using a 1:40 solid to solution ratio and details of the different

time steps can be found in Table 3-3. The original modified SEP was conducted using RES 2 and the SEP with the modified solid-reagent ratio and rate control steps were performed using RES 3.

Table 3-3 Duration of each fraction performed during a modified SEP to determine the potential for a rate control on the mobility of Se from the residual. Samples were named in accordance with the number of hours F4 was performed.

Sample ID	Time (hours since start of experiment)							
	0-2	2-4	4-5	5-29	29-53	53-77	77-78	78-82
RES-24	F1	F2	F3	F4			F5	F4
RES-24 DUP	F1	F2	F3	F4			F5	F4
RES-48	F1	F2	F3		F4		F5	F4
RES-48 DUP	F1	F2	F3		F4		F5	F4
RES-72	F1	F2	F3		F4		F5	F4
RES-72 DUP	F1	F2	F3		F4		F5	F4

To limit microbial activity residual samples were stored in re-sealable plastic bags at 4°C until analysis. All reagents used were analytical grade and, due to the oxidation sensitivity of the residual, all solutions used were prepared in 1L polyethylene bottles under an N_2 atmosphere and bubbled with N_2 gas for at least 10 minutes. All sample preparation and handling was conducted under a N_2 atmosphere to prevent oxidation of the residual. After each step, the samples were centrifuged at 10 000 rpm for 10 minutes and the supernatant was decanted to a 50 mL test tube. Following this, the samples were diluted with 10 mL of DI water, stirred for 5 minutes and centrifuged a second time. The second supernatant was combined with the first in the 50 mL test tube. The supernatant was then filtered using a 0.45 µm syringe filter, diluted with a 2% nitric acid solution to reach a 1 in 10 dilution factor and stored at 4°C until analysis.

Following the SEP, the supernatant was analyzed for selenium concentrations along with 41 additional elements (Li, Be, Al, Sc, Ti, V, Cr, Mn, Fe, Co, Ni, Cu, Zn, As, Rb, Sr, Zr, Ag, Cd, Sn, Sb, Cs, Ba, La, Ce, Pr, Sm, Eu, Gd, Tb, Dy, Ho, Er, Tm, Yb, Lu, Hg, Tl, Pb, Th and U) using Inductively Coupled Plasma Mass Spectrometry in the 4D Laboratories at Simon Fraser University. Samples from the end of the rate controlled experiments were analyzed for total residual Se by aqua regia digestion and subsequent

aqueous phase analysis on the ICP-MS. Mass balance calculations were done to determine the percent of Se being mobilized during each step.

3.2.3. X-ray Absorption Near Edge Structure

X-ray Absorption Near Edge Structure (XANES) analysis was performed at the Advanced Photon Source (APS) in Chicago, Illinois to characterize the selenium speciation in the residual before the SEPs and after each extraction step. Two bending magnet beamlines were used at the APS for XANES analysis during two separate beamtime allocations. 9-BM was used for analysis of the starting residual sample, the residual samples following each fraction for the original SEP and ten Se standards. 20-BM was used to measure residual samples from the modified SEP performed to test for rate controls and an additional Se standard. Samples from the ratio tests were not analyzed due to insufficient sample weights. Table 3-4 provides a summary of the samples analyzed on each beamline and their associated experiments.

Table 3-4 Summary of the residual samples analyzed using XANES at the Advanced Photon Source (APS) and their corresponding experiment.

Beamline	Sample	Experiment description
9-BM	RES 2	Starting residual sample
9-BM	RES 2_B	Starting residual sample - duplicate
9-BM	RES 3	Starting residual sample
9-BM	F1	Residual following Fraction 1 of the SEP (targets selenate)
9-BM	F2	Residual following Fraction 2 of the SEP (targets selenite)
9-BM	F3	Residual following Fraction 3 of the SEP (targets selenides)
9-BM	F4	Residual following Fraction 4 of the SEP (targets elemental)
9-BM	F5	Residual following Fraction 5 of the SEP (targets organic)
20-BM	RES 24	Residual following the SEP with Fraction 4 running for 24 hrs
20-BM	RES 48	Residual following the SEP with Fraction 4 running for 48 hrs
20-BM	RES 72	Residual following the SEP with Fraction 4 running for 72 hrs

In addition to the samples, a series of selenium standards was run for the purpose of linear combination fitting (Table 3-5). This method fits the spectrum of the residual (of unknown composition) to varying proportions of the standards in order to determine the relative amounts of each selenium species in the residual. While this method can identify the composition of an unknown sample accurately, it requires some knowledge of the selenium species present so that the appropriate standards are selected. Based on bulk characterization performed, ten selenium standards, including

barium selenate (Se^{6+}), sodium selenite (Se^{4+}), selenium sulphide (formal valence varies) grey elemental selenium (Se^{0}), iron (II) selenide (Se^{2-}), zinc selenide (Se^{2-}), copper (II) selenide (Se^{2-}) and two organic Se compounds (Se^{2-}): seleno-DL-cystine and seleno-cystamine, were identified and used for comparison to the residual samples . Following the initial XANES analyses, the red allotrope of elemental Se was run at a later date on a different beamline (20-BM) at the APS. All Se standards were purchased commercially, with the exception of red Se^{0}, which was synthesized using the method outlined in Ebels et al. (2006).

Table 3-5 Summary of the Se standards analyzed using XANES at the Advanced Photon Source and their associated valence states. Standards were analyzed using 9-BM unless otherwise stated.

Standard	Se species
Barium selenate	Se^{6+}
Sodium selenite	Se^{4+}
Elemental Se (grey)	Se^{0}
Elemental Se (red)*	Se^{0}
Selenium sulphide	Se**
Iron selenide	Se^{2-}
Zinc selenide	Se^{2-}
Copper selenide	Se^{2-}
Seleno-DL-cystine	Se^{2-} (organoSe)
Seleno-L-methionine	Se^{2-} (organoSe)
Seleno-cystamine	Se^{2-} (organoSe)

* indicates the standard was run on 20-BM. ** the formal valence state of Se in SeS_2 varies.

The samples were shipped to the Canadian Light Source and stored under chilled conditions until analysis to limit biological activity and subsequent sample oxidation. In order to prevent oxidation, individual samples were prepared using Teflon washers sealed in Kapton tape. The Teflon washer was attached to one piece of Kapton tape and the residual was then packed in to the washer and leveled off to minimize air trapped within the sample. An additional piece of Kapton tape was then placed overtop to contain the residual, with the washer providing a seal. Teflon and Kapton were chosen as they are composed of materials that do not interfere with data collection during XANES measurements. Approximately 1g of residual was used for each Kapton tape sealed sample. Standards were prepared by grinding the sample to a fine powder and spreading uniformly onto one layer of Kapton tape and sealed with a second layer. Multiple layers of the prepared standards were used for transmission measurements.

Because the standards were dry powders, the washer was not required to contain the sample.

Se K-Edge Data Collection

Bulk Se K-edge XANES spectra were collected on two bending magnet beamlines (9-BM and 20-BM) at the Advanced Photon Source. Samples were positioned in the X-ray beam at an angle of 45°. XANES spectra of the samples were collected both in transmission and in fluorescence mode using a 12-element Ge solid state Canberra detector or a 4-element Vortex SDD on 20BM and 9BM, respectively. Spectra were collected from ~200eV below to ~250 eV above the Se K-edge absorption edge (12658 eV) with a step size of 0.5 eV near the edge (-20/+30eV). The adsorption edge (E_0) for Se is documented in literature and energy ranges are selected around the E_0 to ensure a large enough range of data is collected for analysis. The 'near edge' region begins at the onset of adsorption and generally extends 30-50eV above E_0. The features in the near edge region are used to identify oxidation state and coordination chemistry. The 'extended region' is the energy range above the near edge region and is generally used for identification of bond lengths and near neighbor identity. The energy range was selected using a silicon (111) double crystal monochromator which provided a monochromatic flux of ~10^{10} photons/sec. 20BM provided an unfocused beam which was set to 4.0x0.8mm where 9BM provided a focused beam that was 0.25x0.25μm. A selenium reference standard was run concurrently in transmission with samples to monitor beamline energy calibration. Ion chambers were filled with N_2 gas at 1 atm on 20BM and 1/3 Ar gas with 2/3 N_2 gas at 1 atm on 9BM. On 9BM, the focused beam resulted in damage to the residual after multiple scans on the same location so nine scans were conducted on different locations. With the unfocused beam on 20BM, damage wasn't a concern and so three scans were run in fluorescence and transmission. Displayed spectra for residual samples were measured in fluorescence and in transmission for Se reference standards.Figure 3-1 provides a schematic representation of the experimental set up that was used for XANES analysis on the 9-BM for reference.

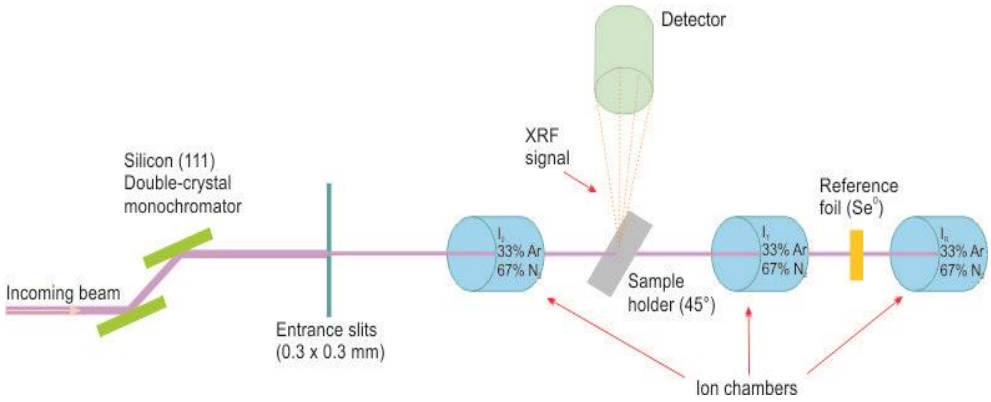

Figure 3-1 Schematic of the experimental set up used on 9-BM at the Advanced Photon Source. Set up was similar for 20BM but with 100% N2 gas in the ion chambers.

Data Analysis

XANES data were averaged and normalized and the background subtracted using standard procedures in the software program Athena (Ravel and Newville, 2005). Following visual inspection, linear combination fitting (LCF) was performed in an attempt to quantify the relative proportions of Se species in the samples. Linear combination fitting is a process where spectra of known standards are added in varying combinations to match or 'fit' the spectra of an unknown sample. In order to do this accurately, the data must be normalized and calibrated to ensure any instrument drift is accounted for and corrected so the data can be properly aligned. In some cases where the sample is very similar to a reference standard, small differences, such as the presence of a different ligand, will cause the spectra to be slightly offset from one another and alignment between the two samples will be slightly shifted. While this method provides a quantitative tool for data analysis, there are several limitations. As with most LCF methods, one of the most important factors is the selection of reference standards. The different selenium species have different energy signatures and if the unknown sample contains a species that was not included in the reference standards, the uncertainty in identifying and quantifying relative proportions may be impacted Additionally, differences in degree of crystalline order or particle size between reference standards and unknown sample can cause differences in spectra shape, particularly towards the end of the fit range in the extended region. In some cases, the sample or the selenium containing components therein could be amorphous or nanoscale, while the reference standards are crystalline and highly ordered. The resulting differences in the extended region can impose further uncertainty in the fits.

For this study, a series of Se combinations were fit to each unknown sample, based on visual inspection and bulk characterization. Weights were not forced between 0 and 1 or forced to sum to 1. Because of the close resemblance between the starting residual and FeSe, E_0 was allowed to float for FeSe during fitting, meaning E_0 could be re-calculated during the LCF process. This introduces the ability to fix any inconsistencies in energy alignment between FeSe and the residual, which likely contains a phase very closely related to FeSe, but with slight differences in charge or ligand presence. Consequently, the sum of the species proportions can reflect the presence of an unknown species that was not included in the standards, and may overestimate some components in an effort to achieve a best fit. Due to these limitations, several fits are provided in the results along with the reduced χ^2 value, with a lower χ^2 indicating a smaller difference between fit and data, nominally indicating better agreement. For each sample, reduced χ^2 values were considered acceptable if they were 2x the lowest χ^2 value achieved for that sample or less.

3.3. Results and Discussion

3.3.1. Bulk Chemical Characterization

Complete chemical results for RES 1, RES 2 and RES 3 can be found in Appendix A. RES 1 was collected from a pilot phase facility, was not used for any experimental work and will not be discussed in this section. RES 2 and RE3 showed slight differences in chemical composition, which may be due to temporal changes in the treatment process. Iron made up a large part of both RES 2 and RES 3 with concentrations of 268 000 mg/kg and 270 000 mg/kg, respectively. Sulphur in the form of sulphide was present with concentrations of 11 300 mg/kg in RES 2 and 13 900 mg/kg in RES 3. Selenium concentrations were similar between the two samples with 1260 mg/kg and 1400 mg/kg detected in RES 2 and RES 3, respectively. Calcium made up a notable portion of the residual with 20 300 mg/kg in RES 2 and 29 100 mg/kg in RES 3. Copper content was 59 mg/kg in RES 2 and 60 mg/kg in RES 3 where zinc concentrations were measured at 223 mg/kg and 532 mg/kg in RES 2 and RES 3, respectively.

Sequential Extraction Procedures

Relative proportions of Se species determined through the eleven SEPs are presented in Table 3-6. A complete summary of the aqueous chemistry following each extraction step for all eleven SEPs can be found in Appendix B. Letters A-K were assigned to each method in Table 3-6 for the purpose of discussion in this section. While SEPs were performed on five Se standards ($BaSeO_4$, SeS_2, Se^0, FeSe, ZnSe), problems were encountered during the procedure that compromised the quality of the results including gas production and expansion within the reactors during F3 of the FeSe and ZnSe samples. The gas production caused leakage from the sample vessel, loss of mass and subsequent introduction of water from the hot water bath into the reactors. While the production of gas indicates the reaction of Se in FeSe and ZnSe, the introduction of water into the experiment caused uncertainty with the results following this step and mechanisms of oxidation beyond F3 were not able to be attributed solely to the added reagents and ultimately selectivity could not be determined for these two standards. For the remaining standards, $BaSeO_4$ dissolved completely in the first step where Se^0 and SeS_2 showed mobility during F4 and to a lesser extent, F5. In the case of Se^0 and SeS_2, only 0.22% and 0.15% of the total Se available for reaction was mobilized during the entire SEP, respectively. Se^0 concentrations reached values approximately three times higher than SeS_2 after F4, suggesting that while the solubility of SeS_2 is lower, the Se is oxidized in the disproportionation reaction and mobilizes under similar conditions to Se^0.

From the initial SEP, the majority of mobilized Se was determined to be elemental with 69.5% and 90.9% of the total Se mobilized during Fraction 4 using methods A and B, respectively. Additionally, method A identified 3.2% as selenate, 2.1% as selenite, 12.9% Se occurring as selenide and 12.3% as organo-Se, where method B yielded 1.0% selenate, 6.4% selenite, 2.0% selenide and 5.4% organo-Se. After mass balance calculations, it was determined that only 2% of the total Se in the starting residual was detected in aqueous phase using method A and 5.8% using method B and therefore, the results cannot be considered representative of the sample..

Table 3-6 A comparison of relative proportions of targeted Se species for 11 different SEP methods, presented as a % of the total Se present in the starting residual sample. For the rate-control testing (24, 48, 72 hrs) F4 was repeated at the end of the experiment (F4-2).

		SEP Method	F1 Selenate	F2 Selenite	F3 Selenide	F4 Elemental Se	F5 Organo-Se	F4-2 Elemental Se	% of Total Se measured as aqueous
Sample Preparation	Freeze/ Crush	A	3.2%	2.1%	12.9%	69.5%	12.3%	-	2%
	Room Temp/Stir	B	1.0%	6.4%	2.0%	90.9%	5.4%	-	5.8%
Solid to Solution Ratio	**1:40**	**C**	**0.9%**	**0.7%**	**2.9%**	**92.2%**	**3.3%**	**-**	**24%**
	1:80	**D**	**1.0%**	**0.9%**	**2.7%**	**85.0%**	**10.4%**	**-**	**20%**
	1:120	**E**	**0.8%**	**1.2%**	**2.5%**	**77.4%**	**18.2%**	**-**	**24%**
	1:160	**F**	**0.8%**	**1.0%**	**2.3%**	**80.6%**	**15.3%**	**-**	**26%**
	1:200	**G**	**0.8%**	**1.0%**	**2.3%**	**73.6%**	**22.4%**	**-**	**27%**
	1:300	**H**	**0.7%**	**1.2%**	**2.3%**	**80.2%**	**15.5%**	**-**	**25%**
Duration of Fraction 4	**24 Hours**	**I**	**0.5%**	**0.7%**	**2.3%**	**86.6%**	**4.0%**	**5.9%**	**32%**
	48 Hours	**J**	**0.4%**	**0.7%**	**1.8%**	**88.8%**	**3.6%**	**4.7%**	**39%**
	72 Hours	**K**	**0.5%**	**0.9%**	**2.0%**	**89.5%**	**2.7%**	**4.5%**	**39%**

Note: bolded lines indicate experiments were done using RES 3, where non-bolded lines were performed using RES 2.

Methods C-H represent the different solid to solution ratios used for the SEP (Table 3-6). While increasing the solution available for reaction with the residual did increase the total Se mobilized during the SEP as compared to methods A and B, there was no significant difference between the ratios tested, which ranged from 1:40 to 1:300. The total Se mobilized ranged from 20-27% and did not increase concurrent with the ratio. Similar to methods A and B, the ratio test SEPs identified the majority of Se as elemental with proportions that ranged from 73.6-92.2%. The next largest fraction identified was organo-Se with 3.3% in method C and 10.4%, 18.2%, 15.3%, 22.4% and 15.5% in methods D, E, F, G and H, respectively. Selenide fractions ranged from 2.3-2.9%, selenite from 0.7-1.2% and selenate from 0.7-1.0% for methods C-H. While the majority of Se was liberated in the step intended to target elemental Se, this is only representative of the 20-27% of total Se that was mobilized during the SEPs and cannot be considered representative of the entire sample. As discussed earlier in Section 3.3.1., SeS_2 was also mobilized during F4, and may be included in the Se liberated during the fourth extraction step along with Se^0. Where an increase in solid to solution ratio from 1:8 in methods A and B to 1:40 in method C did increase total Se yield, further increases in reagent up to 1:300 did not have a significant effect on the amount of Se mobilized. Due to this, a 1:40 solid to solution ratio was used for the remaining SEPs.

Methods I, J and K in Table 3-6 represent the SEPs performed to test possible rate controls by performing Fraction 4 for 24, 48 and 72 hours, respectively. Method I mobilized 32% of the total Se while methods J and K both mobilized 39%. This is an increase from the ratio tests, suggesting kinetics may be a limiting factor in this experiment. It is unclear, however, if an additional time increase would mobilize more Se, as there was no difference between methods J and K regarding total Se. Relative proportions of each Se species were very consistent between methods I, J and K with the majority occurring as elemental (92.5-94%) followed by organo-Se (2.7-4.0%), selenide (1.8-2.3%), selenite (0.7-0.9%) and selenate (0.4-0.5%). A small portion (4.5-5.9%) of the total elemental Se was released when repeating the F4 step which suggests a fragment of the elemental Se may reside in the biomass and is not available for reaction until the organic material has been dissolved.

Of the eleven different SEP methods used, a maximum of 39% of the total Se was accounted for by aqueous Se. During F3, which targets selenides, however, visible volatilization was observed which smelled of H_2S gas. Since the selenides are likely

associated with sulphides, it can be inferred that a portion of the solid-phase Se was lost during the experiment as volatile H_2Se gas. In order to account for this lost fraction, total Se was measured in the remaining residual at the end of the rate-control SEPs and any Se that was unaccounted for was assumed to be lost as H_2Se and therefore present as selenide in the solid-phase. The aqua regia digestions that were conducted showed approximately 73% of total Se was mobilized during the optimized SEP, the rest persisted in solid phase for the duration of the SEPs. Figure 3-2 presents the relative proportions of Se species with the mass balance calculation built in. With H_2Se accounted for, the experiments indicate 22%, 35% and 35% of solid-phase Se occurred as selenide in samples RES-24, RES-48 and RES-72, respectively (Table 3-7). The new, corrected ratios of Se species in the solid-phase can be verified by the XANES results and are further discussed in the next section.

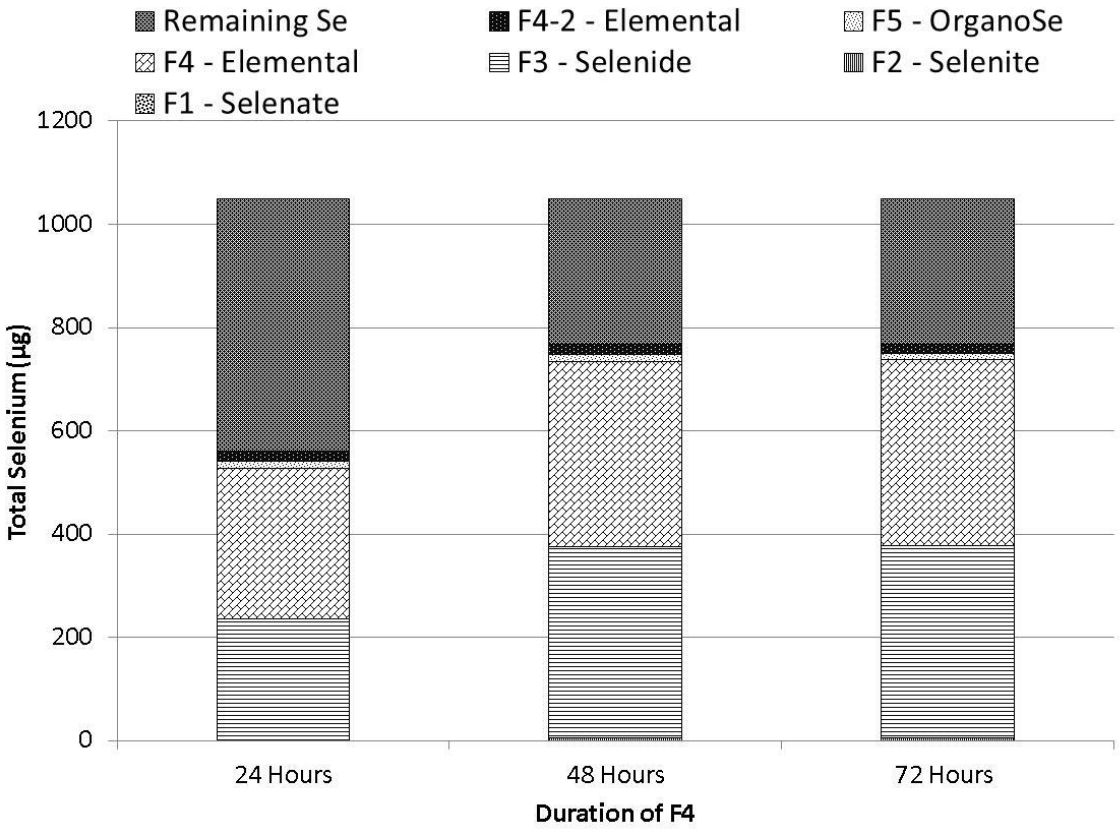

Figure 3-2 Relative proportions of total Se present in the residual samples used for the rate-control SEPs when assumed H_2Se loss is accounted for. Due to linear scale, low Se in F1 and F2 cannot be seen in the figure. The Se measured by aqua regia digestion at the end of the experiment is provided in grey and labelled 'remaining Se'.

Table 3-7 Relative proportions of Se species in the rate-control SEPs with H_2Se loss accounted for. 'Remaining Se' refers to the portion of Se measured at the end of the experiment through aqua regia digestion.

	Relative Proportion of Se Species		
	24 Hrs	**48 Hrs**	**72 Hrs**
F1- Selenate	0.15%	0.16%	0.19%
F2- Selenite	0.21%	0.27%	0.33%
F3- Selenide	22.10%	35.35%	35.37%
F4– Elemental	27.81%	34.17%	34.49%
F5- OrganoSe	1.30%	1.37%	1.05%
F4-2- Elemental	1.91%	1.80%	1.74%
Remaining Se	46.54%	26.88%	26.84%

X-ray Absorption Near Edge Spectroscopy

Se-K edge spectra for the reference standards are shown in Figure 3-3. The prominent peak in the near edge region is often referred to as a "white line" and is indicative of unoccupied Se p-states. E_0, or the 'edge', of a given species corresponds to the energy necessary to remove a core electron and is specific to each species of any element. The E_0 is determined by examining the first derivative of the spectrum. Generally, for a given ligand, higher energy white line or edge positions correspond to the higher oxidation state, with white line positions for SeO_4^{2-} just below 12668 eV, followed by SeO_3^{2-} at ~12665 eV. The white line position for SeS_2, and both allotropes of Se^0 occur near 12660 eV (SeS_2 ~ 0.4 eV higher). The metal selenide compounds possess two prominent features in the near edge region, with the initial peak for CuSe and FeSe occurring near 12660 eV, followed by a more prominent peak near 12666 and 12668 eV, respectively. The prominent peak for ZnSe occurs near 12664 eV and near 12661 eV for the organic compounds (Selenocystamine and Seleno-DL-cystine).

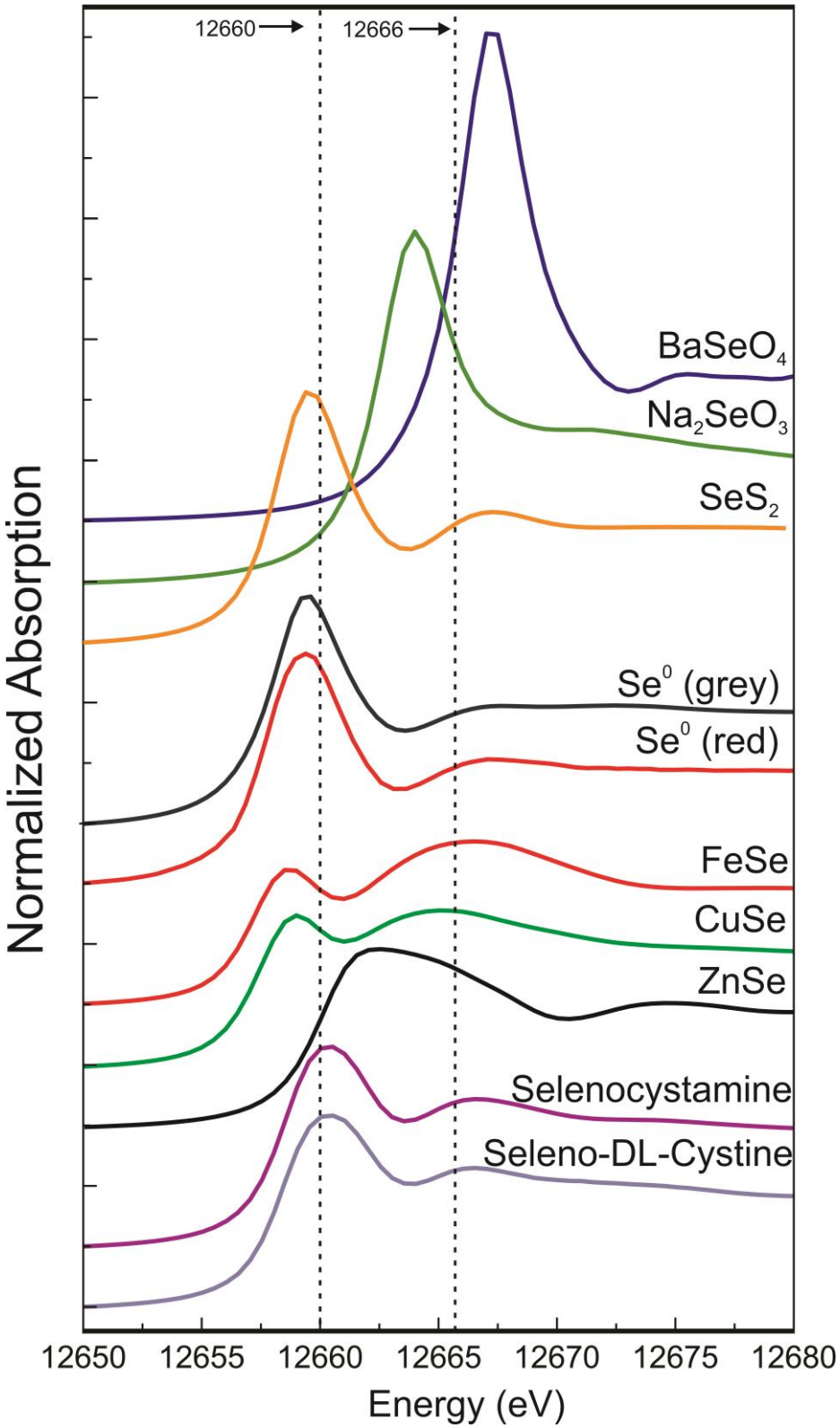

Figure 3-3 **Selenium K-edge spectra for all reference standards used, with reference lines at 12660 and 12666 eV.**

For the purpose of this study it is important to note the similarities in white line position and spectra shape between Se^0 (red) and SeS_2 (Figure 3-4). While this compound is presented as SeS_2, it is difficult to quantify in terms of stoichiometry and has been shown to have many isomers that vary in relative amounts of Se and S (Laitinen, 1987). It most commonly occurs as an 8-member ring molecule with varying Se-S ratios and bonding patterns and can be generally represented as Se_nS_{8-n} (Steudel and Laitinen, 1982). As it was commercially purchased as SeS_2, it will be referred to as this for the purpose of simplification in this document. While it has been suggested that SeS_2 incorporates Se in its elemental form (Hockin and Gadd, 2003; Vogel et al. 2018) the 0.4 eV shift observed between the spectra suggests slightly more energy is required to remove an electron from the Se incorporated in SeS_2 as compared to Se^0. The similarities between the K-edge spectra of Se^0 and SeS_2, make it difficult to distinguish between them, both visually and for the LCF software, when analyzing a multiphase sample (Figure 3-4). Because of this, LCF scenarios using either SeS_2 or Se^0 (red) are presented in Table 3-8 to emphasize the difficulties encountered when trying to fit an unknown multi-phase sample where one or both of these compounds is present. Figure 3-4 provides a comparison of SeS_2 and Se^0 (red) in white line position as well as the first derivative plots, the first peak of which corresponds to the E_0 of each species.

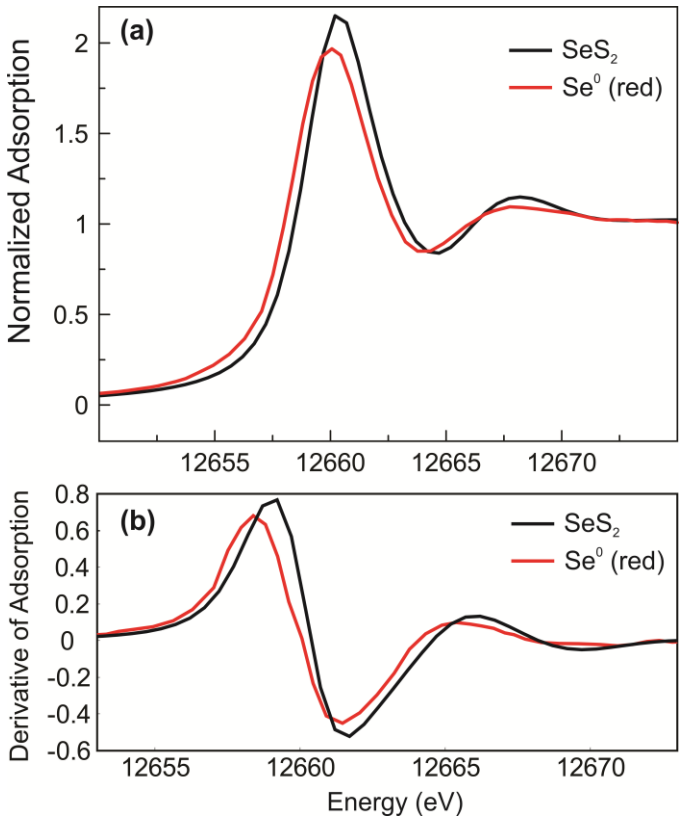

Figure 3-4 Comparing K-edge spectra for SeS_2 to Se^0 (red) (a) and the 1st derivative of adsorption for the same species in (b).

Se K-edge spectra obtained from two residual samples (RES 2 and RES 3) are displayed in Figure 3-5. While the spectra have shapes similar to FeSe and CuSe, the first feature falls at a slightly higher energy for RES 2 as compared to RES 3. LCF analysis indicates the majority phase in both samples is FeSe with 55-57% and 59-70% for RES 2 and RES 3, respectively. RES 3 has higher portions of both CuSe and ZnSe, where RES 2 has a higher proportion of Se^0 (grey) with 24-31% identified as the elemental species in all fit scenarios (Table 3-8). Higher ZnSe in RES 3 is consistent with bulk chemical characterization results which showed RES 3 to have approximately twice the amount of zinc as RES 2. E_0 values for FeSe were allowed to float up to 0.65eV for RES 2 and 0.80eV for the RES 3 fits. While both RES samples were taken from the filter press of the same treatment plant only months apart, the data suggests there is temporal variance in the composition of the residual. This is important to note, as the behavior of Se in the residual may not be consistent throughout the life of the treatment plant. After data collection and further literature review, the absence of $FeSe_2$ as a standard was considered a limiting factor in the accuracy of the LCF results. The white line position of $FeSe_2$ falls near 12660eV, which is the same energy range as Se^0

(grey and red) with similar features in the extended region (Kang et al., 2014). Additionally, the thermodynamic stability field for $FeSe_2$ is much larger than for FeSe and is likely a major component of RES 2 and RES 3 (Figure 1-1). Having $FeSe_2$ missing from the standards could be a factor in why the LCF process did not provide a perfect fit to the data. In addition, it is likely that the portion of the residual that the LCF results indicated to be Se^0 is $FeSe_2$ or a similar species such as $FeS_{2-n}Se_n$. Due to the uncertainties resulting from the absence of $FeSe_2$ from the standards, the term 'iron selenides' will be used to refer to both compounds henceforth in the discussion of this study.

In order to further investigate the relationship between RES 2 and RES 3, additional LCF scenarios were generated to try and determine the additional phase present in RES 2 that would cause its white line position to be slightly higher than RES 3. RES 2 was fit with RES 3 and suspected additional components, one at a time, to see which Se compound was responsible for the observed shift. Since $FeSe_2$ was not available, a scenario was generated where the E_0 for Se_0 (grey) was allowed to 'float'. Since the spectra for Se^0 and $FeSe_2$ are similar, but with slight differences in white line position, the floating Se^0 should serve as an approximation for $FeSe_2$ or a similar iron selenide species for the purpose of the additional LCF. RES 2 was fit with RES 3 in combination with SeS_2, Se^0 (grey), Se^0 (red), and the simulated $FeSe_2$, the results of which are provided in Figure 3-6. Of these scenarios, the best fit was obtained from the combination of RES 3 and Se^0 with the E_0 floating -0.16 eV, which is in the direction of Se^{1-} ($FeSe_2$) but not shifted as far as Se^{2-} (FeSe). This is a good indication that RES 2 is composed of the same Se species as RES 3 but with additional $FeSe_2$.

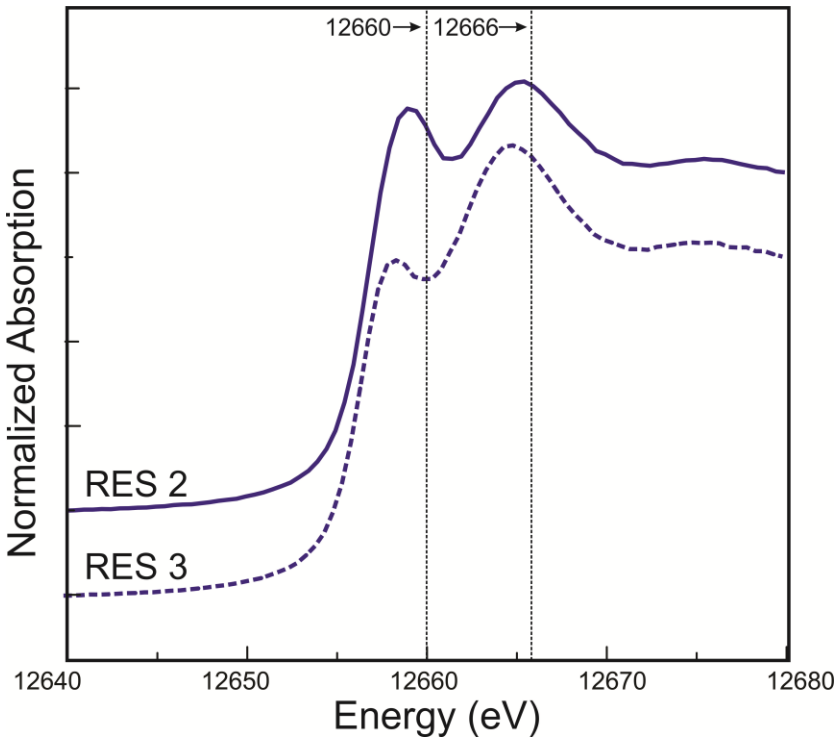

Figure 3-5 **Comparison of Se K-edge spectra for residual samples used in the sequential extraction procedures. RES 2 was used for methods A-B and RES 3 was used for methods C-K.**

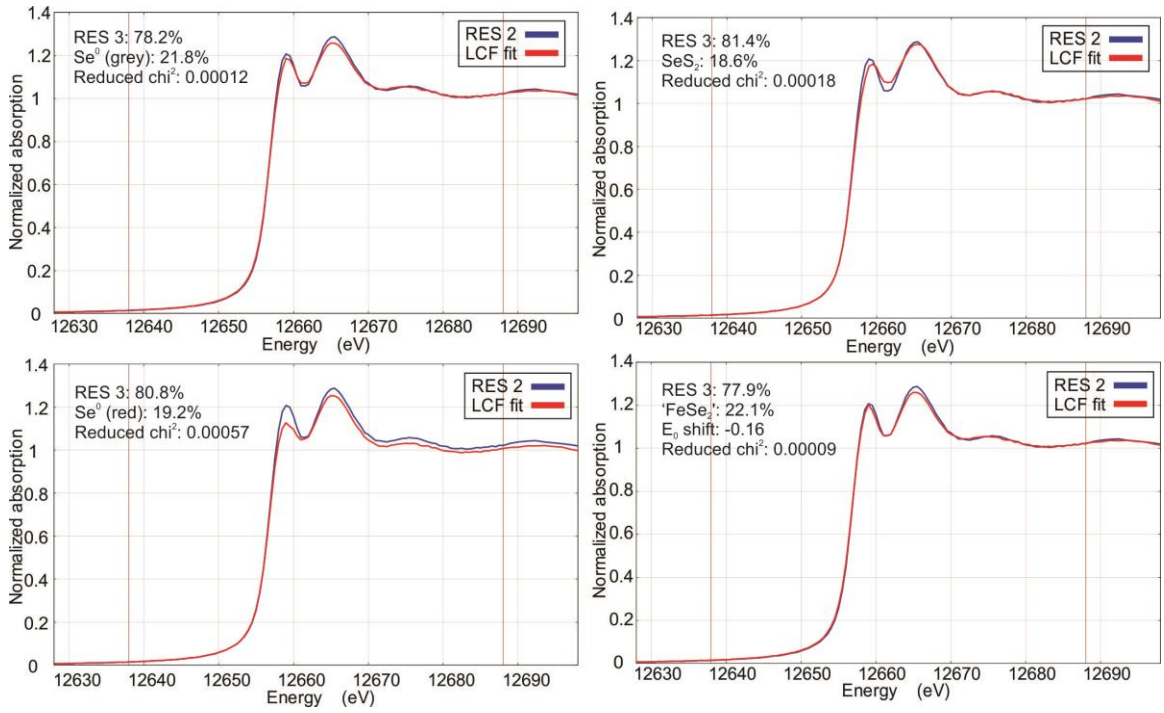

Figure 3-6 LCF scenarios generated for RES 2 by fitting RES 3 with the suspected additional Se phase. Lowest chi^2 value indicates the best fit.

LCF was performed for the starting residual samples (RES 2 and RES 3) as well as the first two fractions of the SEP (F1 and F2) to determine relative proportions of Se species in the mixed phase samples. The remaining samples associated with the SEPs, however, appear to be single phase and so visual inspection was solely relied on for analysis. In order to achieve best fits for F1 and F2, the E_0 for FeSe was allowed to float up to 0.52 eV and 0.53 eV, respectively. The Se K-edge spectra for the solid phase samples following each fraction of the SEP using method B are provided in Figure 3-7 along with RES 2 for comparison. While the spectra shape of F1 and F2 are closely related to RES 2, the white line has shifted to a slightly higher energy (~1 eV), suggesting a loss of a lower energy (reduced) Se species. Since F1 is meant to target selenate, and F2 selenite, this shift indicates an unintentional consequence. LCF results indicate three potential oxidation products, with Se (grey) showing an increase of up to 18% after F1 and 23% after F2 as compared to the starting residual sample (RES 2), Se^0 (red) increasing 41% after F1 and 46% after F2 with SeS_2 increasing 35% and 40% after F1 and F2, respectively. To investigate these further, additional LCF scenarios were generated using F1/F2 and the starting residual, in combination with each of the suspected oxidation products. While the SEP was performed on RES 2 in this case, fit

scenarios using both RES 2 and RES 3 are provided for reference and discussion. The best fit scenario was generated when F1 was composed of 67.2% RES 3 and 32.8% SeS_2 and when F2 was composed of 62.4% RES 3 and 37.6% SeS_2.While the fit scenarios using RES 2 did not yield as low of χ^2 values as RES 3, the best fit was still obtained when SeS_2 was used in combination with the starting residual for both F1 and F2. The results of each fit scenario for F1 can be seen in Figure 3-8 and in Figure 3-9 for F2. These results indicate that SeS_2 may have been produced during the first two extraction steps of the SEP. Hocking and Gadd, (2003) demonstrated the production of SeS_2 in a system with abundant reduced sulphur when selenite was added to solution. Given the high concentrations of sulphur in the residuals, and the mobilization of selenate and selenite during the first two extraction steps, it is possible for SeS_2 to be produced in this system.

In addition to the XANES results, chemical data was analyzed to provide further support and aqueous concentrations of Se, Fe, Cu and Zn following each of the extraction steps from the three rate-controlled SEPs are presented in Table 3-9. Elevated concentrations of Fe and Zn are present following F1 and F2 with Fe and Zn concentrations increasing by two orders of magnitude following F2. The elevated Fe concentrations suggest it is possible that a significant portion of an iron selenide compound was oxidized during at least F2 but only a minor amount in F1, producing a more oxidized Se compound and resulting in the observed shift in white line position relative to RES 3. These observations, in combination with the results of the LCF support the conclusion that the oxidized phase present in F1 and F2 was SeS_2. However, there was insufficient Fe mobilized to account for the apparent 20% decrease in the relative amount of iron selenide and it is questionable where the Zn came from that resulted in the 10% increase in ZnSe. Due to the limitations of the LCF method outlined previously, the results have an unspecified error associated with them and do not represent a completely quantitative method for defining relative proportions of Se species and therefore, should not be taken as absolute values. In addition, a mechanism of oxidation during F1 and F2 has not been identified and further studies will need to be undertaken to determine how this unexpected speciation change occurred.

Table 3-8 **Relative proportions of Se species as determined by linear combination fitting for the starting residual samples as well as samples following Fraction 1 and 2 using method B. Remaining samples associated with SEPs are single phase and are not included.**

Sample ID	Fit number	Reduced χ^2	$BaSeO_4$	$NaSeO_3$	SeS_2	Se^0 (red)	Se^0 (grey)	FeSe	CuSe	ZnSe	Organo-Se	Total
RES 2	1	0.00053		4.1			30.8	57.3		6.9		99.1
RES 2	2	0.00059					24.3	55.5	9.6	9.9		99.3
RES 3	1	0.00095		3.3			10.6	70.3		14.3		98.5
RES 3	2	0.00100						58.8	25.6	13.8		98.2
F1	1	0.00026		1.2			42.7	41.4		14.9		100.2
F1	2	0.00038		0.3		40.9		37		21.7		99.9
F1	3	0.00063		0.2	35.4			52		11.3		98.9
F2	1	0.00020		1.1			47.7	36.3		15.6		100.7
F2	2	0.00031		0.1		45.7		31.5		23		100.3
F2	3	0.00048		0.5	40.4			47.3		11		99.2

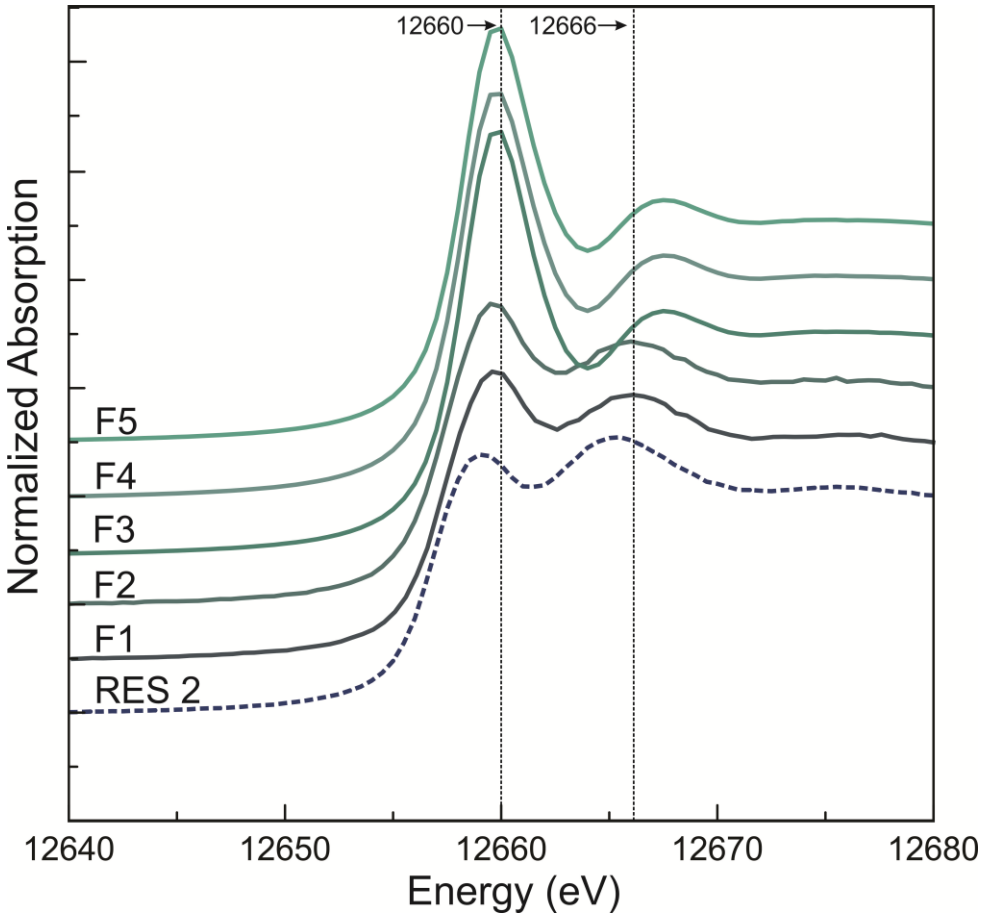

Figure 3-7 **Se K-edge spectra for samples following each fraction of the SEP using method B, compared to the starting residual sample. Energy lines are provided at 12660 and 12666 eV for reference.**

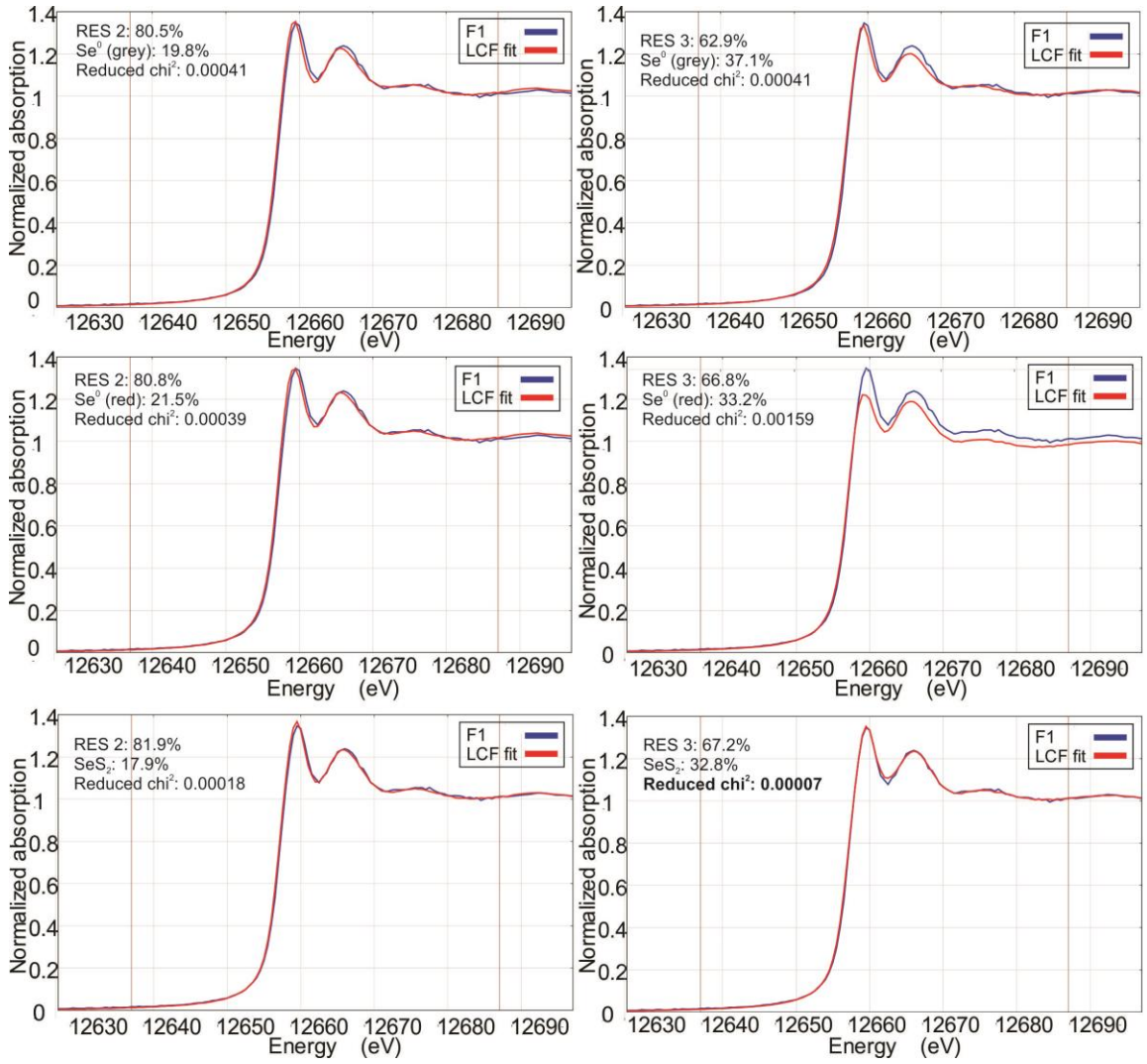

Figure 3-8 LCF scenarios fitting F1 with both starting residual samples and the suspected oxidized Se phase produced during F1. The lowest chi^2 value indicates the best fit and the resulting oxidized phase present after F1.

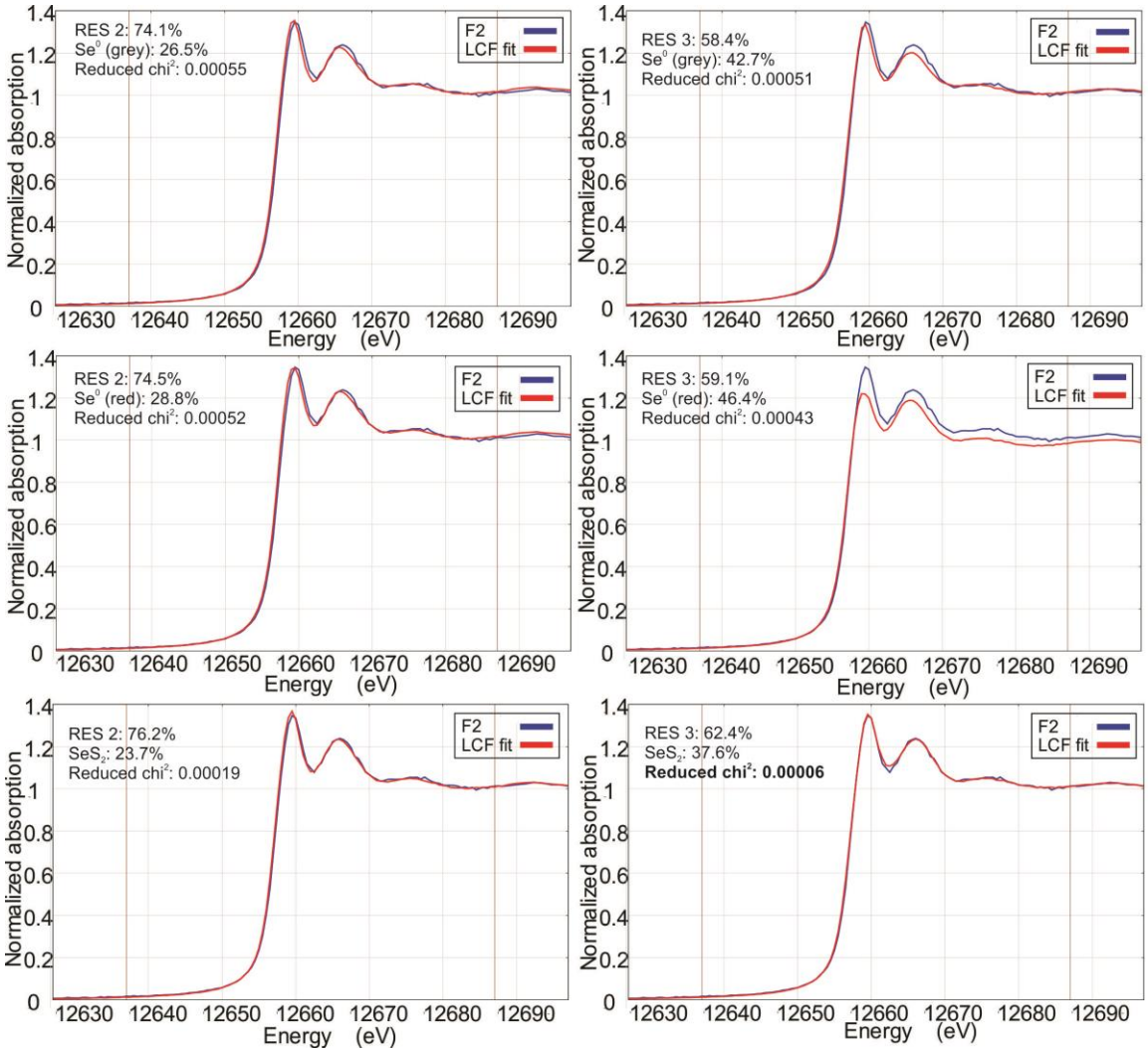

Figure 3-9 **LCF scenarios fitting F2 with both starting residual samples and the suspected oxidized Se phase produced during F2. The lowest chi^2 value indicates the best fit and the resulting oxidized phase present after F2.**

Table 3-9 Aqueous concentrations of Se, Fe, Cu and Zn following each extraction step of the rate-controlled SEPs.

Sample ID	Element	Units	F1 Selenate	F2 Selenite	F3 Selenide	F4 Elemental Se	F5 OrganoSe	F4-2 Elemental Se
RES-24 (Method I)	Se	ug/l	43.0	56.6	179	7.50E+03	330	498
	Fe	ug/l	225	1.01E+04	1.00E+06	5.85E+03	121	61.2
	Cu	ug/l	4.42	3.92	496	2.83	3.06	2.14
	Zn	ug/l	99.7	74.0	6.44E+03	113	8.00	36.5
RES-48 (Method J)	Se	ug/l	46.1	71.9	168	9.27E+03	347	467
	Fe	ug/l	238	1.00E+04	9.20E+05	2.95E+03	137	67.8
	Cu	ug/l	2.97	4.47	458	2.42	5.44	3.42
	Zn	ug/l	11.4	86.0	5.89E+03	61.0	2.60	33.5
RES-72 (Method K)	Se	ug/l	53.4	87.3	179	9.08E+03	276	451
	Fe	ug/l	255	1.10E+04	9.15E+05	2.83E+03	180	44.6
	Cu	ug/l	3.90	4.51	464	3.36	6.34	3.24
	Zn	ug/l	18.9	99.9	5.66E+03	82.8	1.31	33.7

XANES spectra for samples following F3, F4 and F5 of the original SEP bear a close resemblance to SeS_2 (Figure 3-10). Additionally, samples from the end of SEPs using method I (RES-24), J (RES-48) and K (RES-72) are plotted in Figure 3-14 and also compared to SeS_2 as well as Se^0 (red) for reference. While the shapes are very similar, the white line positions of all post-SEP samples are shifted to a slightly higher energy than Se^0 (red) and fall in line with SeS_2. As with the samples from the original SEP (F3, F4 and F5), the post-rate control SEP samples (RES-24, RES-48 and RES-72) are virtually identical to one another. Since SeS_2 was not identified in the starting sample, it can be inferred that it exists in the post-experiment samples as a by-product of Se reaction caused during at least step F3 of the SEP. The occurrence of SeS_2 is plausible after F3, where one of the products of acid volatile sulphide dissolution is H_2S. H_2S has been shown to be a source of reduced sulphur for the production of SeS_2, although a mechanism of Se oxidation would also be required (Fergusson et al., 1962; Rich, 2007).

In addition, a study done by Kang et al., (2014), investigated the interaction of naturally occurring arsenic rich pyrites with selenite over a range of pH and found that Se^0 (red) was the by-product of this reaction at lower pH (<6.10). As discussed earlier in Section 3.3.1, however, Se^0 (red) and SeS_2 have very similar XANES spectra with a shift

of approximately0.4 eV in white line position between them. Kang et al., (2014) noted a small shift between Se^0 (red) and their post experiment samples, but attributed it to data resolution, rather than the presence of a different Se compound. SeS_2 was not included in the reference standards and if it were, the interpretations may have been different. Our interpretation of the data presented in Kang et al., (2014) is that SeS_2 can be produced from the interaction of selenite with iron sulphide minerals at low pH, conditions which were present during F3. The production of SeS_2 during the SEP could be responsible for the ~27% of Se that failed to mobilize during the experiment, as it was not specifically targeted in the process and has been shown to be relatively insoluble.

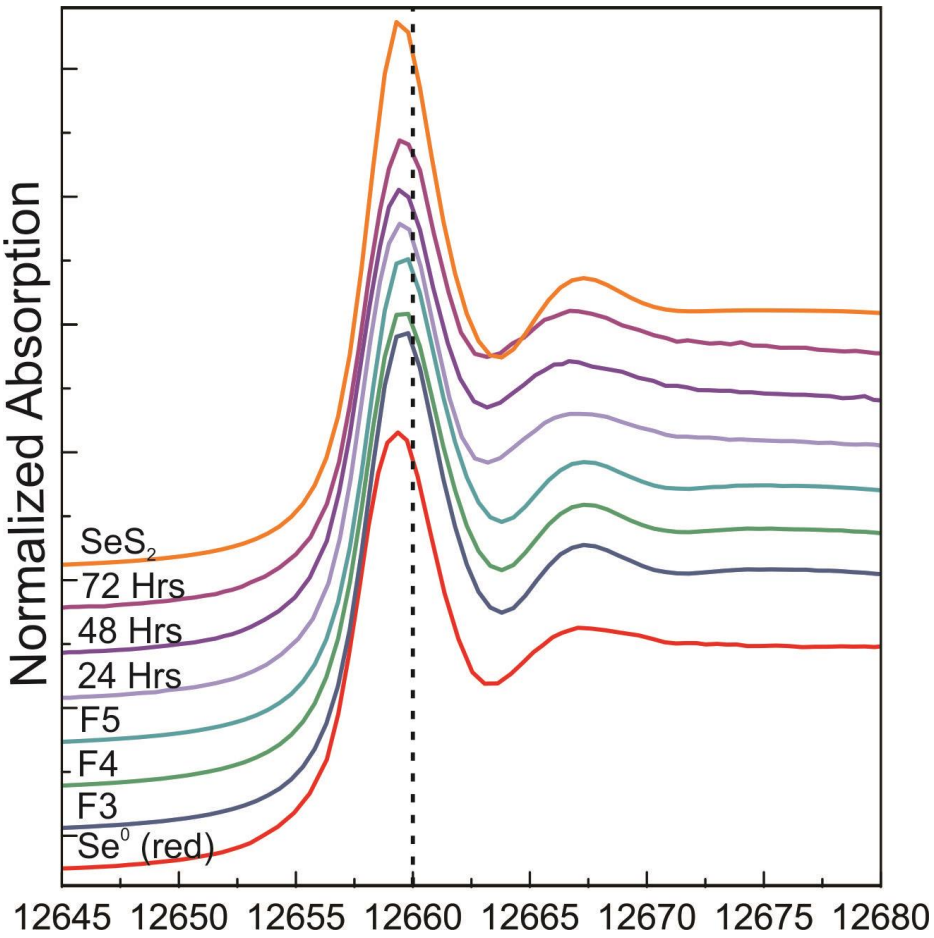

Figure 3-10 Se K-edge spectra for samples following Fractions 3, 4 and 5 using method B compared to Se^0 (red) and SeS_2.

Both solid to solution ratios and reaction rates were found to be factors that influence the mobilization of Se from the residuals, with an increase in either recovering significantly more Se in the step that targets zero valent Se. The optimal solid to solution ratio was determined to be 1:40 and Fraction 4 (elemental Se) required a duration of at

least 48 hours to maximize mobilization. Although 39% of the Se was accounted for in the aqueous phase when using the optimal methods, only 27% was found to persist throughout the experiment and remained in solid phase at the end of the experiments. The remaining Se was lost as H_2Se due to volatilization of metal selenides during Fraction 3. Using the solid-phase Se measured at the end of the rate-controlled experiments and the concentrations in aqueous phase after each extraction step, the calculated relative proportions of selenide are much lower than the portion of selenide as determined by the XANES analysis. Using the optimized SEP, it was determined that selenide and elemental Se each constituted 35% of Se in the residual with minor amounts of selenite, selenite and organoSe compounds (<2%) The limited results from the SEPs conducted on the Se standards also showed the affinity for mobilization of SeS_2 during the step that targets elemental Se, although overall solubility of SeS_2 was relatively low. Due to this, the portion presented as Se^0 could be overestimated and could actually incorporate SeS_2 as well. Additionally, ~27% of Se available for reaction was not mobilized during the experiment and persisted in solid phase. This persistent phase was identified by XANES to be SeS_2, and is likely the result of reactions during the SEP, since it was not identified in the original residual samples. SeS_2 would be particularly resistant to the SEP reagents, due to its insolubility and antimicrobial properties, which would increase its resistance to mobilization (Mitchell et al., 1992). Furthermore, due to the absence of $FeSe_2$ from the standards ambiguity exists with the identification of Se^0 in RES 2 and RES 3, as the XANES spectra of $FeSe_2$ is very similar and was not included. Therefore, while Se^0 may still be present, the relative proportions may have been overestimated by the XANES as well. Heterogeneities were also identified between different samples of the starting residual and through supporting LCF scenarios the difference is thought to be the presence of additional $FeSe_2$ in RES 2 as compared to RES 3.

Although there were some consistencies between the SEPs and XANES, the SEP was found to change the speciation of Se during the procedure through the oxidation of iron and zinc selenides to SeS_2, making it difficult to target specific species accurately. While this was observed in the XANES results and supported by the aqueous chemistry, the mechanism whereby this amount of oxidation would occur in the first two extraction steps is unknown. Additional experiments need to be conducted to

identify this mechanism, as the information regarding the behavior of SeS_2 is relatively limited, especially in residuals.

While SEPs are generally applied to an element of interest across a broad spectrum of soils and sediments, the results of this study emphasize the importance of tailoring a SEP for each specific material. Synthetic residuals may be of particular interest, due to their unique chemical and physical properties. While more rigorous methods of sample characterization are recommended prior to developing an SEP to identify features such as particle size and elemental associations, it is also important to consider oxidation sensitivity, as this was shown to be an unintentional consequence of the first three extraction steps and has the potential to significantly impact the results of an SEP.

Chapter 4.
Investigating Mobility Mechanisms of Se using Batch Experiments and XANES

4.1. Introduction

Selenium (Se) has recently become a contaminant of concern in many parts of the world, including North America, due to its toxicity and propensity to bioaccumulate within food chains (Lemly, 2004). While Se is essential for all lifeforms, it has a very narrow concentration range before causing adverse ecological and health effects. Se in high concentrations can be fatal and even in lower doses has the potential to negatively affect human health and reproduction in fish, birds, amphibians and reptiles (Chapman et al., 2010). For example, larval deformities in Northern Pike were described by Muscatello et al. (2006) because of exposure to Se in mining effluent from a uranium operation in Saskatchewan, Canada. While Se occurs naturally at elevated concentrations in sediments, soils and rocks, it can become mobile under the right chemical conditions, whether naturally or anthropogenically induced. Industrial activities such as mining, agriculture and nuclear-power generation have all demonstrated the potential to mobilize Se into natural water systems (Chapman et al., 2010). Suspended growth biological wastewater treatment systems are currently in use in the mining industry to prevent the release of Se to the environment by removing Se from contaminated wastewater (Lenz et al., 2008; Jain et al., 2015). The by-product of this treatment is a sludge-residual that has Se concentrations as high as 4000mg/kg and requires disposal or tertiary treatment to minimize the risk associated with it.

Se can occur in a variety of different oxidation states that are subject to oxidation-reduction processes and complex biogeochemical cycling (White and Dubrovsky, 1994). The four main Se oxidation states found under natural conditions are Se^{6+}, Se^{4+}, Se^{0} and Se^{2-}. The two highest oxidation states (Se^{6+} and Se^{4+}) form the oxyanions selenate (SeO_4^{2-}) and selenite (SeO_3^{2}-), respectively, which can occur as aqueous species or in solid compounds (Maiers et al., 1988). Se can also exist as crystalline and amorphous allotropes in the elemental state (Se^{0}) (Pejova and Grozdanov, 2001). In addition to elemental Se, zero valent Se has been found to incorporate into SeS_2, which exists generally as an 8-member ring molecule with varying

proportions of Se and S and multiple bonding structures (Vogel et al. 2018). The reduced Se, selenide (Se^{2-}), can be present as aqueous species, as a solid bound with transition metals, or as gaseous forms of hydrogen selenide (White and Dubrovsky, 1994). Se mobility is directly related to 1) the redox state, which controls the speciation in aqueous solution; 2) the sorption properties of the coinciding solid state; and 3) the stability of Se minerals (White and Dubrovsky, 1994). The redox conditions, however, have been demonstrated to be the main control on Se solubility, mobilization and sequestration (Shwartz et al., 2016). While the processes can be microbially facilitated, thermodynamic data indicate that selenide (Se^{2-}) and elemental Se (Se^{0}) should be dominant in reducing environments whereas selenite (SeO_3^{2-}) is dominant in mildly reducing environments to slightly oxidizing, and selenate (SeO_4^{2-}) in oxidizing environments (Jayaweera and Biggar, 1996; White et al., 1991). This study evaluates the redox behavior of Se in the residual produced by biologically treating mine-impacted waters with regards to these thermodynamic data. A series of aqueous geochemical batch experiments were conducted to address the mobility mechanisms of Se in the residual, and, along with solid-phase Se speciation, addresses the question of whether the efficacy of the different remobilization pathways is dependent on selenium speciation within the residual and whether that speciation is affected by the oxidation process. In particular, the occurrence of preferential species mobilization under different oxidation pathways when multiple species are present in the residual was investigated.

4.2. Materials and Methodology

4.2.1. Residual Samples

Residual samples were obtained from the filter press of a suspended growth biological treatment system for mine-impacted waters. Samples were stored in re-sealable plastic bags and kept at 4°C to limit biological activity and subsequent oxidation. Prior to experimental work, subsamples were obtained from the center of the filter cake to ensure the samples had no prior contact with oxygen.

4.2.2. Batch Experiments

Geochemical batch experiments were conducted on the residual (RES) and four Se standards (Na_2SeO_3, SeS_2, Se^{0} and ZnSe) to evaluate Se oxidation reaction

mechanisms and rates. The RES and SeS_2 experiments were conducted simultaneously for 64 and 46 days, respectively. The experiments for the remaining standards were conducted approximately 10 weeks later for a total of 25 days. Batches were sampled on a 2 or 3 day interval for the first 2 weeks and then approximately every 4 days for the remainder of the experiments.

Three oxidants (O_2, Fe^{3+} and NO_3^-) at different concentrations were used to simulate mildly oxidizing or highly oxidizing conditions. For each of the redox conditions, the pH was either left unbuffered at the natural pH of the solution or controlled with HCl at pH 2.5. For the oxygen experiments, de-ionized water was used and either left open to the atmosphere to simulate highly oxidizing conditions or sealed to limit the oxygen available (~170mL of headspace) and simulate mildly oxidizing conditions. Ferric iron and nitrate solutions were prepared in an N_2 atmosphere and then bubbled with N_2 gas for 10 minutes to ensure the intended oxidant was isolated in solution. $FeCl_3$ was used to prepare 0.1 mmol (mildly oxidizing) and 10 mmol (highly oxidizing) iron solutions, and $NaNO_3$ was used to prepare 1.0 mmol (mildly oxidizing) and 100 mmol (highly oxidizing) nitrate solutions. All reagents used were analytical grade. Following the first round of experiments, the highest Se mobilization was observed under mildly oxidizing conditions; therefore, only the lower concentration of the two oxidants was used for each of the remaining Na_2SeO_3, Se^0 and ZnSe experiments.

Residual samples were prepared by freezing with liquid nitrogen and grinding to a coarse powder. Each batch reactor was prepared using a 500 mL re-sealable polyethylene bottle. A 1:10 solid:solution ratio was prepared by adding 30 g of sample to 300 g of oxidizing solution. For the Se standards, the weight used was calculated to equal the mass of Se present in 30 g of the residual, and 300 g of oxidizing solution was used to ensure the same Se:solution ratio. The batch reactors were left at room temperature for the duration of the experiment.

Apart from the oxygen batches, sampling was done in an N_2 atmosphere to prevent unintentional oxidation. Prior to each sampling event, the pH and the oxidation-reduction potential (ORP) of the solution were measured and recorded. In the controlled pH experiments, HCl was added prior to sampling to adjust the pH to 2.5. The solution was then sampled using a syringe and a 0.45 µm filter. Following this, three separate 1 mL aliquots of the supernatant were transferred to 15 mL test tubes and diluted to a

ratio of 1 in 10 with either 2% nitric acid for analysis of cations by inductively coupled plasma–atomic emission spectrometry (ICP-AES) and ICP-MS, or de-ionized water for analysis of anions by ion chromatography. The aqueous samples were analyzed at the SFU Hydrogeochemistry Laboratory and SFU 4D Laboratories. Trace elements were measured using two methods with Na, Ca, Mg, Fe, S and Si measured using a Horiba Jobin Yvon Ultima 2 ICP-AES and 44 additional elements using a Thermo Fisher iCAP QC ICP-MS (Li, Be, Al, Sc, Ti, V, Cr, Mn, Co, Ni, Cu, Zn Ga, As, Se, Rb, Sr, Zr, Ag, Cd, Sn, Sb, Cs, Ba, La, Ce, Pr, Nd, Sm, Eu, Gd, Tb, Dy, Ho, Er, Tm, Yb, Lu, Hg, Tl, Pb, Bi, Th and U). The ICP-AES has a measurement error of ±3% where the ICP-MS has an error of ±10%. Elements that had potential mass interferences with argon were measured using a collision cell where ions collide and react with He gas to eliminate these interferences. Major anions (Cl^-, NO_3^-, NO_2^-, SO_4^{2-}, Br^-, F^- and PO_4^{3-}) were measured using a Dionex ICS-3000 SP IC, which as an error of ±3%. After each sampling event the reactors were vigorously stirred to ensure no concentration gradients within the vessels occurred. At the end of the experiments, the solid-phase fraction was retained for Se-species characterization.

4.2.3. X-ray Absorption Near Edge Structure

X-ray Absorption Near Edge Structure (XANES) measurements were performed at the Canadian Light Source (CLS) in Saskatoon, Saskatchewan and at the Advanced Photon Source (APS) at the Argonne National Laboratory in Lemont, Illinois to characterize the selenium speciation in the residual before and after the batch experiments. The first run was performed at the CLS and included the starting residual and the samples associated with the batch experiments. Additional runs were performed at the APS for the purpose of measuring additional Se standards that were identified as missing after the first round of data collection. Table 4.1 provides a summary of the samples analyzed at each light source and their associated experiments.

Table 4-1 Summary of the residual samples analyzed using XANES and the corresponding experiments.

Light Source	Sample Name	Experiment description
CLS	RES 2_1	Starting residual sample
CLS	RES 2_2	Starting residual sample - duplicate
CLS	RES 2_3	Starting residual sample - duplicate
CLS	O2-O	O_2 oxidant - open to atmosphere
CLS	O2-O 2.5	O_2 oxidant - open to atmosphere with pH at 2.5
CLS	O2-C	O_2 oxidant - closed to atmosphere
CLS	O2-C 2.5	O_2 oxidant - closed to atmosphere with pH at 2.5
CLS	NO3 1.0	NO_3 oxidant using 1.0 mmol $NaNO_3$
CLS	NO3 1.0 2.5	NO_3 oxidant using 1.0 mmol $NaNO_3$ with pH at 2.5
CLS	NO3 100	NO_3 oxidant using 100 mmol $NaNO_3$
CLS	NO3 100 2.5	NO_3 oxidant using 100 mmol $NaNO_3$ with pH at 2.5
CLS	Fe 0.1	Fe oxidant using 0.1 mmol FeCl
CLS	Fe 0.1 2.5	Fe oxidant using 0.1 mmol FeCl with pH at 2.5
CLS	Fe 10	Fe oxidant using 10 mmol FeCl
CLS	Fe 10 2.5	Fe oxidant using 10 mmol FeCl with pH at 2.5

In addition to the samples, a series of Se standards were run for comparison to identify Se species present in the residual samples. Based on the bulk characterization performed, ten selenium standards were identified to be of interest and were run at the CLS, including: barium selenate (Se^{6+}), sodium selenite (Se^{4+}), grey elemental selenium (Se^0), iron selenide (Se^{2-}), zinc selenide (Se^{2-}), copper selenide (Se^{2-}) and three organic Se compounds (Se^{2-}): seleno-DL-cystine, seleno-L-methionine and seleno-cystamine. Following the first round of XANES experiments, the red allotrope of elemental Se and SeS_2 (valence state varies) were run at a later date at the APS. All Se standards were purchased commercially, with the exception of red Se^0, which was synthesized using the method outlined in Ebels et al. (2006).

In all cases, samples were shipped to the light source under chilled conditions and kept refrigerated until analysis to limit biological activity and sample oxidation. Samples were prepared using Teflon washers sealed in Kapton tape and the standards were prepared by grinding the sample to a fine powder and then spreading the standard on and sealing between layers of Kapton tape.

XANES data were averaged and normalized and the background subtracted using standard procedures in the software program Athena (Ravel and Newville, 2005). Linear combination fitting (LCF) was attempted to quantify the relative proportions of Se species in the samples. While this method provides a quantitative tool for data analysis, there are several limitations. If the unknown sample contains a species that was not included in the reference standards, the program is unable to accurately quantify relative proportions if that species is substantially different than the standards being used. Additionally, differences in degree of crystalline order or particle size between reference standards and unknown sample will cause differences in spectra shape, particularly towards the end of the fit range in the extended region. In this study, the residual sample could contain amorphous or nanoscale components, while the reference standards are crystalline and highly ordered. The resulting differences in the extended region can be difficult for the LCF program to accurately fit. Because of the differing physical properties between the reference standards and residual samples, attempts at LCF were unsuccessful and a qualitative approach by means of visual inspection was used instead. The visual inspection compares peaks and features in the unknown residual samples to those of the standards in order to identify the main components.

4.2.4. Se K-Edge Data Collection

Canadian Light Source

Bulk Se K-edge XANES spectra were collected on the Very Sensitive Elemental and Structural Probe Employing Radiation from a Synchrotron (VESPERS) 07B2-1 beamline at the Canadian Light Source. Samples were positioned in front of the X-ray beam at an angle of 45°. XANES spectra of the samples were collected in fluorescence mode using a 4-element silicon drift Vortex detector. Spectra of the selenium standards were collected in both transmission and fluorescence mode. Spectra were collected from ~200 eV below the edge to ~250 eV above the Se K-edge absorption edge (12658 eV) with a step size of 0.5 eV through the edge region (-20/+30 eV) itself. The energy range was selected using a silicon (111) double crystal monochromator, which provided a flux of ~10^{10} photons/sec. The focused beam intermediate slit size was set to 0.8 mm wide and 0.8 mm tall. A selenium reference standard (grey elemental selenium) was run periodically between samples for beamline energy calibration. Ion chambers were filled with 100% N_2 gas (1 atm). Samples were initially measured by performing 3 scans on 3

separate spots for a total of nine scans. Due to evidence of beam damage in some samples, a second run was performed on an undamaged region with 1 scan at 9 separate spots, for a total of nine scans.

Advanced Photon Source

Bulk Se K-edge XANES spectra were collected for Se^0 (red) on 20-BM and for SeS_2 on 9BM, both bending magnet beamlines at the APS. Samples were positioned in front of the X-ray beam at an angle of 45°. XANES spectra of the samples were collected in both transmission and in fluorescence mode using a 12-element Ge solid state Canberra detector and a 4-element Vortex SDD detector on 20BM and 9BM, respectively. Spectra were collected from ~200 eV below the edge to ~250 eV above the Se K-edge absorption edge (12658 eV) with a step size of 0.5 eV through the edge region (-20/+30 eV) itself. The energy range was selected using a silicon (111) double crystal monochromator which provided a monochromatic flux of ~10^{10} photons/sec. The focused beam size was set to 0.25 x 0.25 µm. A selenium reference standard was run concurrently in transmission with samples to monitor beamline energy calibration. Ion chambers were filled with N_2 gas at 1 atm on 20BM and 1/3 Ar gas with 2/3 N_2 gas at 1 atm on 9BM. On 9BM, nine scans were run on different spots to account for possible beam damage in both fluorescence and transmission. On 20BM, three scans were run on the same spot, as beam damage was not a concern. All scans were imported and merged in Athena (Ravel and Newville, 2005). Displayed spectra for residual samples were measured in fluorescence, with transmission data used for Se reference standards.

4.3. Results and Discussion

4.3.1. Mobility Mechanisms

A complete summary of the aqueous chemistry from the batch experiments along with concurrent pH and ORP measurements can be found in Appendix C and D, respectively. Figure 4-1 provides Se concentrations for the duration of each batch experiment using O_2, NO_3^- and Fe^{3+} as oxidants. The highest Se concentrations were observed in the mildly oxidizing-unbuffered pH experiments for all three oxidants. In this scenario, Se reached maximum concentrations of 310, 392 and 331 µg/L in the O_2, NO_3^- and Fe^{3+} experiments, respectively (Figure 4-1). Maximum concentrations were reached

after 16 days in the O_2 and NO_3^- experiments and 18 days in the Fe^{3+}experiment, followed by a steady decline until 31 days when Se concentrations stabilized under 150 µg/L in the NO_3^- experiment and under 100µg/L in the O_2 and Fe^{3+} experiments. Given that the total Se present in each batch available for reaction was 37800 µg, the maximum concentrations reached only represent 0.25%, 0.31% and 0.26% in the O_2, NO_3^- and Fe^{3+} experiments, respectively, which is a very small portion of the total Se. The highly oxidizing scenarios reached peak Se concentrations of 169, 236 and 140 µg/L for the O_2, NO_3^- and Fe^{3+} experiments, respectively, at the same time steps as the mildly oxidizing scenarios (Figure 4-1). Low pH seemed to inhibit the mobility of Se, with the concentrations staying in the range of 34 to 141 µg/L for the O_2 experiments, 61 to 177 µg/L for NO_3^- and 15 to 139 µg/L for Fe^{3+}. While the highest mobility would be expected under the most oxidizing conditions, the batch experiments show that the simulated mildly oxidizing conditions were most efficient in mobilizing Se. The trend observed with the peak in Se concentrations at 16-18 days, followed by the steady decline could be due to the oxidant being consumed, followed by the subsequent reduction of the aqueous Se, or from the aqueous Se adsorbing onto the surface of the residual. Since the anion data shows steady concentrations of NO_3^- for the duration of the experiment, it is unlikely that the oxidant was fully consumed in this time frame (Figures 4-2, 4-3, 4-4). It is possible, however, that reduced species, such as iron, in the residual are reacting with selenate/selenite and removing it from aqueous phase by forming Se^0. Additionally, aqueous Se, which would be dominated by selenite (SeO_3^{2-}) under mildly oxidizing conditions, may also be adsorbing onto the surface of the residual causing it to be undetectable in solution.

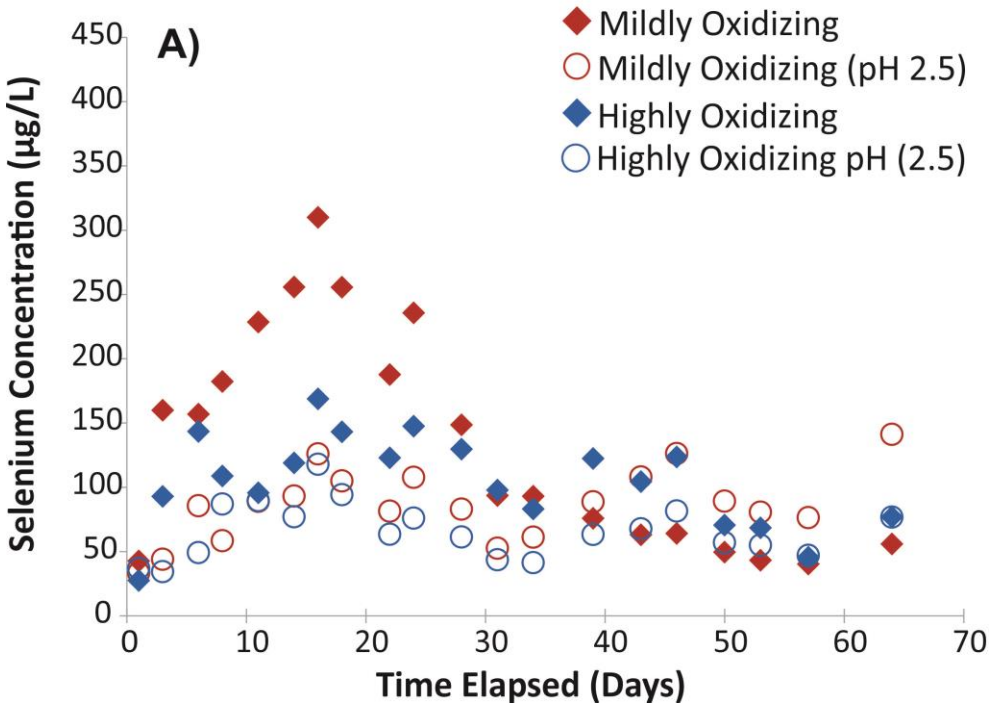
A)
Mildly Oxidizing
Mildly Oxidizing (pH 2.5)
Highly Oxidizing
Highly Oxidizing pH (2.5)
Selenium Concentration (µg/L)
Time Elapsed (Days)
0
50
100
150
200
250
300
350
400
450
0
10
20
30
40
50
60
70

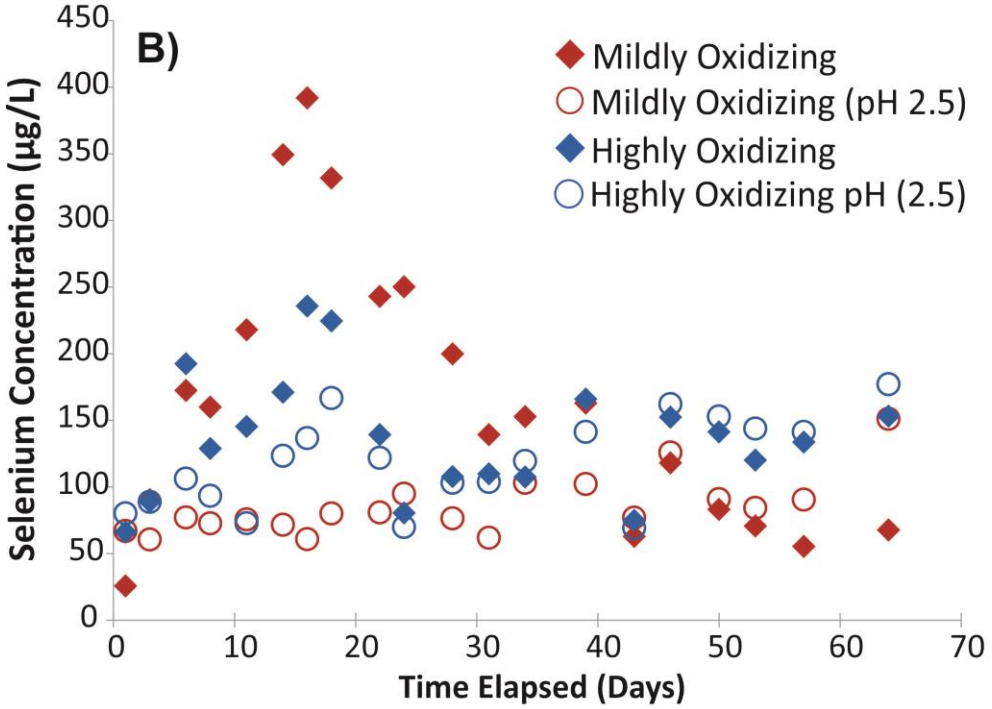
B)
Mildly Oxidizing
Mildly Oxidizing (pH 2.5)
Highly Oxidizing
Highly Oxidizing pH (2.5)
Selenium Concentration (µg/L)
Time Elapsed (Days)
0
50
100
150
200
250
300
350
400
450
0
10
20
30
40
50
60
70

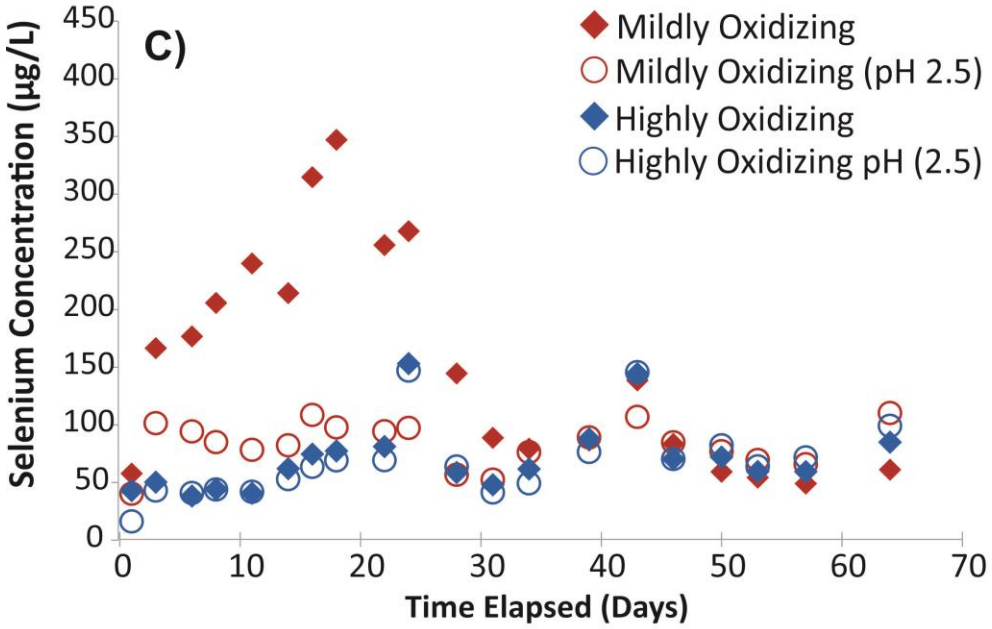

Figure 4-1 Selenium concentrations for the duration of the batch experiments. O_2 (A), NO_3- (B) and Fe^{3+} (C) experiments with mildly oxidizing conditions represented by red markers and highly oxidizing by blue. Low pH (2.5) represented by open circles.

In the O_2 experiments, NO_3^-, Cl^- and SO_4^{2-} concentrations consistently increase under low pH conditions, regardless of ORP, reaching maximum concentrations of 113, 6921 and 385 mg/L, respectively (Figure 4-2). The increase in Cl^- is consistent with the addition of HCl^- to control pH, where NO_3^- and SO_4^{2-} concentrations suggest oxidation of organic material is taking place with the subsequent release of associated reduced nitrogen and sulphur species followed by their further oxidation in solution. SO_4^{2-} concentrations may also be due to the oxidation of monosulphides by O_2, NO_3^- and Fe^{3+}. Any Fe^{2+} released during the oxidation of FeS would further oxidize to Fe^{3+} in solution, providing an additional source of oxidant. Under the unbuffered pH conditions, however, little evidence of sulphur oxidation is observed, indicating a potential pH control on SO_4^{2-} occurrence, potentially due to the instability of Fe^{3+} at higher pH. O_2 has the greatest effect on PO_4^{3-} concentrations, with the unbuffered pH experiments reaching maximum concentrations of 21 mg/L and at low pH, 11 mg/L (Figure 4-2). The PO_4^{3-} in solution could be due to oxidation of phosphorous incorporated in organic matter or desorption from the surface of the residual. The mildly oxidizing conditions in the NO_3^- and Fe^{3+} experiments reached PO_4^{3-} concentrations as high as 17 and 24 mg/L, respectively, with virtually no PO_4^{3-} in the highly oxidizing scenarios (Figure 4-3 and 4-4).

In the NO_3^- experiments SO_4^{2-} reached maximum concentrations of 300 mg/L in the low pH scenarios and 169mg/L under highly oxidizing-unbuffered pH conditions. Negligible SO_4^{2-} was detected under mildly oxidizing-unbuffered pH conditions, which indicates the occurrence of sulphur and Se may not be analogous, since that environment proved to be conducive to Se mobility (Figure 4-3). Similar to the O_2 experiments, Cl^- levels increase in the low pH scenarios reaching maximum concentrations of 8475 mg/L, due to the addition of HCl^- throughout the experiment to control pH. NO_3^- concentrations are controlled by the $NaNO_3^-$ used as an oxidant and remain relatively constant for the duration of the experiments, suggesting extensive consumption of the oxidant did not occur. However, due to the upper calibration limits of the IC, there is an error associated with the higher NO_3^- values causing them to be substantially higher (up to a factor of 4) than expected.

SO_4^{2-} levels reached their maximum under highly oxidizing-unbuffered pH and highly oxidizing-low pH conditions in Fe^{3+} experiments after 43 days, with concentrations of 293 mg/L and 250 mg/L, respectively (Figure 4-4). The mildly oxidizing-low pH conditions were also effective in oxidizing sulphur, with SO_4^{2-} concentrations reaching 213 mg/L after 46 days. Similar to the NO_3^- and O_2 experiments, SO_4^{2-} concentrations in the mildly oxidizing-unbuffered pH scenarios show minimal evidence of sulphur oxidation (Figure 4-4). While the highly oxidizing-unbuffered pH conditions mobilized sulphur when Fe^{3+} was the oxidant, it is important to note the pH of this batch was consistently ~3, and a pH control on SO_4^{2-} occurrence is still likely. Nitrate concentrations in the Fe^{3+} experiments generally ranged between 0 and 182 mg/L, suggesting some nitrogen oxidation was taking place, but not increasing or decreasing over the duration of the experiments (Figure 4-4).

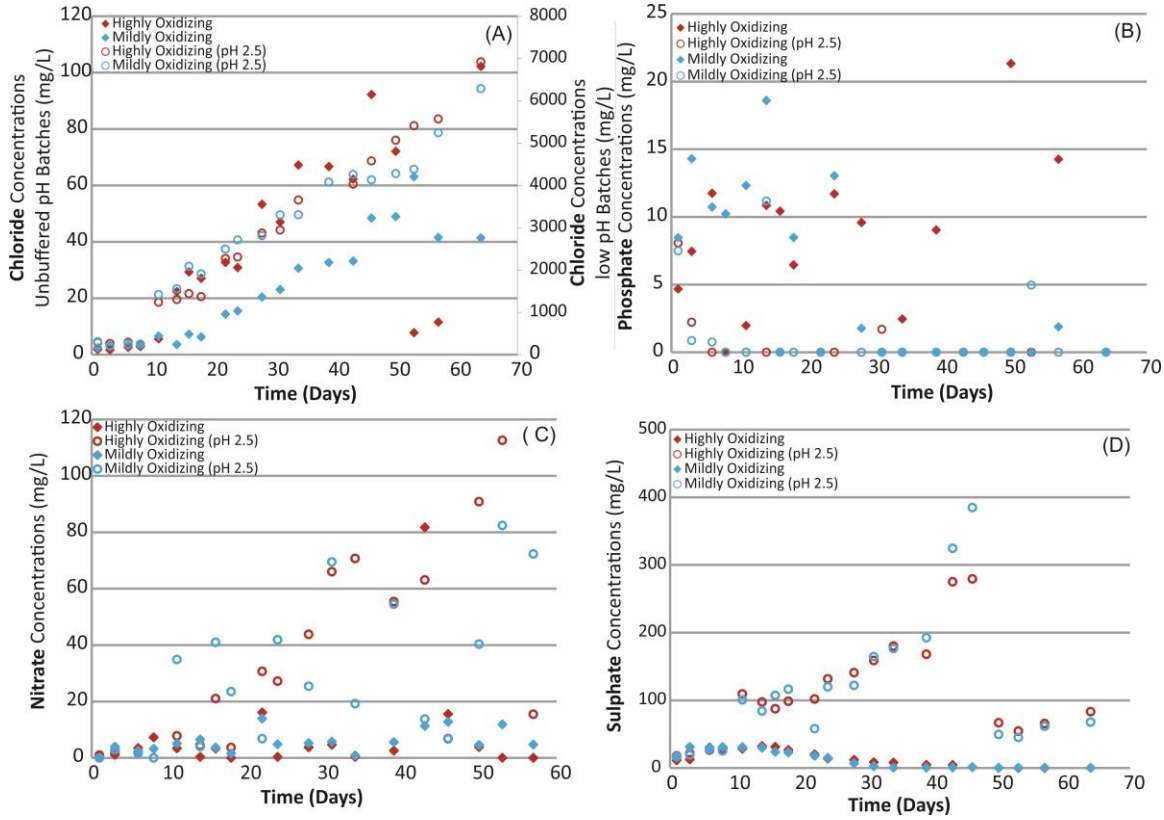

Figure 4-2 **Chloride (a), phosphate (b), nitrate (c) and sulphate (d) concentrations over the duration of the batch experiments using O_2 as the oxidant. Mildly oxidizing conditions are represented in red and highly oxidizing in blue with low pH represented by an open circle. Note the secondary axis for the chloride concentrations in the low pH batch reactors.**

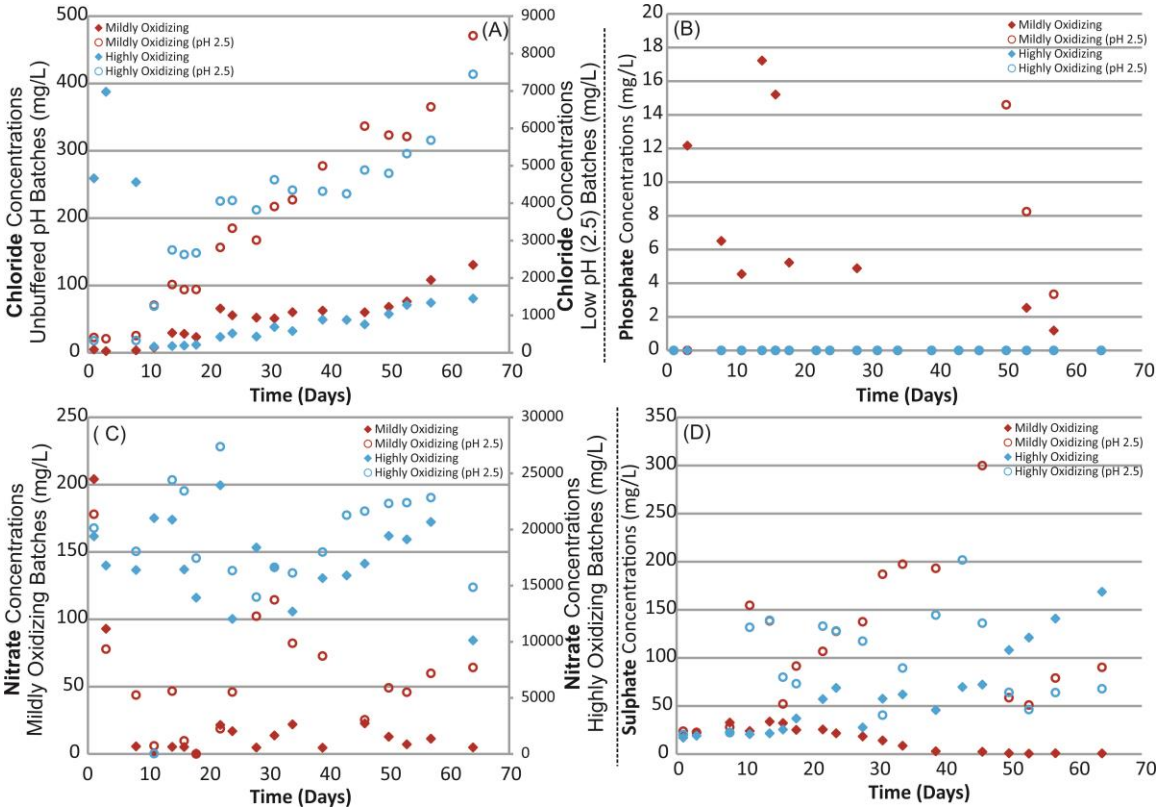

Figure 4-3 **Chloride (a), phosphate (b), nitrate (c) and sulphate (d) concentrations over the duration of the batch experiments using NO_3^- as the oxidant. Mildly oxidizing conditions are represented in red and highly oxidizing in blue with low pH represented by an open circle. Note the secondary axis for the chloride concentrations in the low pH batch reactors as well as for nitrate concentrations in the highly oxidizing batches.**

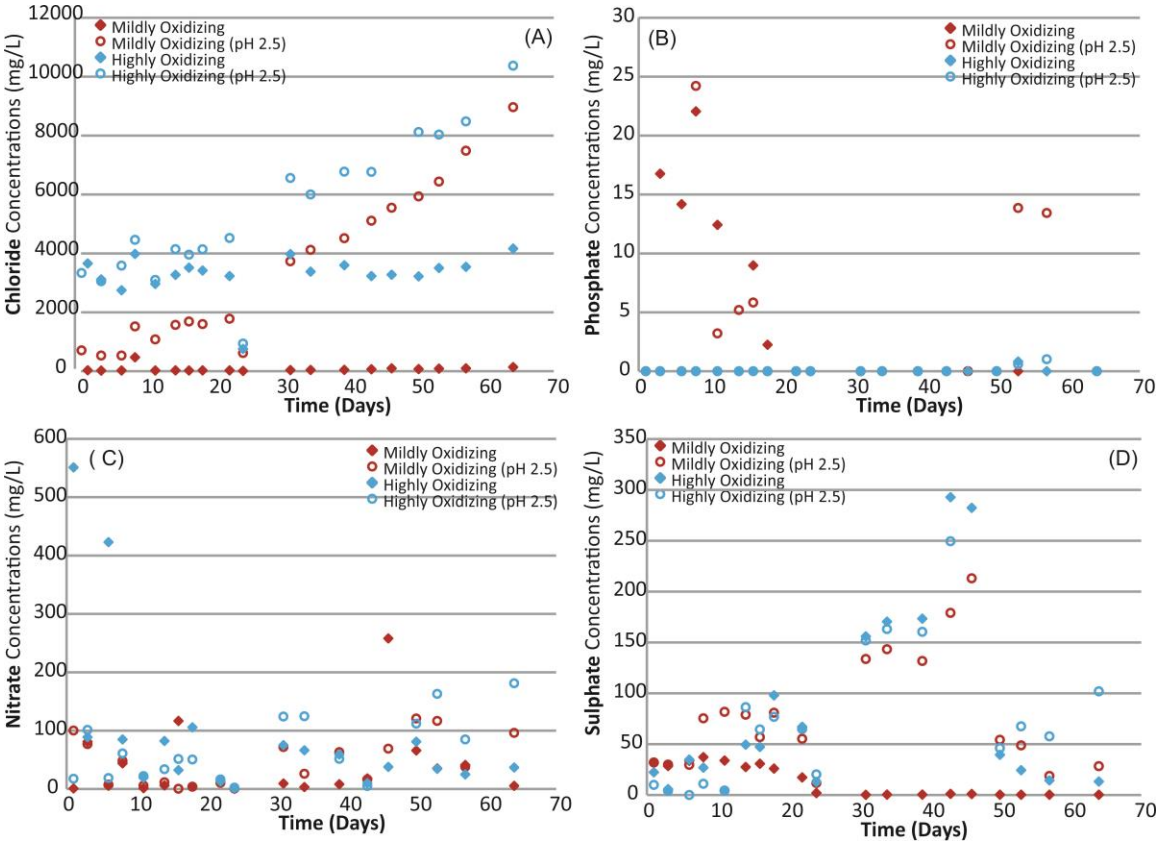

Figure 4-4 Chloride (a), phosphate (b), nitrate (c) and sulphate (d) concentrations over the duration of the batch experiments using Fe^{3+} as the oxidant. Mildly oxidizing conditions are represented in red and highly oxidizing in blue with low pH represented by an open circle.

In each of the batches, a combination of elements other than Se showed noteworthy trends, including: calcium (Ca), chromium (Cr), copper (Cu), iron (Fe), magnesium (Mg), manganese (Mn), nickel (Ni), zinc (Zn) and uranium (U). These trends can be seen in Figures 4-5, 4-6, and 4-7 for the O_2, NO_3^- and Fe^{3+} experiments, respectively. Note that concentrations in Figures 4-5 to 4-7 are presented as 3-day moving averages to smooth data for ease of interpretation. In general, the unbuffered pH experiments show elevated concentrations of these elements at the beginning of the experiment followed by a steady decline. This decline is likely due to the adsorption of the trace elements onto the surface of the residual following their initial release concurrent with the dissociation of associated minerals. Contrarily, the low pH scenarios show a steady increase of these elements for the duration of the experiments. A steady increase in Ca during the low pH experiments suggests the dissolution of carbonate minerals and the subsequent release of commonly associated trace elements (Rimstidt

et al. 1998). The instability of Fe and Mn oxides at pH's <2.5 can result in their dissolution and the subsequent loss of adsorption sites as well as the release of associated trace elements, causing concentrations to increase as the experiment progresses. Additionally, adsorption sites tend to be dominated by a positive charge at low pH which results in the attraction of anions, rather than cations to the surface.

An exception to the general trends is the highly oxidizing scenario using NO_3^-, where the U and Ni increase initially, then decrease reaching their lowest concentrations at approximately 34 days and then increase again for the remainder of the experiment, forming a 'U' shaped trend, with Mn and Zn showing the inverse in the same scenario. The peak in Mn concurrent with low U concentrations suggests conditions in the batch reactor were more reducing between 20 and 50 days, which can be confirmed by ORP measurements made during the experiment (Figure 4-8). ORP and pH for the duration of the remaining experiments can be found in Appendix D. The reducing conditions are reflected by the release of Mn into solution by dissolution of MnS or a $MnCO_3$, both of which incorporate Mn in the 2+ oxidation state. The decrease in Mn^{2+} at 50 days is then a reflection of the system shifting to a more oxidizing state, which would cause the subsequent increase in ORP after 57 days. While Mn occurs as an aqueous cation in reducing conditions, oxidized Mn isn't soluble and usually precipitates as Mn-oxides, hydroxides and oxyhydroxides (Sposito, 1989). The inverse is true for U, which occurs in aqueous form in oxidizing conditions, but is relatively insoluble in reducing conditions where it forms minerals such as uraninite (Reeder and Schoonen, 2006). The absence of U in the low pH experiments is likely related to its propensity to form uranyl carbonate anion species in systems where carbonate is abundant, whether from higher pH or dissolution of carbonate minerals (Reeder and Schoonen, 2006). The uranyl carbonate anions would have a high affinity for adsorption onto the positively charged surfaces at low pH and therefore would be expected to be at very low concentrations.

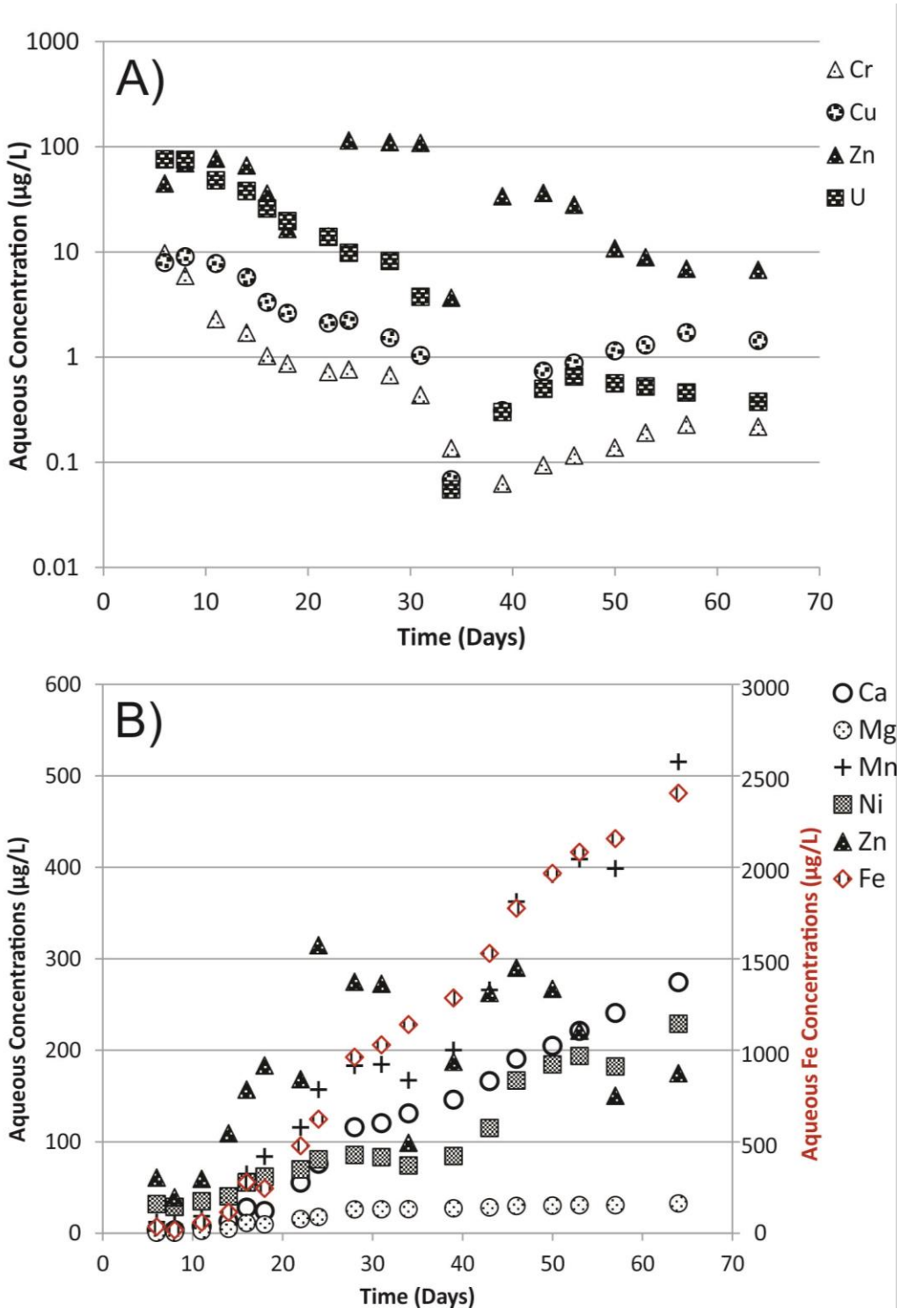
A)
Aqueous Concentration (µg/L)
1000
100
10
1
0.1
0.01
0
10
20
30
40
50
60
70
Time (Days)
Cr
Cu
Zn
U
B)
Aqueous Concentrations (µg/L)
600
500
400
300
200
100
0
3000
2500
2000
1500
1000
500
0
Aqueous Fe Concentrations (µg/L)
Time (Days)
Ca
Mg
Mn
Ni
Zn
Fe

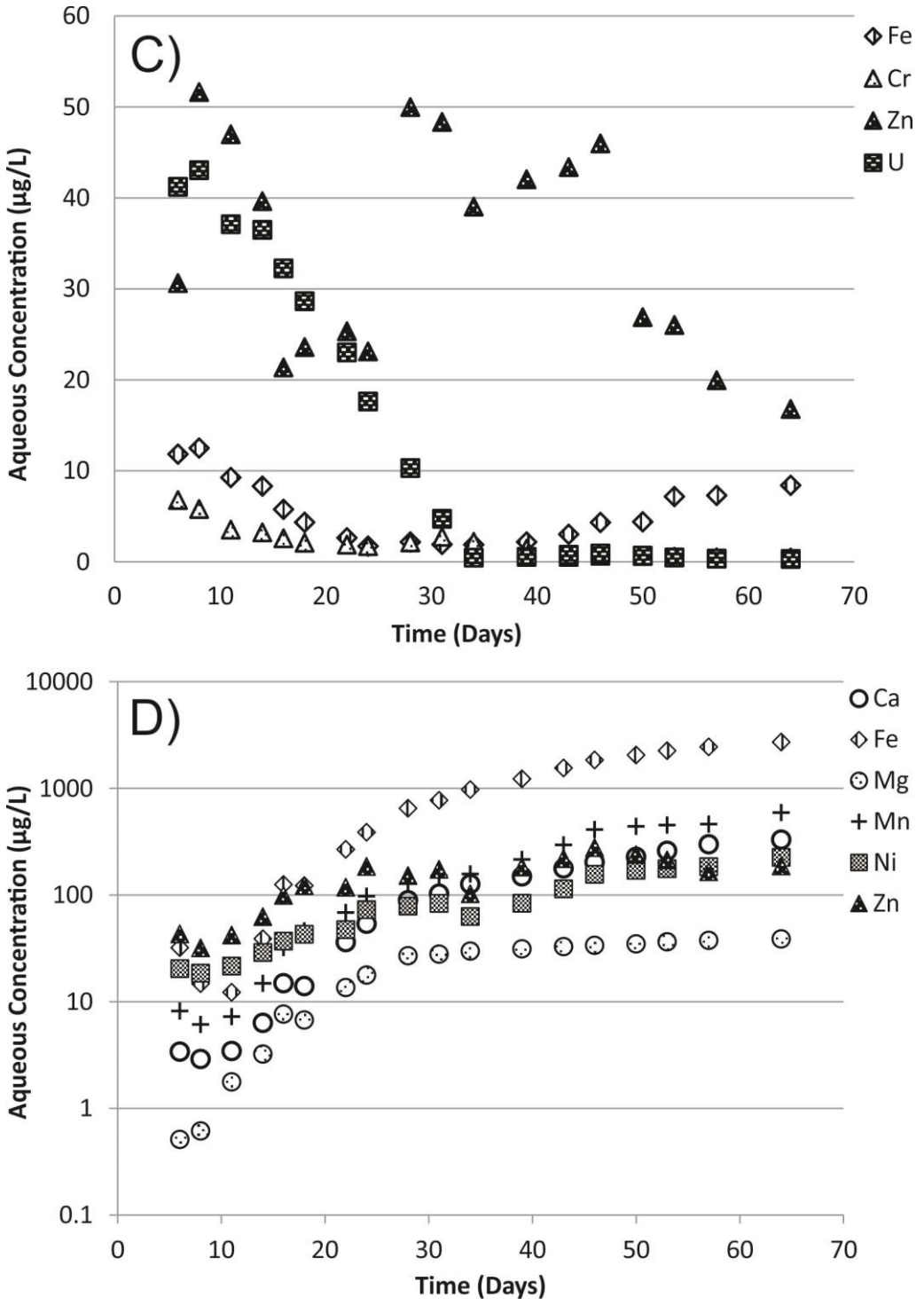

Figure 4-5 **Elements of interest for the (A) mildly oxidizing scenario (B), mildly oxidizing (pH 2.5) (C), highly oxidizing (D) and highly oxidizing (pH 2.5) over the duration of the batch experiments using O_2 as the oxidant. Note the difference in scales for each of the scenarios and the secondary axis for iron concentrations in panel (B). Concentrations for Ca, Mg and Fe are presented in mg/L.**

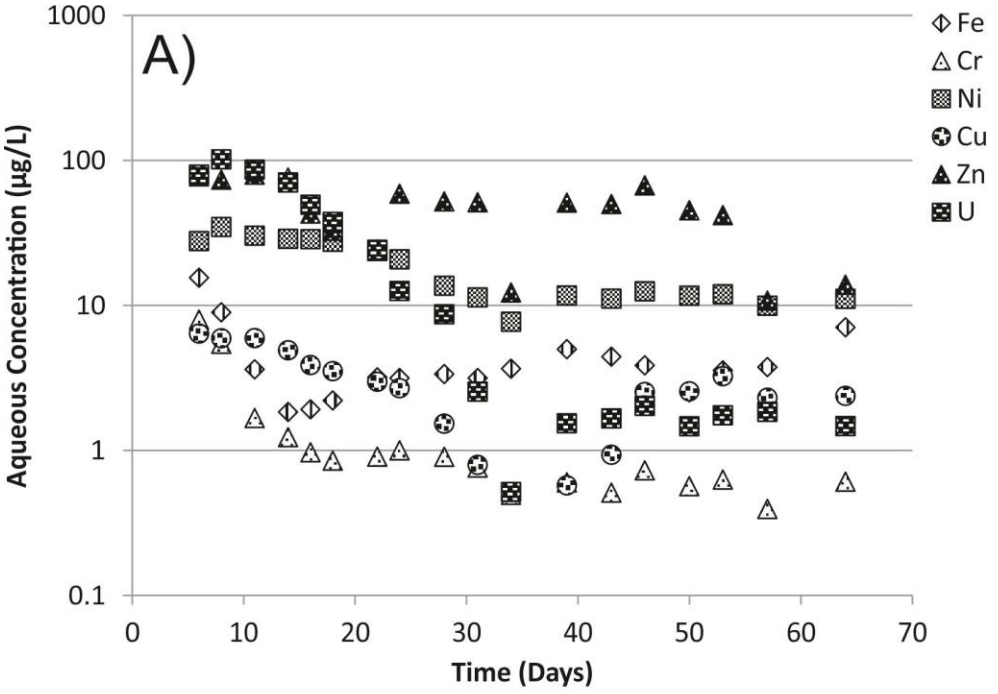
A)
Aqueous Concentration (µg/L)
1000
100
10
1
0.1
0
10
20
30
40
50
60
70
Time (Days)
Fe
Cr
Ni
Cu
Zn
U

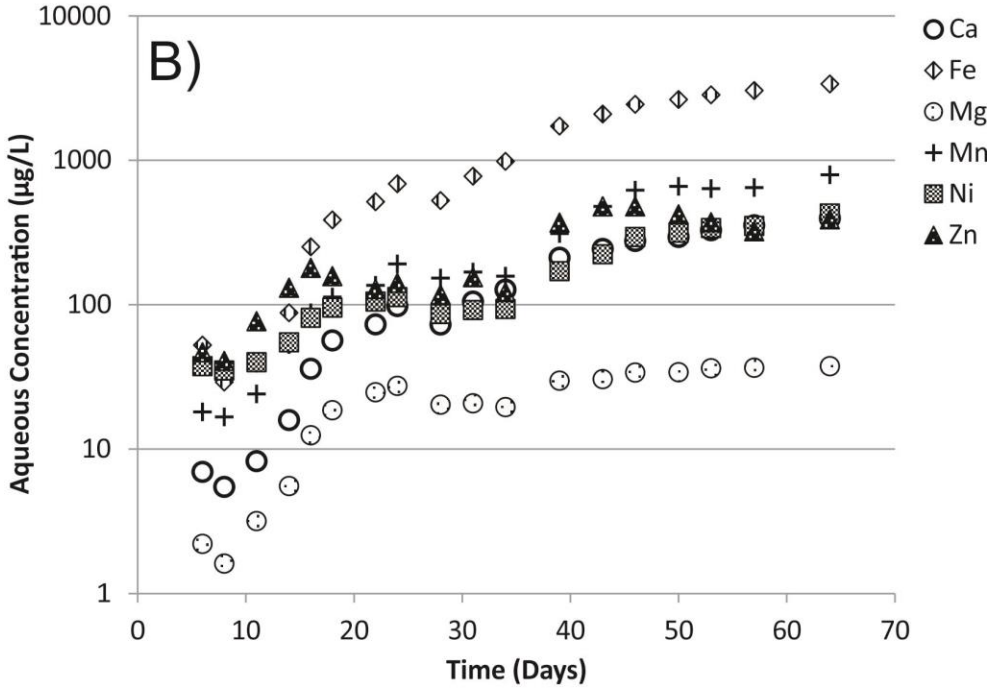
B)
Aqueous Concentration (µg/L)
10000
1000
100
10
1
0
10
20
30
40
50
60
70
Time (Days)
Ca
Fe
Mg
Mn
Ni
Zn

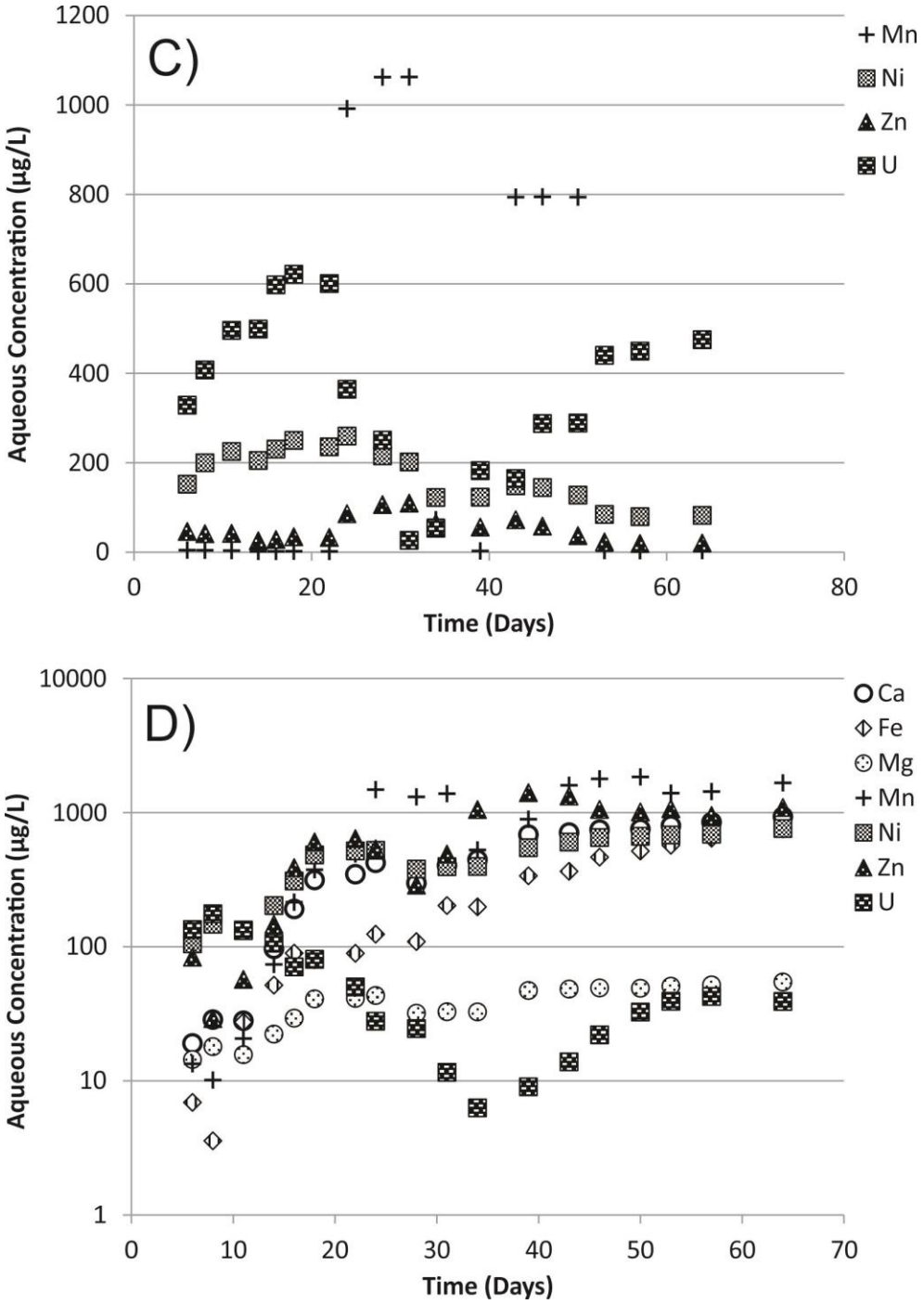

Figure 4-6 **Elements of interest for the (A) mildly oxidizing scenario (B), mildly oxidizing (pH 2.5) (C), highly oxidizing (D) and highly oxidizing (pH 2.5) over the duration of the batch experiments using NO_3^- as the oxidant. Note the difference in scales for each of the scenarios. Concentrations for Ca, Mg and Fe are presented in mg/L**

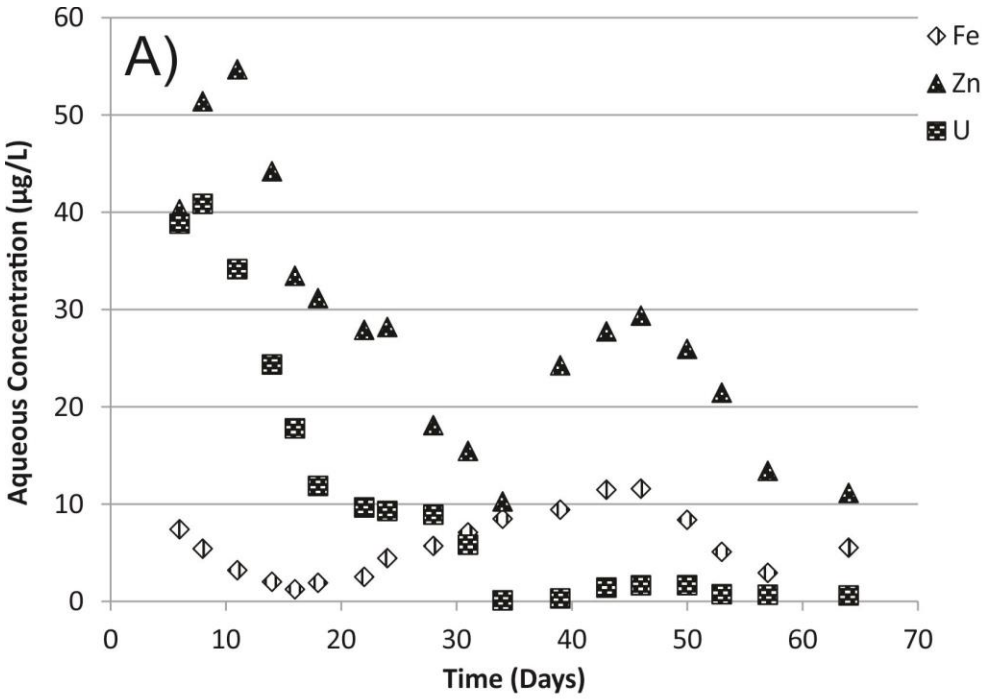
A)
Fe
Zn
U
Aqueous Concentration (µg/L)
Time (Days)
0
10
20
30
40
50
60
70

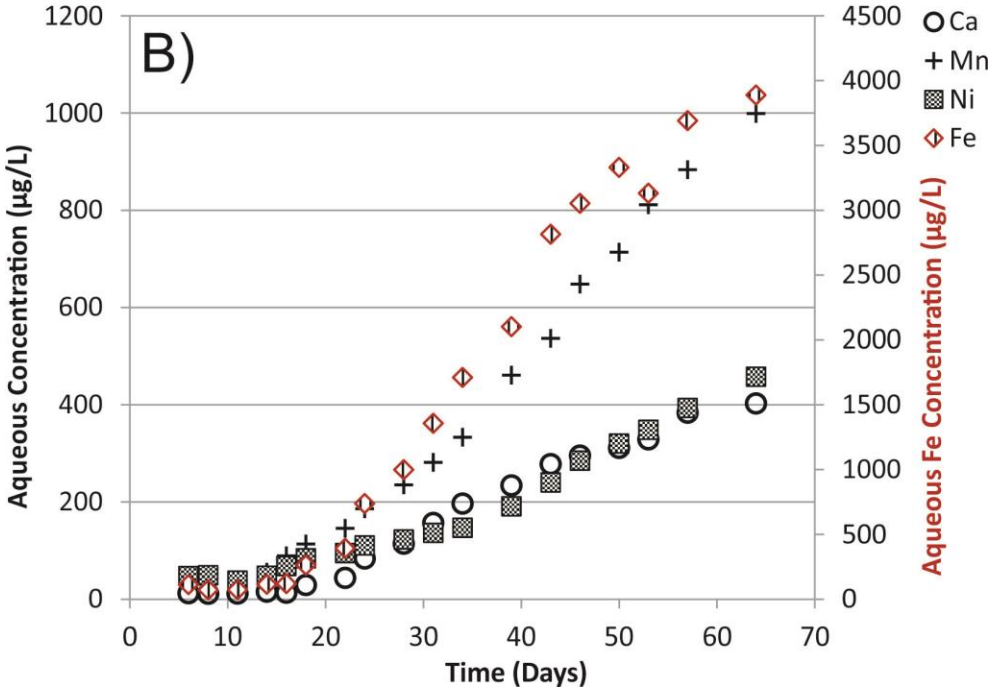
B)
Ca
Mn
Ni
Fe
Aqueous Concentration (µg/L)
Aqueous Fe Concentration (µg/L)
Time (Days)
0
200
400
600
800
1000
1200
500
1000
1500
2000
2500
3000
3500
4000
4500

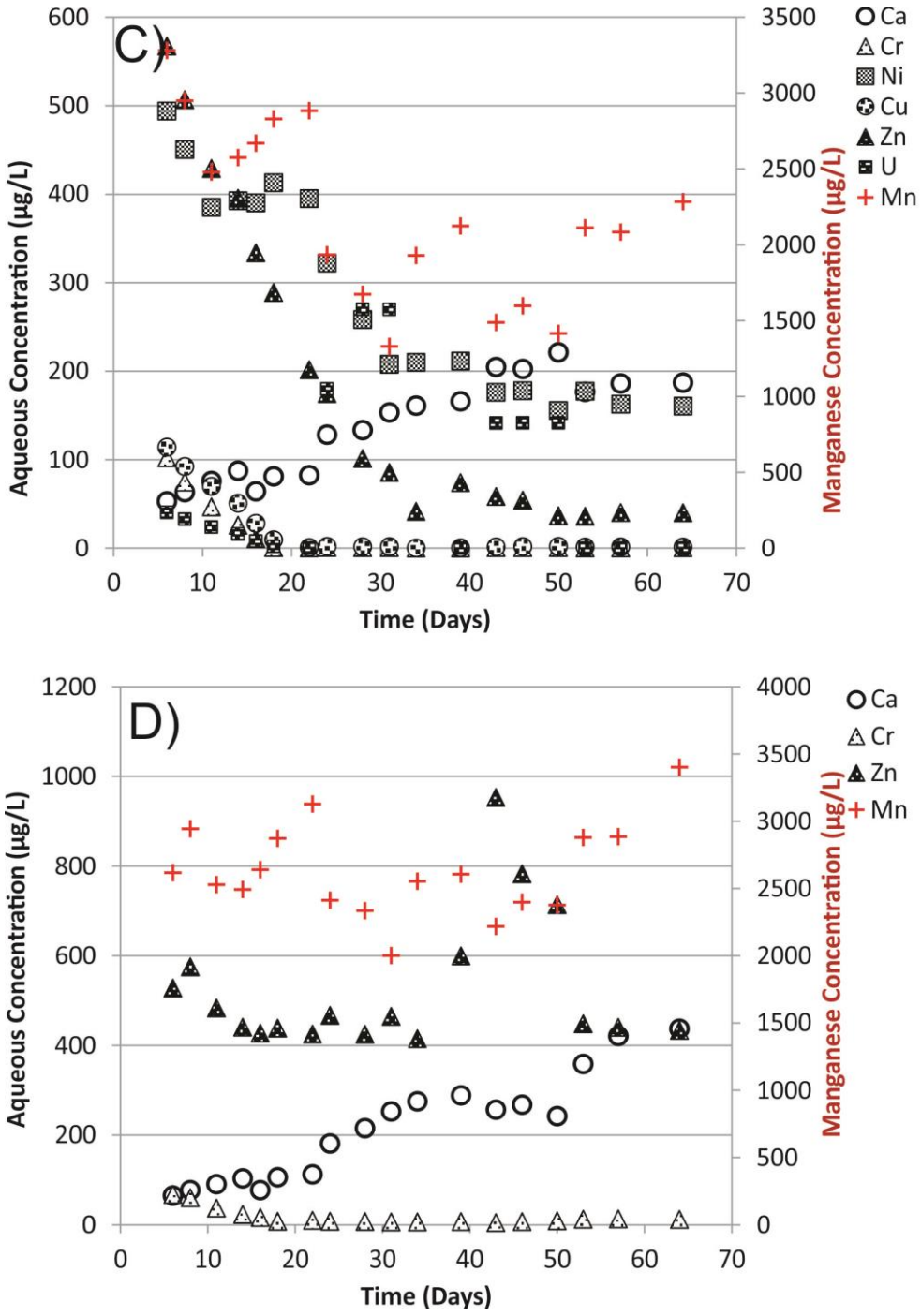

Figure 4-7 **Elements of interest for the (A) mildly oxidizing scenario (B), mildly oxidizing (pH 2.5) (C), highly oxidizing (D) and highly oxidizing (pH 2.5) over the duration of the batch experiments using Fe^{3+} as the oxidant. Note the difference in scales for each of the scenarios.Note the difference in scales for each of the scenarios. Manganese is presented in red and on a secondary scale in the highly oxidizing scenarios. Concentrations for Ca, Mg and Fe are presented in mg/L**

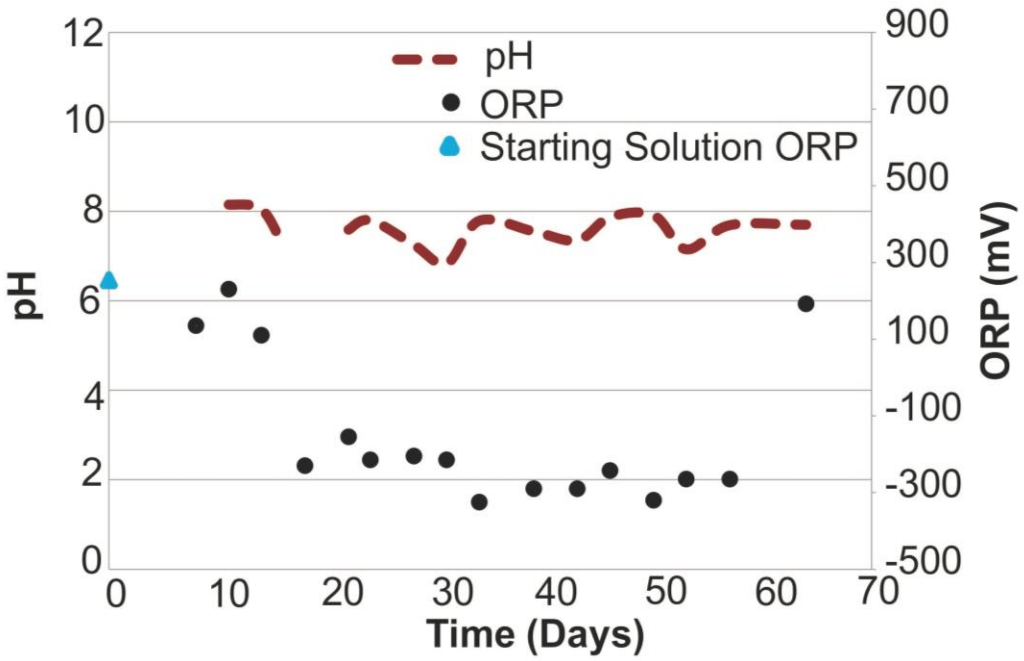

Figure 4-8 pH and ORP over the duration of the highly oxidizing scenario (NO3 100) using NO_3^- as an oxidant. Blue triangle represents ORP of the starting NO_3^- solution used.

Se concentrations over the duration of the batch experiments performed on the Se reference standards are presented in Figure 4-9. A complete summary of the chemistry data throughout these experiments can be found in Appendix E. Na_2SeO_3 reached concentrations that exceeded 4.0E5 µg/L in O_2, NO_3^- and Fe^{3+} experiments, regardless of the pH control (Figure 4-9). This is expected, due to the high solubility of SeO_3^{2-}. For the remaining standards (Se_0, ZnSe and SeS_2) the low pH inhibited the mobility of Se, with concentrations that did not exceed 246, 190 and 156µg/L for the O_2, NO_3^- and Fe^{3+} experiments, respectively (Figure 4-9). SeS_2 also demonstrated very low solubility, with concentrations remaining below 25µg/L in all scenarios. Se concentrations in the Fe^{3+} experiments remained below 260µg/L regardless of the pH control, but it should be noted that the pH of the uncontrolled Fe^{3+} solutions were ~3 for the duration of the experiments. In the ZnSe O_2 and NO_3^- experiments, Se increased steadily, with concentrations reaching 1710 and 829µg/L after 25 days, respectively. Se was mobilized from Se^0 in the O_2 and NO_3^- experiments as well, with concentrations that ranged from 227 to 645µg/L and 316 to 673µg/L, respectively, with no notable ascending or descending trend (Figure 4-9). O_2, NO_3^- and Fe^{3+} did not have a discernable difference on Se mobility in the standards, assuming the low Se mobility in the Fe^{3+}

experiments was the result of the low solution pH. With the exception of SeO_3^{2-}, which is stable in aqueous form, ZnSe had the highest affinity for oxidation, followed by Se^0, with SeS_2 proving to be stable even under oxidizing conditions.

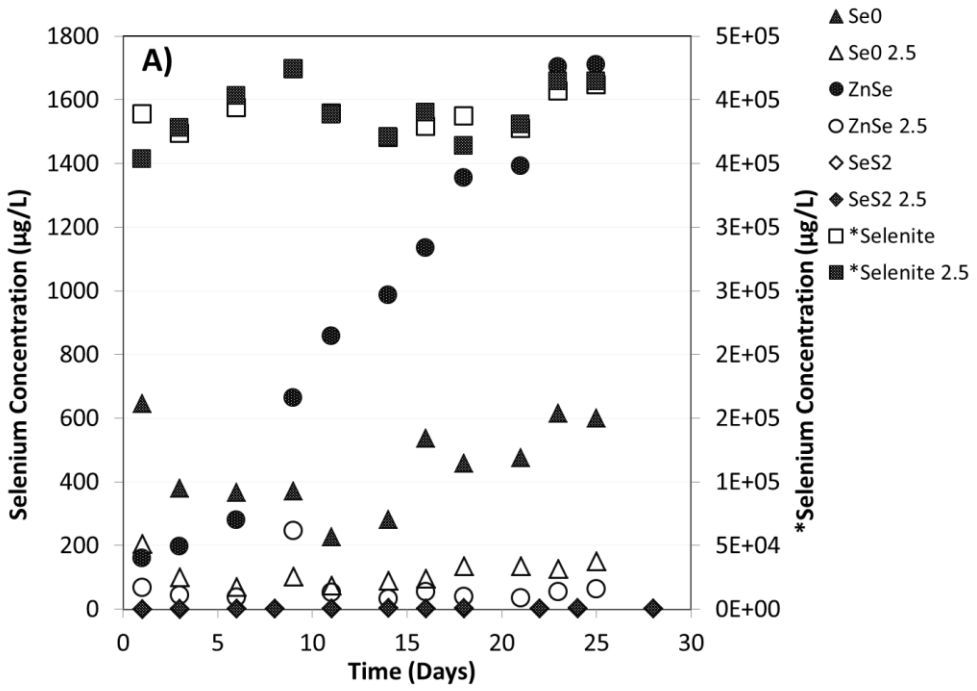
A)
Selenium Concentration (µg/L)
*Selenium Concentration (µg/L)
Time (Days)
Se0
Se0 2.5
ZnSe
ZnSe 2.5
SeS2
SeS2 2.5
*Selenite
*Selenite 2.5

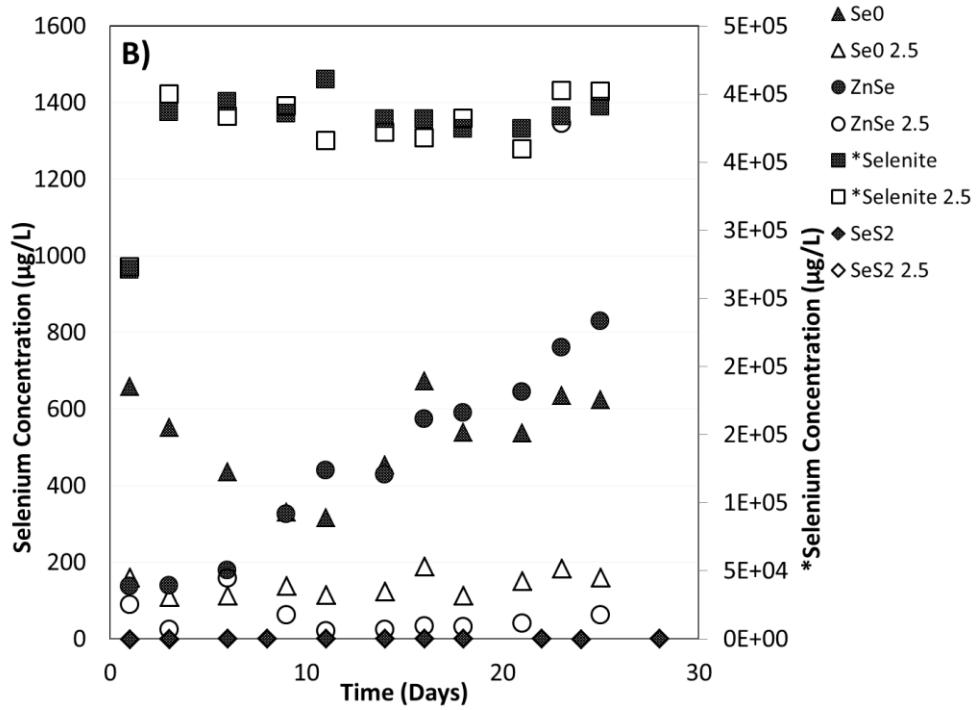
B)
Selenium Concentration (µg/L)
*Selenium Concentration (µg/L)
Time (Days)
Se0
Se0 2.5
ZnSe
ZnSe 2.5
*Selenite
*Selenite 2.5
SeS2
SeS2 2.5

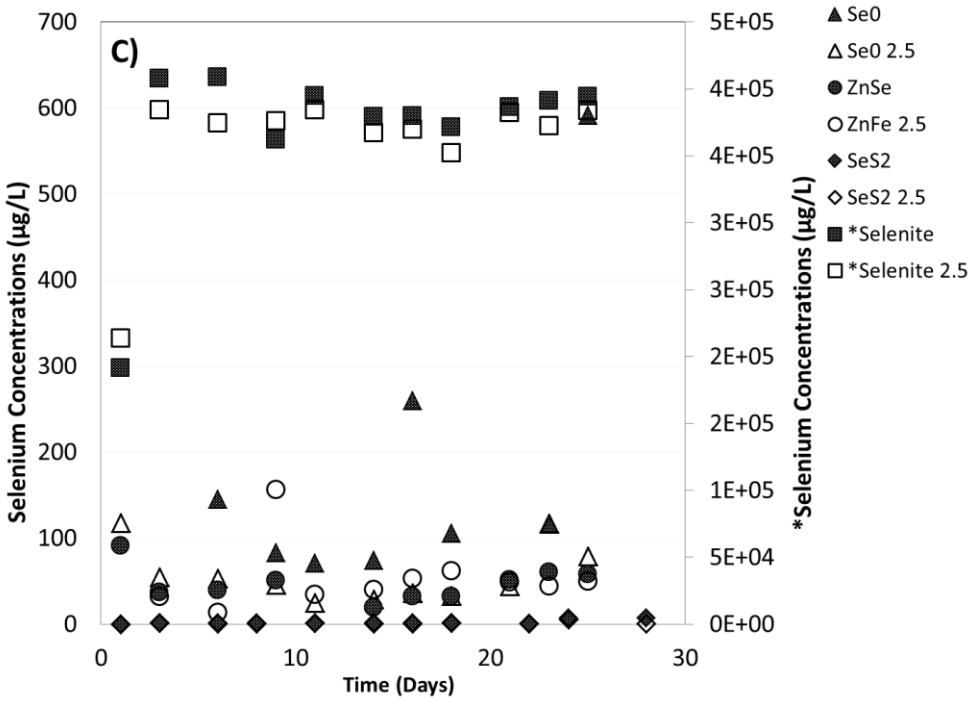

Figure 4-9 Selenium concentrations over the duration of the batch experiments performed on the selenium standards using O_2 (A), NO_3^- (B) and Fe^{3+} (C) as oxidants. Selenite is presented on a secondary axis due to high concentrations. Low pH scenarios are represented by open markers

4.3.2. Solid-phase Speciation

Se-K edge spectra for the reference standards are shown in Figure 4-10. The prominent peak in the near edge region is often referred to as a “white line” and is indicative of unoccupied Se p-states. E_0, or the ‘edge’, of a given species corresponds to the energy necessary to remove a core electron and is influenced by both oxidation state and ligand number and type coordinating the target element. In XAFS, the E_0 is determined by examining the first derivative of the spectrum. Generally, for a given ligand, higher energy white line or edge positions corresponds to the higher oxidation state, with white line positions for SeO_4^{2-} just below 12668 eV, followed by SeO_3^{2-} at 12664.6 eV. The K-edge for SeS_2, and both allotropes of Se^0 occur near 12660 eV (SeS_2 ~ 0.4 eV higher). The metal selenide compounds possess two prominent features in the near edge region, with the initial peak for CuSe and FeSe occurring at 12660 eV, followed by a more prominent peak at 12666 and 12667.7 eV, respectively. The prominent peak for ZnSe occurs at 12664 eV. K-edge positions for the organic

compounds occur at 12661 eV (Selenocystamine and Seleno-DL-cystine) and 12662 eV (L-Selenomethionine).

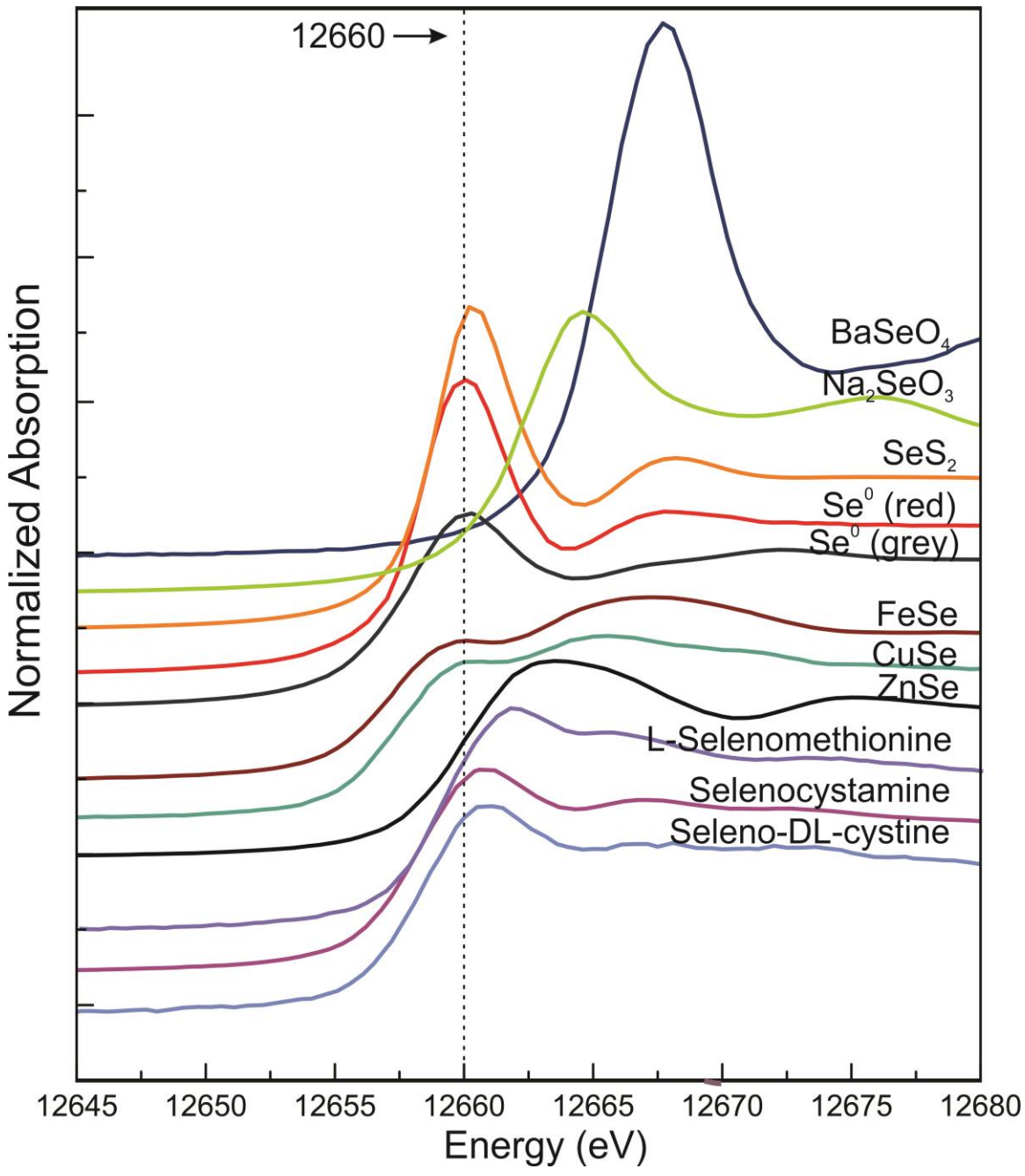

Figure 4-10 Selenium K-edge spectra for all reference standards used, with the K-edge for elemental Se (12660 eV) provided for reference.

Figure 4-11 provides a comparison of the starting residual sample (RES 2) compared to the suspected principle components. While the spectrum closely resembles CuSe and FeSe, the white line position of RES 2 occurs ~0.8 eV lower than the selenides and differences can be observed in the extended edge region. Minor variances can occur if the residual contains a phase very closely related to a standard, but with small changes in charge or ligand presence (i.e. from a more electropositive ligand resulting in less covalence and more charge on the Se). This can account for the slight shift in white line position between RES 2 and the metal selenides. Figure 4-12 provides the first derivative plots of RES 2 compared to FeSe and CuSe for better reference to differences in E_0. In Figure 4-11, a less structured peak can be observed in the extended region at ~12677 in RES 2 that is not present in FeSe or CuSe. While Se^0 (grey) has a similar feature at higher energy (~12672 eV), it is likely there is a phase present that is missing from the standard, such as $FeSe_2$, which has a white line position near 12660 eV, similar features in the extended region as Se^0 and a larger thermodynamic stability field than FeSe. Sequential extraction procedures (SEP) and XANES analysis was conducted as part of Chapter 3 to determine the speciation of Se in the residual. The results of the SEP and XANES analysis were in agreement, identifying the majority of RES 2 to be an iron selenide with some zinc selenide and approximately one third Se^0 (grey). However, due to the absence of $FeSe_2$ from the standards, and its similarity to Se^0, the relative proportion of Se^0 could be overestimated by the XANES analysis.

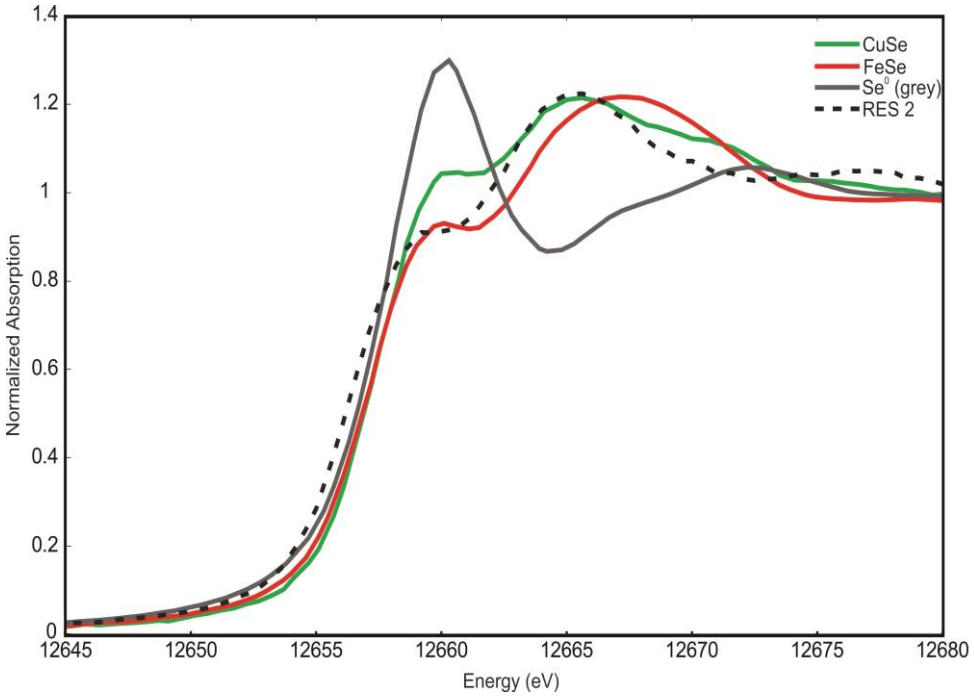

Figure 4-11 Provides the Se K-edge spectra of the starting residual sample (RES 2) compared to the suspected principle components.

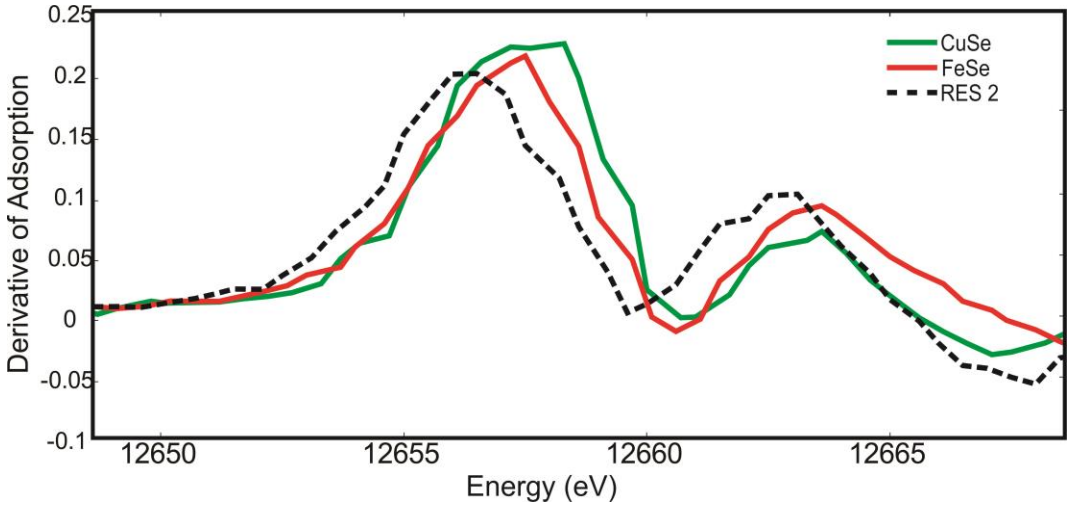

Figure 4-12 First derivative plot of RES 2 compared to CuSe and FeSe. The first peak on the plot corresponds to the E_0. A lower E_0 can be observed in RES 2 compared to the reference standards.

Figure 4-13 presents RES 2 compared to the post-experiment samples from the O_2 batches. For the purpose of discussion, batch scenarios are discussed with a short-hand notation using the oxidant, followed by the concentration in mmol used and '2.5' if the pH was being buffered with HCl. In the case of oxygen, a 'C' indicates the batch reactor was kept closed to simulate mildly oxidizing conditions and an 'O' indicates it

was left open for highly oxidizing conditions. While the aqueous concentrations throughout the batch experiments indicated the majority Se mobilization was taking place in the mildly oxidizing-unbuffered pH scenario (O2 C), the XANES show the least amount of change in this scenario compared to the starting residual. The remaining batches, however, show a significant change in speciation, which suggests the oxidation of a large portion of the reduced Se to an intermediate phase took place, rather than to a completely oxidized aqueous species.

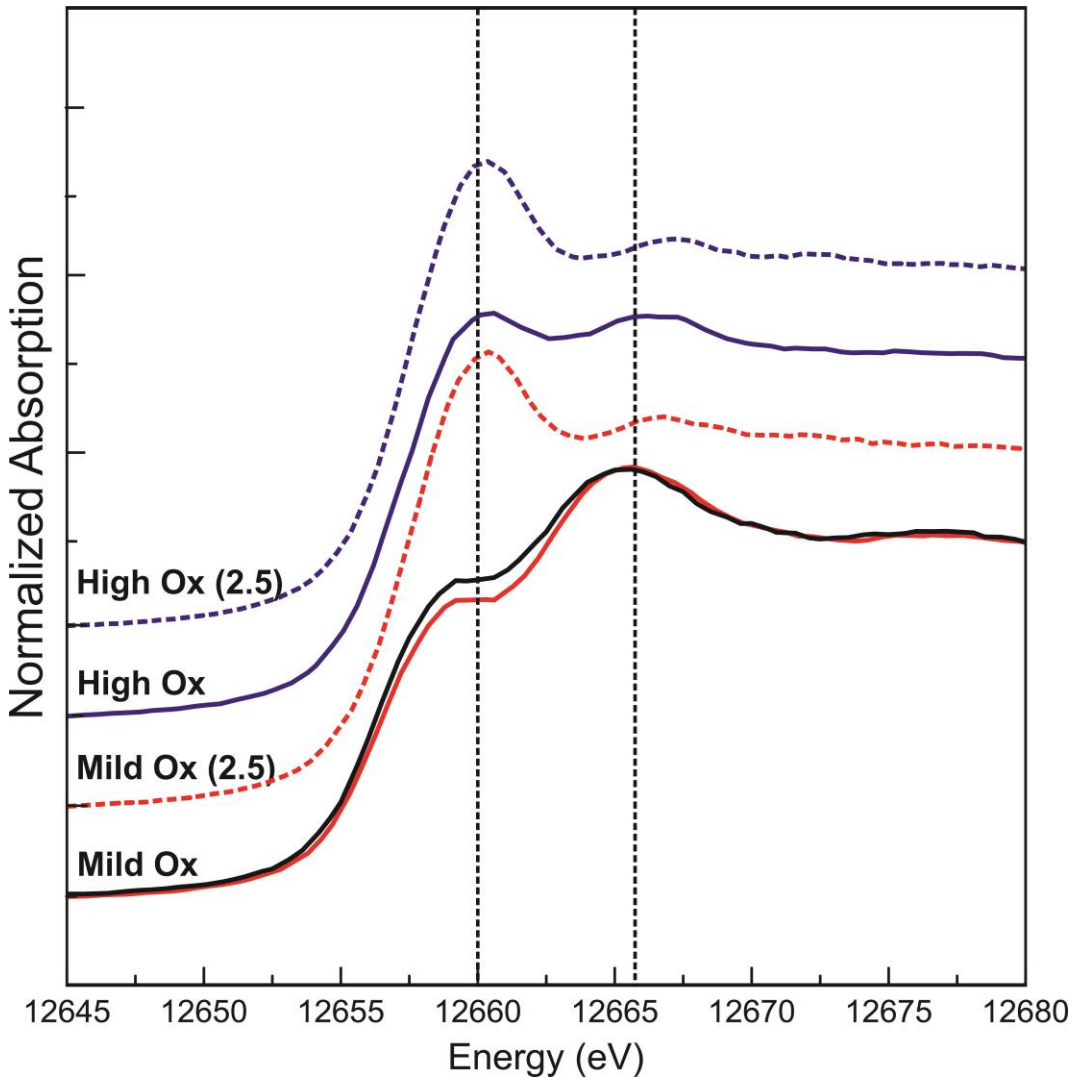

Figure 4-13 Selenium K edge spectra for starting residual (RES 2 in black) compared to post-batch experiment samples using O_2 as an oxidant. Mildly oxidizing scenarios are in red and highly oxidizing in blue. Vertical lines at 12660 and 12666 eV are provided as reference.

O2 C shows very little difference from RES 2 with both O2 C and RES 2 clearly dominated by a metal selenide phase but with observable differences at ~12660 eV and ~12666 eV. SeS_2 and both allotropes of Se^0 have white line positions near 12660 eV, suggesting one or more of these oxidized species is present in O2 C. Similarly, the white line position of selenate occurs near 12668 eV and may be contributing to the higher energy differences between O2 C and RES 2 as an adsorbed phase onto the surface of the residual. The highly oxidizing-unbuffered pH scenario (O2 O) showed significantly more evidence of oxidation while still maintaining features similar to metal selenides. The mildly oxidizing- and highly oxidizing-low pH scenarios (O2 C 2.5, O2 O 2.5), however, bear little resemblance to the starting residual and are likely dominated by less-reduced species. White line positions for O2 O, O2 C 2.5 and O2 O 2.5 all occur near 12660 eV (slightly above) meaning SeS_2 or either allotrope of Se^0 could be contributing. The changes in the low pH scenarios are consistent with observations from the SEPs conducted as part of Chapter 3, where after the third extraction step (F3), which targets acid volatile sulphides and selenides using HCl, a new phase resembling SeS_2 was formed and persisted for the remainder of the experiment.

In addition to peak location, the amplitude should also be considered. Upon comparison of SeS_2/Se^0 reference spectra to RES 2, it is clear that the white line peaks are nearly double the amplitude in the standards. This is not the case when comparing O2 O, O2 C 2.5 and O2 O 2.5 to RES 2, and the smaller differential between peak heights suggests there is another species contributing, possibly an unidentified organoSe compound. Peaks in these three samples also occur in the extended region near 12666 eV and 12672 eV. Se^0 (red) and SeS_2 both have secondary peaks near 12667 eV which are likely contributing to these features as well as Se^0 (grey) having a peak which aligns near 12672 eV. While Se^0 (grey) has a discernable feature near 12672 eV, the similarities between SeS_2 and Se^0 (red) make them difficult to distinguish in multiphase samples and to ultimately conclude which of the two is present. Figure 4-14 provides a comparison between white line position and E_0 for SeS_2 and Se^0 (red) which shows an offset in white line position of approxiamtely0.4eV and similar features in the extended region. While it is possible to discern the differences in the reference standards, it is much more of a challenge to do so in multi-phase samples when there are contributions from more reduced/oxidized species that can cause the small shift observed between SeS_2 and Se^0 (red).

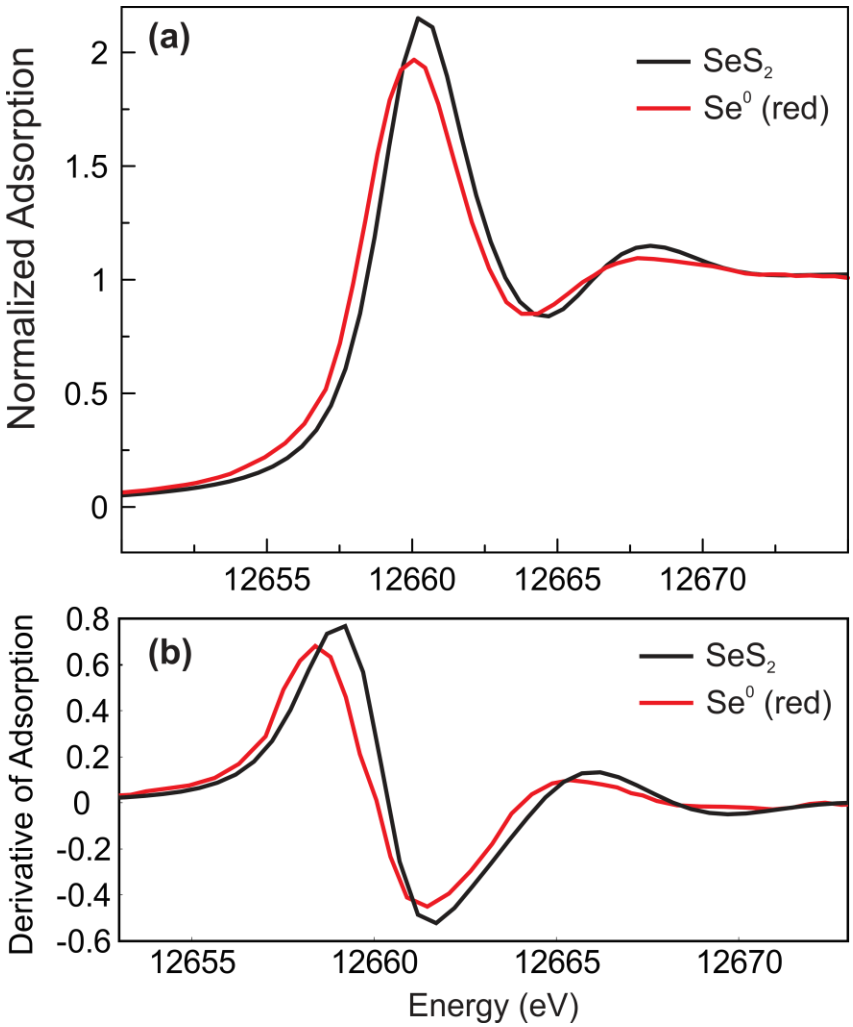

Figure 4-14 Comparison of the white line position (a) and the 1st derivative of the Se K-edge spectra for Se^0 (red) and SeS_2. The first peak of the derivative plot represents the E_0.

A comparison of RES 2 and the post-experiment samples from the NO_3^- batches is provided in Figure 4-15. Similar to the O_2 experiments, the mildly oxidizing-unbuffered pH sample (NO3 1.0) shows very little change from the starting residual. Higher energy along the edge jump and near 12660 eV suggests the presence of an oxidized species, likely SeS_2, Se^0 (red) or Se^0 (grey), given their white line positions (~12660 eV). The mildly oxidizing-low pH sample (NO3 1.0 2.5) likely contains a majority of oxidized species, while still retaining features that are likely due a minor contribution from metal selenides, such as the broad peak near 12667 eV which sits between the second Fe/CuSe peak and higher energy peaks in the extended region of the Se^0 and SeS_2 spectra. In addition to peak location, the lower white line to jump ratio compared to the highly oxidizing samples indicates a higher contribution from reduced species. Both

highly oxidizing samples (NO3 100 and NO3 100 2.5) show the most evidence of oxidation, regardless of the pH control. Both spectra overlap almost completely with one another, have white line positions approximately 0.5eV higher than Se^0 and bear close resemblance to SeS_2/Se^0 (red). The 0.5eV shift in white line position suggests the post-experiment sample is comprised of SeS_2, rather than Se^0. Geoffroy, et al., 2011 demonstrated the production of SeS_2 in a system with selenite and sulphides present when the pH remains between 1.7 and 7, conditions which exist in the NO_3^- experiments. Additionally, NO_3 100 and NO3 100 2.5 have amplitudes similar to the reference standards, suggesting the oxidized phase comprises more of the post-experiment samples than comparable samples from the O_2 experiments. Features in the extended region correlate well with the second peak of Se^0 (red) and SeS_2 near 12667 eV and of Se^0 (grey) near 12672 eV. Both NO3 100 and NO3 100 2.5 have little resemblance to the starting residual or metal selenide compounds, indicating the vast majority of reduced Se was oxidized, making it possible to identify a single phase (SeS_2) as the oxidation product.

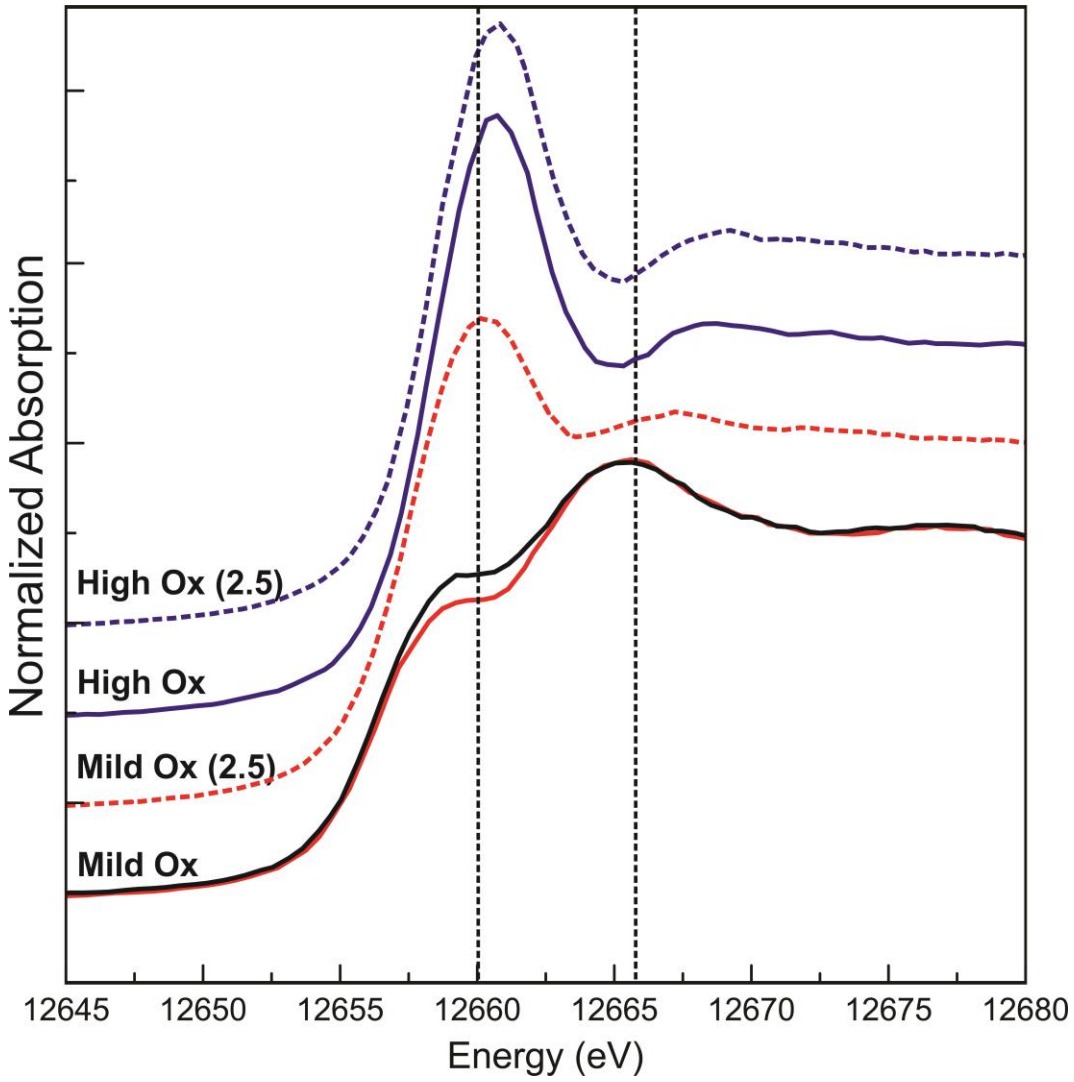

Figure 4-15 Selenium K edge spectra for starting residual (RES 2 in black) compared to post-batch experiment samples using NO_3^- as an oxidant. Mildly oxidizing scenarios are in red and highly oxidizing in blue. Vertical lines at 12660 and 12666 eV are provided as reference.

A comparison of RES 2 to the post-experiment samples from the Fe^{3+} batches is provided in Figure 4-16. Similar to O_2 and NO_3^-, the mildly oxidizing-unbuffered pH (Fe 0.1) sample showed the least evidence of oxidation in the XANES, despite the higher concentrations of aqueous Se detected during the batch experiments. The white line of Fe 0.1 occurs at a slightly higher energy (~1 eV) than RES 2 suggesting oxidation occurred, likely to Se^0 or SeS_2, which have their white lines near 12660 eV (Figure 4-14). A shift in the second peak to energy of approximately12666 eV indicates a possible contribution from selenate, likely adsorbed to the surface of the residual. The highly oxidizing-unbuffered pH (Fe 10) and mildly oxidizing-low pH (Fe 0.1 2.5) samples have

spectra that closely resemble Se^0 (red) and SeS_2 with secondary peaks occurring near 12666 eV, which is slightly lower energy than the corresponding SeS_2/Se^0 (red) peaks, suggesting a small residual contribution from a metal selenide phase. The spectrum of the highly oxidizing-low pH (Fe 10 2.5) sample showed no resemblance to the starting residual and appears single phase, suggesting the vast majority of reduced Se was oxidized. The white line position and secondary features of the Fe 10 2.5 spectrum suggests the oxidation product is Se^0, rather than SeS_2 like the highly oxidized NO_3^- samples.

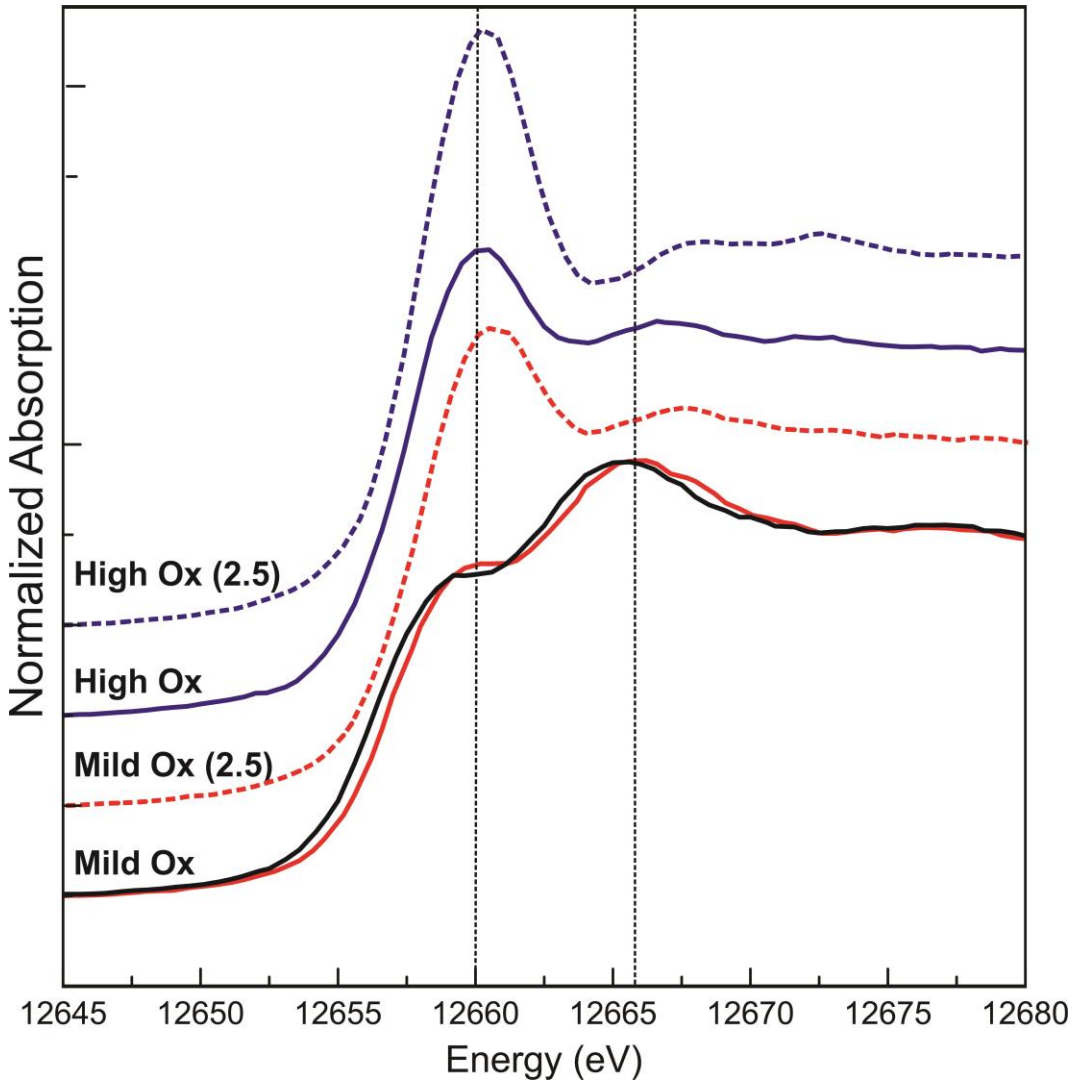

Figure 4-16 Selenium K edge spectra for starting residual (RES 2 in black) compared to post-batch experiment samples using Fe^{3+} as an oxidant. Mildly oxidizing scenarios are in red and highly oxidizing in blue. Vertical lines that correspond to the K edge of Se^0 (12660 eV) and the second peak of CuSe (12666 eV) are provided as reference.

Several studies have demonstrated the production of Se^0 through the oxidation of Fe(II)-bearing selenide minerals (Breynaert et al., 2008; Charlet et al., 2007; Myneni et al., 1997; and Sudipta et al., 2010). Additionally, the respiration of selenium oxyanions by certain types of bacteria has been shown to produce both intra- and extra-cellular Se^0 nanoparticles with monoclinic structure (Se^0 red), making the Se^0 by-product stable within the biomass of the residual for the duration of the batch experiments, if this were to occur (Jain et al., 2015; Oremland et al., 2004). Furthermore, studies have also shown the production of SeS_2 under low pH conditions in the presence of reduced sulphur species (Fergesson et al., 1962 and Geoffroy et al., 2011,). These findings support the possibility that Se^0 is being produced through the oxidation of selenide in the batch reactors. Furthermore, the production of SeS_2 has been documented in low pH conditions by Fergeson et al. (1962) through the reaction of selenite during pyrite dissolution and could be an equally likely oxidation product as Se^0. While the spectra for Fe 10 2.5, NO3 100 and NO3 100 2.5 appear to be single phase, which makes it possible to discern between these two oxidation products, the remaining samples still retain features from a reduced form of Se, making it difficult to identify a single oxidation product. It is therefore reasonable to assume that either Se^0 or SeS_2 is being produced during the oxidation of selenide in all O_2 scenarios, as well as Fe 0.1, Fe 0.1 2.5, Fe 10, NO3 1.0 and NO3 1.0 2.5. Although elevated aqueous concentrations of Se weren't detected in the highly oxidizing and low pH experiments, significant oxidation was occurring, but only to the production of Se^0 or SeS_2. It is likely that any aqueous Se would be quickly reduced by the iron selenides and reduced sulphur present in the residual. The added oxidants (O_2, NO_3^-, Fe^{3+}) would also be reacting with sulphides and iron selenide minerals, and since Fe^{3+} is stable at low pH, these conditions would promote additional oxidation, which was observed in the XANES spectra where the highly oxidizing-low pH scenario using Fe^{3+} showed no trace of selenide phase in the post-experiment sample. The production of Se^0 is thermodynamically favored as its stability field expands across a wide range of pH at reducing to mildly oxidizing conditions (Figure 1-1). However, while the oxidation state of Se in SeS_2 differs slightly from Se^0, Geoffry et al. (2011) demonstrated a large overlap in the stability fields of Se^0 and SeS_2 by testing the solubility of SeS_2 under a variety of redox and pH conditions, suggesting SeS_2 would also be favored as an oxidation product in the batches where redox was constrained to the sulphide stability field. The redox conditions in the batches

would likely stay in the Se^0 stability field until the added oxidant or the organic matter was consumed.

While the mildly oxidizing-unbuffered pH scenario using O_2, NO_3^- and Fe^{3+} had the highest concentrations of aqueous Se during the batch experiments, they showed the least amount of oxidation in the XANES and the maximum amount mobilized was 0.31% of the total Se available for reaction. In addition, Se concentrations reached their peak at 16-18 days, after which the Se was likely removed from solution by adsorption onto the residual surface or reduced to Se^0. The remaining scenarios (highly oxidizing and low pH) showed significant oxidation of selenide to elemental Se in the post-experiment XANES samples but little aqueous Se throughout. These results are likely thermodynamically controlled, as the redox-pH conditions of the batch reactors were in the range of the Se^0 stability field, with the exception of the mildly oxidizing-unbuffered pH scenario which had increased pH but low ORP resulting in the experiments staying predominantly in the FeS_2 stability field. The low pH conditions had the greatest amount of oxidation in the O_2 and Fe^{3+} batches, likely due to the stability of Fe^{3+} in these conditions providing additional oxidant for the reactions to occur. In addition, trends in trace elements as well as SO_4^{2-} suggest that monosulphides and carbonate minerals may be important components of the residual. If the conditions simulated in the batches were to persist in nature and remain in the range of Se^0 (and SeS_2) stability, the risk posed by the residual would be relatively low, as the oxidation observed did not produce high levels of mobile Se in most scenarios, and when it did the majority of Se was removed from aqueous phase by adsorption or reduction within 18 days. Because of the limited data available for SeS_2 production and stability and the error associated with the XANES measurements resulting from the missing $FeSe_2$ standard along with difficulties associated with qualitatively assessing multi-phase samples, further experiments are needed to verify the production of SeS_2 in the presence of NO_3^-.

Chapter 5. Conclusions and Recommendations

While selenium (Se) is naturally occurring, industrial activities can facilitate its mobility into the environment making Se an element of increasing concern. Se presence in natural waters is a major issue due to its toxicity and rapid bioaccumulation within food chains. Mobility of Se is directly related to the redox state which controls the speciation in aqueous solution, the sorption properties of the coinciding solid state, as well as the stability of selenium minerals. In general, the higher the oxidation state, the more mobile Se will be. Due to the increasing concern, biologically facilitated water treatment systems are being used at industrial sites to remove the Se from the water before it's discharged off-site. The by-product of this treatment is solid-phase sludge residual with elevated Se concentrations. This research focused on characterization of 2 samples of residual from a water treatment facility by determining Se speciation, element associations and mobility mechanisms. Solid phase Se speciation was determined using sequential extraction procedures (SEP) and X-ray Absorption Near Edge Spectroscopy (XANES). Mobility mechanisms were investigated through a series of aqueous geochemical batch experiments that were conducted under a variety of redox and pH conditions. The batch experiments, in combination with XANES analysis on the solid phase post-experiment samples, provided insight into the vulnerability of specific Se species under varying redox and pH conditions.

5.1. Conclusions

5.1.1. Solid Phase Selenium Speciation

Bulk chemical characterization identified 1260 mg/kg Se in RES 2 and 1400 mg/kg in RES 3. Chemical compositions varied slightly between the two samples, but both had ~27% Fe, with moderate sulphur content and elevated concentrations of Ca, Cu and Zn. Heterogeneities identified in the bulk characterization were supported by XANES measurements which showed the spectra of RES 2 shifted to a slightly higher energy (~1eV) than RES 3. Additional LCF scenarios identified the composition of RES 2 to be similar to RES 3 but with an additional component that was suspected to be $FeSe_2$ or a similar iron selenide species. Since the samples were taken from the filter press of the same treatment plant only months apart, the difference in composition between RES

2 and RES 3 indicates there is temporal variance in the composition of the residual. This is important to note since the behavior of Se in the residual may not be consistent throughout the operating life of the treatment plant.

The SEPs required optimization from the initial method and eleven different variations of the method were attempted before an optimal procedure was reached. It was found that at least a 1:40 solution to solid ratio was required, along with 48 hour duration of the step for extracting the elemental Se component (Fraction 4). In addition, a portion of the Se fraction was lost as volatile H_2Se during the acid volatile sulphide/selenide step (Fraction 3). This volatile phase was accounted for by subtracting the total Se measured in aqueous phase after each extraction step and the remaining Se measured at the end of the SEP in solid phase (~27%) from the total Se present in the starting residual sample. With the H_2Se accounted for, the SEPs identified an average of 0.2% of the total Se as selenate, 0.3% as selenite, 35% as selenides, 34% as elemental,1.2% as an organically associated phase and 27% as a persistent phase that is thought to be SeS_2 produced during the procedure. While there were some commonalities between the SEPs and XANES, the XANES results indicated that the majority fraction of both RES 2 and RES 3 was an iron selenide compound, identified spectrally and semi-quantitatively through the use of linear combination fitting (LCF) with a smaller portion occurring as elemental Se. While SEPs were conducted on the Se standards with the hope of providing supporting information for interpretations, the results of these SEPs were compromised for FeSe and ZnSe due to a loss of mass and introduction of water into the sample vials caused by gas production and expansion in the hot water bath during F3. In addition, complete mobilization of Se was not achieved for any of the standards tested. SeS_2 and Se^0, however, showed similar behavior as they were both mobilized during F4, which targeted elemental Se, although the overall solubility of SeS_2 was relatively low. The release of SeS_2 during F4 could result in an overestimation of the elemental portion of Se as determined by the SEPs. Furthermore, the absence of $FeSe_2$ as a standard could also overestimate the portion identified as Se^0 due to the similarities between their spectra.

Solid phase samples following each fraction of the original SEP were analyzed using XANES to determine the efficiency of the SEP and ensure each fraction was targeting the appropriate species. While the spectra following F1 and F2 were closely related to the starting residual (RES 2), a slight shift to higher energy (~1eV) was

observed, suggesting the loss of a lower energy (reduced) Se species. Since F1 is meant to target selenate and F2 selenite, a shift to higher energy would not be expected and indicates a change in composition of the residual, rather than the removal of a targeted Se species. LCF was done where F1 and F2 were fit with the starting residual and the suspected oxidation products. This method determined the oxidation product during both F1 and F2 to be SeS_2. Following F3, which targets metal selenides assuming they are analogous with metal sulphides, a single phase is left and remains consistent for the remainder of the SEP. This is also observed in the post-rate controlled SEP samples, the spectrum of which resembles the spectra produced following F3, F4 and F5 of the original SEP. The persistent phase is nearly identical to SeS_2 and while this compound has already been shown to form during F1 and F2, could also be the result of the reaction between H_2S and selenite in F3, which has been documented in the past to produce selenium sulphide compounds. The insolubility of SeS_2 and its antimicrobial properties could cause it to persist for the duration of the SEP, since the redox reactions required for mobility are often bacterially facilitated, owing to the 27% Se that remained in the post experiment SEP samples.

5.1.2. Mobility Mechanisms

Although thermodynamics would predict the highest Se mobility under highly oxidizing conditions, the highest concentrations of Se were detected in the mildly oxidizing-unbuffered pH batch reactors for all three oxidants (O_2, NO_3^- and Fe^{3+}). In these reactors, concentrations reached a peak after 16-18 days, followed by a sharp decline and stabilization after 31 days. This decline was likely due to adsorption of aqueous Se, likely selenite under mildly oxidizing conditions, onto the surface of the residual or the reduction of aqueous Se. While elevated concentrations were detected, they only amounted to a maximum of 0.31% of the total Se available for reaction, suggesting the Se in the residual is quite stable in the simulated redox conditions. While aqueous Se concentrations were highest under mildly oxidizing-unbuffered pH conditions, the post-experiment XANES results showed the least evidence of oxidation under these conditions with spectra that closely resembled the starting residual. In the O_2 batches, the low pH scenarios showed the most oxidation, where the greatest extent of oxidation was observed under highly oxidizing conditions in the NO_3^- reactors, regardless of pH. All Fe^{3+} scenarios were efficient in oxidizing Se (with the exception of

the aforementioned mildly oxidizing-unbuffered pH scenario) but the highly oxidizing-low pH sample showed the greatest amount of oxidation. While oxidation was evident in all samples, only select spectra showed virtually complete oxidation of the starting selenide phase and the resulting oxidation products were able to be identified. For the NO_{3-} experiments, both highly oxidizing reactors resulted in a single phase in the post-experiment samples which was identified to be SeS_2 based on the white line position and subsequent spectrum shape. For the Fe^{3+} scenarios, the highly oxidizing low pH reactor showed complete oxidation of selenide to Se^0. In the remaining NO_3^- and Fe^{3+} reactors, and all O_2 experiments, however, post-experiment samples appeared to be mixed phase and so a single oxidation product could not be determined. It can be inferred, however, that either SeS_2 or Se^0 are equally likely oxidation products.

The lowest aqueous Se concentrations were measured in the low pH reactors regardless of oxidant, suggesting low pH conditions inhibit the mobility of Se. This was further supported by the data from the batch experiments conducted on the Se standards which also showed low mobility under low pH conditions, with the exception of Na_2SeO_3 which is highly soluble. Additionally, SeS_2 exhibited very low solubility in all redox-pH conditions, with ZnSe and Se^0 displaying moderate mobility potential as steady, low concentration increases were observed in unbuffered pH conditions. While Se an S often behave analogously, the highest SO_4^{2-} concentrations were detected under low pH conditions, suggesting either the occurrence of reduced S and Se or the mechanisms of mobility differ between the two elements.

A number of trace elements (Ca, Cr, Cu, Fe, Mg, Mn, Ni, Zn and U) showed notable trends throughout the batches with steady increases observed under low pH conditions and an initial decrease followed by a steady decrease for unbuffered pH conditions. Under unbuffered pH conditions, the initial increase is thought to be due to the solubility of trace element-containing minerals and the decrease due to adsorption of these elements onto the surface of the residual. Under low pH conditions, however, Mn and Fe oxides are not stable and a large portion of adsorption sites would contain a positive charge, causing the concentrations of trace elements to increase throughout the duration of the experiment as associated minerals continue to dissolve. One exception to these trends was observed in the highly oxidizing-unbuffered pH NO_3^- reactor where a decrease in ORP was observed from ~20-50 days, concurrent with a dip in U and Ni concentrations and a peak in Mn and Zn values. This trend is potentially due to an

increase in Mn^{2+}, which generated more reducing conditions and shifted the focus of the microbial community. Once the Mn^{2+} was consumed, conditions returned to oxidizing after ~50 days.

5.2. Recommendations

In order to better characterize the residual, and to address the possibility of Se occurring as nanoparticles, it is recommended that Transmission Electron Microscopy (TEM) be conducted in combination with elemental mapping on the residual samples. TEM provides significantly higher resolution than other conventional methods and has the potential to achieve resolution below 50 picometers (pm). With this resolution, TEM has the capability to identify properties such as chemical identity, crystal orientation and electronic structure. The detailed characterization that the TEM provides can more accurately advise Se reference standard selection for XANES analysis and hopefully resolve the issues encountered with the physical and chemical differences between the residual and the standards. In addition to characterization of the residual, in-situ TEM provides an opportunity to observe chemical reactions as they are taking place through the use of specialized sample holders and liquid-phase electron microscopy. Variations of the batch experiments or SEPs can be constructed to collect real-time data and pin point the oxidation mechanisms.

In addition to TEM, synchrotron based micro X-ray Fluorescence Spectroscopy (XRF) provides further opportunity for detailed sample characterization. XRF is a non-destructive method for determination of elements in the ppm or ppb concentration range and would be useful for determining oxidation state as well as chemical associations in the case where it is unclear how much selenide is associated with each metal. By selecting appropriate energies of the incoming X-rays (similar to XANES), chemical maps can be generated in relation to Se oxidation state and chemical bonding. Quantification of each Se oxidation state could be determined using XRF and used as a comparative method to XANES and SEPs.

While more detailed characterization of the residual is important, it is recommended that the SEPs be repeated with a gas capture system in place during Fraction 3. With a gas capture system in place, the gas can then be bubbled through a solution and Se concentrations measured and fully accounted for. This allows

verification of the portion of Se that was identified as selenide through calculation and XANES in this study. Once detailed characterization is conducted with TEM and XRF methods, the SEP can be further tailored to the residual to maximize the accuracy of the procedure. TEM or other detailed characterization methods are also recommended on samples following F1, F2 and F3 to verify the presence of SeS_2 as an oxidation product.

Variations in the batch experiments are recommended to gain further understanding into the oxidation mechanisms of Se in the residuals. Since oxidation of Se only made it to Se^0 in select reactors, increasing the duration of the batch experiments would serve to investigate the rates of these reactions and help determine if complete oxidation to Se^{4+} or Se^{6+} would be achieved given more time. Additionally, a complete suite of experiments should be conducted in sterile conditions to assess the role of microbes in the oxidation of Se and the rate at which these reactions proceed.

It is also recommended that XANES measurements be conducted on the post-experiment batch samples on a different beamline, as the data resolution on the VESPERS line used at the CLS was poor due to the beam quality at the time of measurements. This will provide further insight into the production of SeS_2 during the NO_3^- , as LCF may be more effective with better quality data.

Following the additional batch experiments, it is recommended that column experiments be conducted under constant ORP and pH conditions to gain understanding of Se behavior in a system with more resemblance to the natural environment or landfill conditions, where the residual may end up residing. Maintaining constant ORP for the duration of the column experiments will confirm the whether the adsorption effects observed in the mildly oxidizing-natural pH reactors after 16-18 days occur. The constant ORP will rule out the possibility that oxidant is being consumed and the presence of reduced species in solution (Fe^{2+}, Mn^{2+}, etc.) is driving the ORP down, causing Se to de-mobilize from solution.

While this research provided useful insight into the occurrence and behavior of Se in the residuals produced from biological waste water treatment of mine-impacted waters, further research needs to be done to gain a full understanding. The recommended characterization techniques should resolve the challenges encountered during the SEPs and XANES and hopefully identify Se compounds that were missing

from the reference standards used in this study. Additionally, further batch and column experiments will provide further comprehension of the rates associated with the oxidation of Se in the residuals as well as the role of microbes. The results of this study, along with the recommended follow up research, should help to quantify the risk posed by Se in the residuals and ultimately reduce the threat to the surrounding environment and human health.

References

Bethke, C., & University of Illinois at Urbana-Champaign. (2005). Geochemist's workbench. Golden: RockWare Inc.

Balistrieri, L. S., & Chao, T. T. (1987). Selenium Adsorption by Goethite. *Soil Science Society of America*, *51*(5), 1145–1151. http://doi.org/10.2136/sssaj1987.03615995005100050009x

Balistrieri, L. S., & Chao, T. T. (1990). Adsorption of selenium by amorphous iron oxyhydroxide and manganese dioxide. *Geochimica et Cosmochimica Acta*, *54*(3), 739–751. http://doi.org/10.1016/0016-7037(90)90369-V

Bleiman, N., & Mishael, Y. G. (2010). Selenium removal from drinking water by adsorption to chitosan-clay composites and oxides: Batch and columns tests. *Journal of Hazardous Materials*, *183*(1-3), 590–595. http://doi.org/10.1016/j.jhazmat.2010.07.065

Breynaert, E., Bruggeman, C., & Maes, A. (2008). XANES-EXAFS analysis of se solid-phase reaction products formed upon contacting Se(IV) with FeS2 and FeS. *Environmental Science and Technology*, *42*(10), 3595–3601. https://doi.org/10.1021/es071370r

Chapman, P.M., Adams, W.J., Brooks, M.L., Delos, C.G., Luoma, S.M., Maher, W.A., Ohlendorf, H.M., Presser, T.S. and Shaw, D.P. (2010). Ecological Assessment of Selenium in the Aquatic Environment. *In Summary of the SETAC Pellston Workshop on Ecological Assessment of Selenium in the Aquatic Environment, 22-28 February 2009, Pensacola, Florida, USA.*

Chao, T.T. & Sanzolone, R.F. (1989). Fractionation of soil selenium by sequential partial dissolution. *Soil Science Society of America Journal, 53,* 385-392.

Charlet, L., Scheinost, A.C., Tournassat, C., Greneche, J.M. and Gehin, A. (2007).Electron transfer at the mineral/water interface: Seleneium reductino by ferrous iron sorbed on clay. *Geochimica et Cosmochimica Acta, 71(23*), 5731-5749.

Cutter, G.A. (1992). Selenium in reducing water. *Science, 217*, 829-831.

Dowdle, P. R., & Oremland, R. S. (1998). Microbial oxidation of elemental selenium in soil slurries and bacterial cultures. *Environmental Science and Technology*, *32*(23), 3749–3755. http://doi.org/10.1021/es970940s

Dungan, R. S., & Frankenberger, W. T. (1999). Microbial transformations of selenium and the bioremediation of seleniferous environments. *Bioremediation Journal, 3(3), 171-188.* https://doi.org/10.1080/10889869991219299

Ebels, J., Spirk, S. & Pietschnig, R. A facile lab scale synthesis of red selenium. *In Proceedings of the 10th Int. Electron. Conf. Synth. Org. Chem.*, 1–30 November 2006; Sciforum Electronic Conference Series, Vol. 10, 2006 , d002

Ensminger, J.T., Braunstein, H., Copenhaver, E.D., and Pfuderer, H.A. (1981) Coal: origin, classification, and physical and chemical properties. *In Environmental Health and Control Aspects of Coal Conversion - an Information Overview, Vol. I., Report No. ORNL/EIS-94.* Prepared by Oak Ridge National Laboratory, April 1977.

Fergusson, J.E., Pratt, G.M., Rodley, G.A. and Wilkins, C.J. (1962). Selenium-sulphur solid solutions. *Journal of Organic and Nuclear Chemistry, (24),* 157-160.

Fe´vrier, L., Martin-Garin, A. and Leclerc, E. (2007). Variation of the distribution of coefficient (Kd) of selenium in soils under various microbial states. *Journal of Environmental Radioactivity, 97,* 189-205.

Geering, H.R., Cary, E.E., Jones, L.H.P., Allaway, W.H. (1968). Solubility and redox criteria for the possible forms of selenuim in soils. *Soil Science Society of America Journal, 32*, 35-40.

Geoffroy, N. and Demopoulos, G.P. (2011). The elimination of selenium (IV) from aqueous solution by precipitation with sodium sulfide. *Journal of Hazardous Materals, 185,* 148-154.

Hocking, S.L., and Gadd, G.M. (2003). Linked redox precipitation of sulfur and selenium under anaerobic conditions by sulfate-reducing bacterial biofilms. *Applied and Environmental Microbiology, 69(12),* 7063-7072.

Holm, J., Palace, V.P., Wautier, K., Evans, R. E., Baron, C. L., Podemski, C., Siwik, P. and Sterling, G. (2003). An assessment of the development and survival of wild rainbow trout (Oncorhynchus mykiss) and brook trout (Salbelinus fontinalis) exposed to elevated selenium in an area of active coal mining. *The Big Fish Bang - Proceedings of the 26th Annual Larval Fish Conference, 2003.*

Jain, R., Seder-colomina, M., Jordan, N., Dessi, P., Cosmidis, J., Hullebusch, E. D. Van, & Weiss, S. (2015). Entrapped elemental selenium nanoparticles affect physicochemical properties of selenium fed activated sludge. *Journal of Hazardous Material, 295*, 193–200. http://doi.org/10.1016/j.jhazmat.2015.03.043

Jayaweera, G.R., and Biggar, J. W. (1996). Role of Redox Potential in Chemical Transformations of Selenium in Soils. *Soil Science Society of American Journal, 60*, 1056-1063.

Kang, M., Bardelli, F., Charlet, L., Gehin, A., Shchukarev, A., Chen, F., Morel, M.C., Ma, B., and Liu, C. (2014). Redox reaction of aqueous selenite with As-rich pyrite from Jiguanshan ore mine (China): Reaction products and pathway. *Applied Geochemistry, 47,* 130-140.

Kang, M., Ma, B., Bardelli, F., Chen, F., Liu, C., Zheng, Z., Wu, S. and Charlet, L. (2013). Interaction of aqueous Se(IV)/Se(VI) with FeSe/FeSe2: Implication to Se redox process. *Journal of Hazardous Materials, 248-249,* 20-28.

Laitinen, R.S. (1987). Selenium sulfide ring molecules. *Acta Chemica Scandinavica, 41,* 361-376.

Lemly, D. A. (2004). Aquatic selenium pollution is a global environmental safety issue. *Ecotoxicology and Environmental Safety, 59*, 44–56. http://doi.org/10.1016/S0147-6513(03)00095-2

Lenz, M., & Lens, P. N. L. (2008). The essential toxin : The changing perception of selenium in environmental sciences. *Science of the Total Environment, The*, *407*(12), 3620–3633. http://doi.org/10.1016/j.scitotenv.2008.07.056

Lenz, M., Van Hullebusch, E. D., Farges, F., Nikitenko, S., Borca, C. N., Grolimund, D., & Lens, P. N. L. (2008). Selenium speciation assessed by X-ray absorption spectroscopy of sequentially extracted anaerobic biofilms. *Environmental Science and Technology*, *42*(20), 7587–7593. http://doi.org/10.1021/es800811q

Lussier, C., Veiga, V. and Baldwin, S. (2003). The geochemistry of selenium associated with coal waste in the Elk River Valley, Canada. *Environmental Geology, 44*, 905-913.

Maiers, D. T., Wichlacz, P. L., Thompson, D. L., & Bruhn, D. F. (1988). Selenate reduction by bacteria from a selenium-rich environment. *Applied and Environmental Microbiology*, *54*(10), 2591–2593.

Masscheleyn, P. H., Delaune, R. D., & Patrick, Jr., W. H. (1990). Transformations of selenium as affected by sediment oxidation-reduction potential and pH. *Environmental Science & Technology*, *24*(1), 91–96. http://doi.org/10.1021/es00071a010

Masscheleyn, P. H., Delaune, R. D., & Patrick, Jr., W. H. (1991). Arsenic and Selenium Chemistry as Affected by Sediment Redox Potential and pH. *Journal of Environment Quality*, *20*(3), 522. http://doi.org/10.2134/jeq1991.00472425002000030004x

Mitchell,S.L., Nickson, R.M. and Waring, R.H. (1992). The biological activity of selenium sulfide. *Sulfur Reports, 13(2),* 279-289.

Muscatello, J.R., Bennett, P.M., Himbeault, K.T., Belknap, A.M. and Janz, D.M. (2006). Larval deformities associated with selenium accumulation in northern pike (Esox Lucius) exposed to metal mining effluent. *Environmental Science and Technology, 40*(2), 6506-6512.

Myneni, S.C.B, Tokunaga, T.K., and Brown, G.E. (1997) Abiotic selenium transformations in the presence of Fe(II,III) oxides. *Science, 278,* 1106-1109.

Neal, R. H., & Sposito, G. (1989). Selenate Adsorption on Alluvial Soils. *Soil Science Society of America Journal*, *53*, 70. http://doi.org/10.2136/sssaj1989.03615995005300010013x

Patrick, W. H., Williams, B. G., & Moraghan, J. T. (1973). A simple system for controlling redox potential and pH in soil suspensions. *Soil Science Society of America Journal, 37*, 331–332.

Pejova, B.; Grozdanov, I. (2001). Solution growth and characterization of amorphous selenium thin films-Heat transformation to nanocrystalline gray selenium thin films. *Applied Surface Science, 177*, 152–157.

Plant, J. A., Bone, J., Voulvoulis, N., Kinniburgh, DG., Smedley, PL., Fordyce FM. and Klinck, B., 11.2 - Arsenic and Selenium, In Treatise on Geochemistry (Second Edition), edited by Heinrich D. Holland and Karl K. Turekian, Elsevier, Oxford, 2014, Pages 13-57

Presser, T.S. and Swain, W.C., (1990). Geochemical evidence for Se mobilization by the weathering of pyritic shale, San Joaquin Valley, California, U.S.A. *Applied Geochemistry*, *5,* 703-717.

Ravel, B and Newville, M. (2005). ATHENA, ARTEMIS, HEPHAESTUS: data analysis for X-ray absorption spectroscopy using IFEFFIT*. Journal of Synchrotron Radiation, 12,* 537–541. doi:10.1107/S0909049505012719

Rich, R. (2007). *Inorganic Reactions in Water*. Springer, New York, New York.

Rimstidt, D.L., Balog, A., & Webb, J. (1998). Distribution of trace elements between carbonate minerals and aqueous solutions. *Geochimica et Cosmochimica Acta, 62(11),* 1851-1863.

Reeder, R. J., & Schoonen, M. A. A. (2006). Metal speciation and its role in bioaccessibility and bioavailability. *Reviews in Mineralogy & Geochemistry, 64*, 59–113. https://doi.org/10.2138/rmg.2006.64.3

Ryan, B. and Dittrick, M, (2000). Selenium in the Mist Mountain Formation of southeast British Columbia. *British Columbia Ministry of Energy and Mines, Geological Fieldwork 2000, Paper 2001-1,* 337-362.

Schwartz, G. E., Rivera, N., Lee, S., Harrington, J. M., Hower, J. C., Levine, K. E., Hsu-kim, H. (2016). Leaching potential and redox transformations of arsenic and selenium in sediment microcosms with fly ash. *Applied Geochemistry*, *67*, 177–185. http://doi.org/10.1016/j.apgeochem.2016.02.013

Shaheen, S. M., Frohne, T., White, J. R., & Delaune, R. D. (2016). Redox-induced mobilization of copper, selenium, and zinc in deltaic soils originating from Mississippi (U.S.A.) and Nile (Egypt) River Deltas : A better understanding of biogeochemical processes for safe environmental management. *Journal of Environmental Management, 186(2)*, 131-140. http://doi.org/10.1016/j.jenvman.2016.05.032

Sposito, G. (1989). The Chemistry of Soils. Oxford University Press, Oxford 1989. http://doi.org/10.1002/ange.19901020446

Steudel, R. and Laitinen, R. (1982). Cyclic selenium sulfides. *Topics in Current Chemistry, 102,* 179-197.

Stolz, J. F., Basu, P., & Oremland, R. S. (2002). Microbial transformation of elements: The case of arsenic and selenium. *International Microbiology*, *5*(4), 201–207. http://doi.org/10.1007/s10123-002-0091-y

Chakraborty, S., Bardelli, F., and Charlet, L. (2010). Reactivities of Fe(II) on calcite: selenium reduction. *Environmental Science and Technology, 44,* 1288-1294.

Szlachta, M., & Chubar, N. (2013). The application of Fe – Mn hydrous oxides based adsorbent for removing selenium species from water. *Chemical Engineering Journal*, *217*, 159–168. http://doi.org/10.1016/j.cej.2012.11.100

Vejahati, F., Xu, Z., & Gupta, R. (2010). Trace elements in coal : Associations with coal and minerals and their behavior during coal utilization – A review. *Fuel*, *89*(4), 904–911. http://doi.org/10.1016/j.fuel.2009.06.013

Vogel, M., Fischer, S., Maffert, A., Hubner, R., Scheinost, A.C., Franzen, C., and Steudtner, R. (2018). Biotransformation and detoxification of selenite by microbial biogenesis of selenium-sulfur nanoparticles. *Journal of Hazardous Materials, 344,* 749-757.

Wen, H., & Carignan, J. (2007). Reviews on atmospheric selenium : Emissions , speciation and fate. *Atmospheric Environment, 41(34)*, 7151–7165. http://doi.org/10.1016/j.atmosenv.2007.07.035

Weres, O., Jaouni, A. R., & Tsao, L. (1989). The distribution, speciation and geochemical cycling of selenium in a sedimentary environment, Kesterson Reservoir, California, U.S.A. *Applied Geochemistry*, *4*(6), 543–563. http://doi.org/10.1016/0883-2927(89)90066-8

Weres, O., Bowman, H.R., Goldstein, A., Smith, E.C., Tsao, L. and Harnden, W., 1990. The effect of nitrate and organic matter upon mobility of selenium in groundwater and in a water treatment process. *Water, Air, and Soil Pollution*, *49*, 251-272.

White, A. F., & Dubrovsky, N. M. (1994). Chemical oxidation-reduction controls on selenium mobility in groundwater systems. *Selenium in the Environment*, 185–221.

White, A. R. T. F., Benson, S. M., & Yee, A. W. (1991). Geochemical Parameters Influencing Selenium Mobility. *Water Resources Research*, *27*(6), 1085–1098.

White, C., Sayer, J. A., & Gadd, G. M. (1997). Microbial solubilization and immobilization of toxic metals: Key biogeochemical processes for treatment of contamination. *FEMS Microbiology Reviews*, *20*(3-4), 503–516. http://doi.org/10.1016/S0168-6445(97)00029-6

Wright, M. T., & Parker, D. R. (2003). Critical Evaluation of the Ability of Sequential Extraction Procedures To Quantify Discrete Forms of Selenium in Sediments and Soils. *Environmental Science and Technology, 37*(20), 4709–4716.

Wright, W. G. (1999). Oxidation and Mobilization of Selenium by Nitrate in Irrigation Drainage. *Journal of Environmental Quality, 28,* 1182-1187.

Zhang, Y., & Moore, J. N. (1996). Selenium fractionation and speciation in a wetland system. *Environmental Science and Technology*, *30*(8), 2613–2619. https://doi.org/10.1021/es960046l

Appendix A.

Bulk Solid Phase Chemistry – RES 1, RES 2 & RES 3

Description:

The accompanying excel sheet summarizes the analysis conducted by ALS Laboratories for the bulk solid-phase chemical characterization of the three residual samples used for this research.

Filenames:

Appendix A_Bulk Chemistry Summary.xlsx

Appendix B.

Aqueous Chemistry – Sequential Extraction Procedures

Description:

The accompanying Excel sheets include a summary of the complete aqueous chemistry associated with the sequential extraction procedures.

Filename:

Appendix B_SEP Data Sheets.xlxs

Appendix C.

Aqueous Chemistry – Batch Experiments (RES 2)

Description:

The accompanying Excel sheets include a summary of the complete aqueous chemistry associated with the batch experiments conducted on the residual samples.

Filename:

Appendix C_Batch Data Sheets_Residual Samples.xlxs

Appendix D.

pH and ORP Figures – Batch Experiments (RES 2)

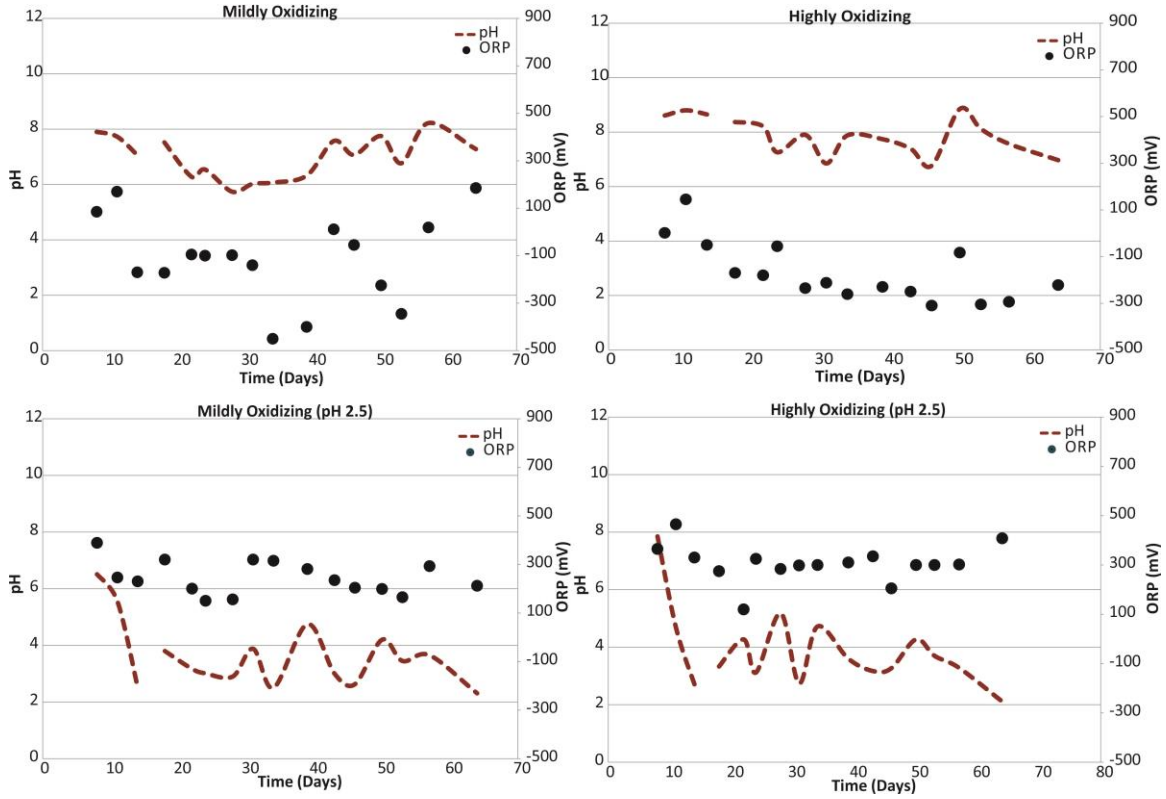

Figure D-1 pH and ORP measurements for the duration of the batch experiments using O2 as an oxidant. pH is represented by the red dashed line and the left axis and ORP is represented by black dots and measured on the right axis.

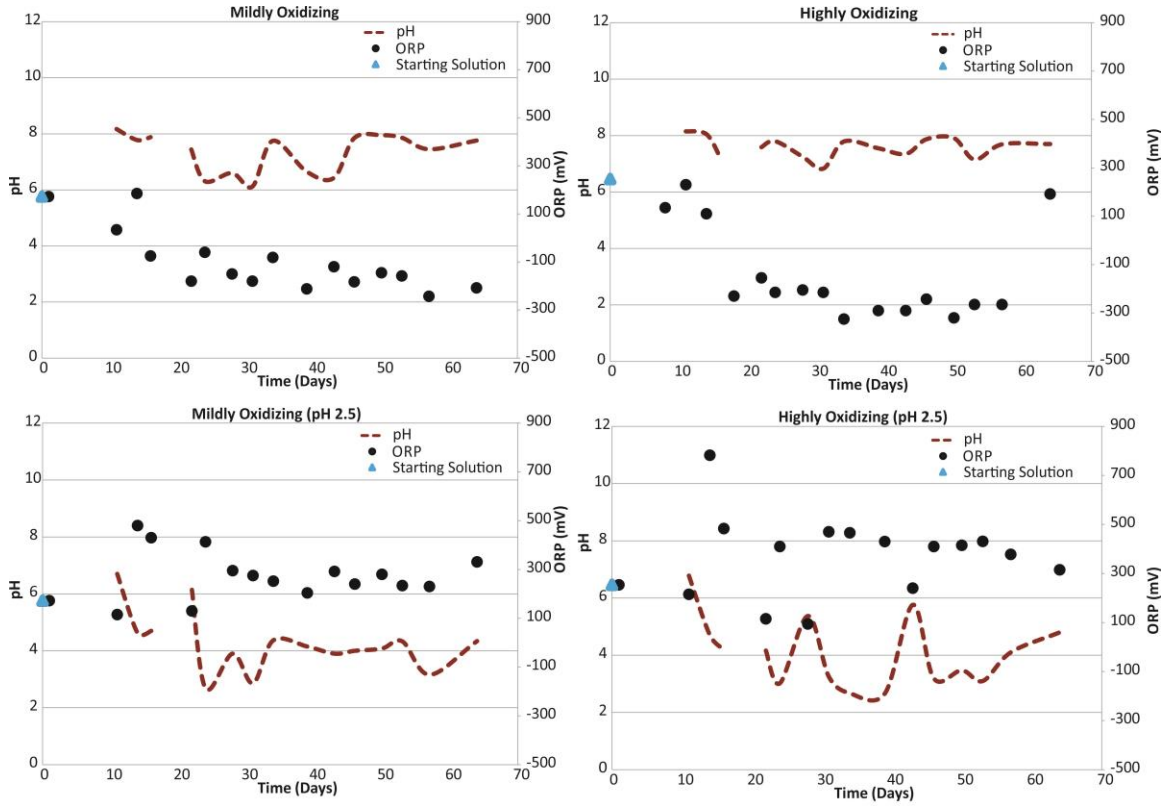

Figure D-2 **pH and ORP measurements for the duration of the batch experiments using NO3- as an oxidant. pH is represented by the red dashed line and the left axis and ORP is represented by black dots and measured on the right axis. The ORP of the starting solution us represented by a blue triangle.**

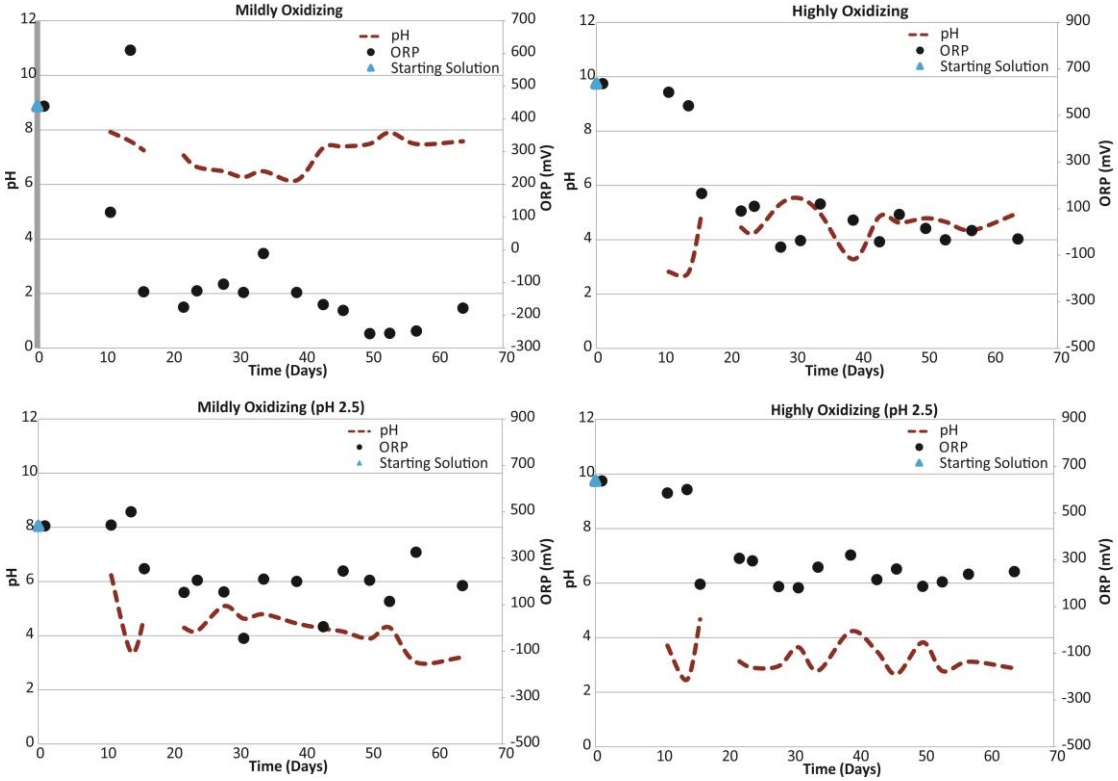

Figure D-3 pH and ORP measurements for the duration of the batch experiments using Fe3+ as an oxidant. pH is represented by the red dashed line and the left axis and ORP is represented by black dots and measured on the right axis. The ORP of the starting solution us represented by a blue triangle.

Appendix E.

Aqueous Chemistry –
Batch Experiments (Selenium Standards)

Description:

The accompanying Excel sheets include a summary of the complete aqueous chemistry associated with the batch experiments conducted on the selenium standards.

Filename:

Appendix E_Batch Data Sheets_Selenium Standards.xlxs